

## ABSTRACT

Title of Dissertation : ALLOSTERY AND GROEL: EXPLORING THE  
TENETS OF NESTED COOPERATIVITY

Jennifer Suzanne Gresham, Doctor of Philosophy, 2004

Dissertation Directed By: Professor George H. Lorimer  
Department of Chemistry and Biochemistry

Despite a wealth of structural and biochemical studies on the functional cycle of the *E. coli* chaperonins GroEL and GroES, no model proposed to date accounts for all the effects seen experimentally by the various allosteric ligands: ATP, ADP, SP, GroES, and  $K^+$ . The work in this dissertation explores the various allosteric transitions in the GroEL reaction cycle and offers a refined model for nested cooperativity that successfully accounts for the effects of these ligands. Initial studies take advantage of a single ring variant, termed SR1, to examine the allosteric properties of GroEL in the absence of complicating interactions arising from negative cooperativity. Initial rates of ATP hydrolysis by GroEL and SR1 as a function of ATP concentration were fit to an equation that makes no arbitrary assumptions. A novel role for  $K^+$  and SP is proposed, which suggests they help regulate the negative cooperativity and control the timing of the chaperonin cycle. The kinetics of association of GroES to the *trans* ring of the asymmetric complex were also studied, using stopped flow fluorescence energy transfer

(FRET), revealing that conditions which accelerate dissociation of the *cis* ligands also accelerate association to the *trans* ring. This, along with previous work obtained by our lab, suggests that the allosteric signal transmitted between the rings for *cis* ligand release is the binding of ATP to the T state of the *trans* ring. A mechanism for the formation of symmetrical particles, termed “footballs,” is suggested.

ALLOSTERY AND GROEL: EXPLORING THE TENETS OF NESTED  
COOPERATIVITY

By

Jennifer Suzanne Gresham

Thesis or Dissertation submitted to the Faculty of the Graduate School of the  
University of Maryland, College Park, in partial fulfillment  
of the requirements for the degree of  
Doctor of Philosophy  
2004

Advisory Committee:  
Professor George H. Lorimer, Chair  
Professor Dorothy Beckett  
Professor Marco Colombini  
Professor Victor Muñoz  
Professor Devarajan Thirumalai

©Copyright by

Jennifer Suzanne Gresham

2004

## ACKNOWLEDGEMENTS

Special thanks to my advisor, Dr. George Lorimer, for his superb mentorship and optimism. It is an honor to have worked with you. Thanks also to my committee for their time and support in completing this degree on time.

I am deeply indebted to Dr. John Grason, who always offered his assistance when it was needed and served as a sounding board for many of my ideas, experiments and conclusions. He also graciously served as the first editor of this document.

Dr. Kahn's laboratory kindly allowed me to use their Cary UV/Spec for several of the experiments contained in this dissertation.

Thanks to all my friends: Jim Watson, Emily Weinert, D'Anne Spence, Ranjani Varadan, Lusiana Widjaja, John and Jen Grason, Fabiani Oliva and Mourad Sadqi. You helped to make this experience fun as well as educational.

Finally, thanks to my husband, Kyle, and his family (Dave, Linda, Ross, Jessy, and Nicole) for such wonderful support and encouragement. I am so lucky to be a part of this family.

## TABLE OF CONTENTS

List of Figures	vi
List of Tables	ix
List of Abbreviations	x
Chapter 1: Introduction and Specific Aims	1
1.1 GroE Architecture	2
1.2 The Chaperonin Reaction Cycle	4
1.3 Allosteric Effects	10
1.4 Active versus Passive Models for Folding	13
1.5 Specific Aims	17
Chapter 2: General Methods and Experimental Procedures	19
2.1 Protein Concentrations	20
2.2 Bradford Assay	20
2.3 Polyacrylamide Gel Electrophoresis (PAGE)	21
2.4 Purification of GroEL	21
2.5 Purification of SR1	25
2.6 Purification of GroES	26
2.7 Purification of His-Tagged GroES	27
2.8 Coupled Enzyme ATPase Assay	28
2.9 Preparing Unfolded Substrate Proteins	31
2.10 Computer software	31
Chapter 3: Probing Allosteric Interactions with the Single Ring Variant, SR1	32
3.1 Introduction	33
3.2 Methods Specific to Chapter 3	37
3.2.1 Assaying GroES Release and SP Encapsulation in SR1 Using His-tagged GroES	37
3.2.2 Gel Filtration Using HPLC	38
3.2.3 Site Directed Mutagenesis	38
3.2.4 Oxidation of SR1 <sup>IAX</sup> with Diamide	39
3.2.5 Gel Quantitation of the Reaction Coordinate	40
3.3 Results	41
3.3.1 Verifying the Oligomeric Structure of SR1	41
3.3.2 The Effect of Unfolded Substrate Protein and GroES on SR1 ATPase Activity	44
3.3.3 Response of SR1 <sup>IAX</sup> ATPase Activity to Oxidation	48
3.3.4 Modeling the Effects of Oxidation in SR <sup>IAX</sup>	48
3.3.5 The Effect of Left Site versus Right Site Mutations	52

## TABLE OF CONTENTS (CONT.)

3.4 Discussion	55
3.4.1 Implications for the Allosteric Model	55
3.4.2 A New Oxidative Model from SR1 <sup>IAx</sup>	57
3.4.3 The Nature of Inter-Ring Communication	58
Chapter 4: Examining the Effects of Potassium on the Allosteric Properties of GroEL: A New Equation for Nested Cooperativity	60
4.1 Introduction	61
4.2 Methods Specific to Chapter 4	64
4.2.1 Purification of Recombinant Rabbit Pyruvate Kinase	64
4.2.2 ATPase Assay Using the Cary 100 Bio UV Spectrophotometer	66
4.2.3 ATPase of GroEL and SR1 at Variable Potassium Concentrations	67
4.2.4 Fitting Data to the Nested Cooperativity Equations	68
4.3 Results	69
4.3.1 Examining the Effects of Potassium Concentration on the ATPase Activity of SR1	69
4.3.2 Fitting SR1 ATPase Activity to the Exclusive and Nonexclusive Binding Equations	70
4.3.3 Examining the Effects of Potassium on the ATPase Activity of GroEL	73
4.3.4 Fitting the GroEL ATPase Data to the Exclusive and Nonexclusive Binding Equations	74
4.4 Discussion	78
4.4.1 Evaluating a New Equation for Nested Cooperativity	78
4.4.2 A Proposal for the Role of Potassium	80
Chapter 5: Stopped Flow Analysis of GroES Association to the Asymmetric Complex: Looking at Inter-Ring Communication	82
5.1 Introduction	83
5.2 Methods Specific to Chapter 5	86
5.2.1 Purification and Labeling of Mutant Proteins	86
5.2.2 Stopped-flow Fluorescence Measurements	88
5.2.3 GroEL versus GroES Competitor Experiments	91
5.3 Results	91
5.3.1 GroES Association to the Trans Ring is Diffusion Limited	91
5.3.2 Comparing the Kinetics of Association and Dissociation	94
5.3.3 The Effects of K <sup>+</sup> on Association and Dissociation	96
5.3.4 Utilizing GroEL Traps to Study Symmetric Complex Formation	98

## TABLE OF CONTENTS (CONT.)

5.3.5	Testing for Symmetric Complexes Using a Steady State FRET Analysis	101
5.4	Discussion	103
5.4.1	GroES Association and Dissociation Are Tightly Coupled Events	103
5.4.2	The Effects of Potassium	104
5.4.3	The Evidence for Symmetric Complexes	105
Chapter 6:	Summary and Final Discussion	107
Appendix:	Derivation of Equations for Nested Cooperativity in GroEL	113
References		118

## LIST OF FIGURES

1-1	Crystal Structures of GroEL and the Asymmetric Complex	3
1-2	Cartoon of the GroEL Reaction Cycle	5
1-3	Conformational Changes Induced Upon Ligand Binding	8
1-4	Movement of SP Binding Sites in the Transition from T to R'	8
1-5	The Model of Nested Cooperativity as Applied to GroEL	11
2-1	GroEL <sup>wt</sup> Purification	24
2-2	Tryptophan Fluorescence of GroEL, Pre- and Post-Acetone Treatment	25
2-3	GroES <sup>wt</sup> Purification	27
2-4	Coupled Enzyme ATPase Assay	29
2-5	Monitoring ATP Hydrolysis in Real Time	29
3-1	Contact Sites at the Inter-Ring Interface of GroEL	33
3-2	Initial Velocities of ATP Hydrolysis by GroEL	36
3-3	An Intra-Subunit Salt Bridge Is Replaced with Two Cysteines	37
3-4	SDS Gel of SR1 <sup>IAX</sup> with Increasing Amounts of Diamide	40
3-5	Binomial Distribution for SR1 <sup>IAX</sup>	42
3-6	Native Gel and Western Blot of GroEL <sup>wt</sup> and SR1	43
3-7	SR1 Remains a 7-mer in the Presence of Nucleotide	44
3-8	ATPase Assays of SR1	45
3-9	SR1 Can Bind and Encapsulate SP	47

3-10	Inhibition of Fractionally Oxidized SR1 <sup>IAX</sup> by GroES	49
3-11	Modeling the Effects of Oxidation Using the Model for GroEL <sup>IAX</sup>	51
3-12	Applying the New Model to SR1 <sup>IAX</sup> and GroEL <sup>IAX</sup>	52
3-13	Native Gel Reveals that GroEL <sup>LSM</sup> is a 14-mer	53
3-14	ATPase Activity of GroEL <sup>LSM</sup> , ±GroES	54
4-1	The Original Model for Nested Cooperativity in GroEL	62
4-2	Nested MWC Model for Cooperativity in GroEL	63
4-3	Purification of Rabbit Pyruvate Kinase E117K	67
4-4	ATPase of SR1 at Various Potassium Concentrations	69
4-5	The $V_{\max}$ for SR1 is Not Affected By Changing Potassium Concentrations	70
4-6	Evaluating the Exclusive Binding Assumption in SR1	72
4-7	Potassium Affects both $V_{\max}$ and $k_R$ in GroEL	74
4-8	The Reciprocal Nature of the Allosteric Ligands ATP and $K^+$	75
4-9	Evaluating the Exclusive Binding Assumption in GroEL	76
5-1	The GroEL Reaction Cycle	84
5-2	Schematic of Stopped Flow Experiment	90
5-3	Long Time Course Association Data	92
5-4	GroES Association is Diffusion Limited	94
5-5	Association and Dissociation Data, ±ADP and ±SP, at 100 mM and 10 mM $K^+$	95
5-6	Figure 5-6: The Effects of $K^+$ on Mean Residence Time, ±ADP	97
5-7	Monitoring Dissociation Using an EL and ES Trap, ±ADP	99

5-8	Adding Denatured Substrate Protein to the GroEL and GroES Trap Experiments	100
5-9	Looking for Symmetric Complex Formation Using Steady State FRET	103
A-1	The Microscopic Species Possible with One Ligand Bound to the Single Ring	114

## LIST OF TABLES

3-1	Thermocycler Conditions for PCR-based Mutagenesis	39
4-1	Parameters Derived from Fits of SR1 ATPase Data to the Nonexclusive Binding Equation	73
4-2	Parameters Derived from Fits of GroEL ATPase Data to the Nonexclusive Binding Equation	77
5-1	Observed Rate Constants at Variable GroES <sup>A</sup> Concentrations	93
5-2	Comparison of Mean Residence Times at 100 mM and 10 mM K <sup>+</sup>	97

## LIST OF ABBREVIATIONS

[X]	concentration of X
ADP	adenosine diphosphate
$\alpha$ -LA	$\alpha$ -lactalbumin (bovine)
Amp	ampicillin
AMP-PNP	5'-adenylylimidodiphosphate
ATP	adenosine triphosphate
BSA	bovine serum albumin
cryo-EM	cryo-electron microscopy
Cys	cysteine
DEAE	diethylaminoethyl (weak anionic exchanger)
DMF	N,N-dimethylformamide
DNA	deoxyribonucleic acid
dNTP	deoxyribonucleoside triphosphate
DTT	dithiothreitol
<i>E. coli</i>	<i>Escherichia coli</i>
EDTA	ethylenediaminetetraacetic acid
F5M	fluorescein-5-maleimide
FRET	fluorescence resonance energy transfer
GdnHCl	guanidinium hydrochloride
GroEL <sup>D</sup>	GroEL E315C labeled with IAEDANS
GroEL <sup>IAx</sup>	GroEL D83C/K327C (intra-subunit double cys pair)
GroEL <sup>LSM</sup>	GroEL E102A, K105A, and M11A ( <b>Left Site Mutations</b> )
GroEL <sup>wt</sup>	wild-type GroEL

GroES <sup>A</sup>	GroES 98C labeled with F5M
GroES <sup>his</sup>	GroES with His <sub>6</sub> tag
GroES <sup>wt</sup>	wild-type GroES
His	histidine
IAEDANS	5-(((2-iodoacetyl)amino)ethyl)amino) naphthalene-1-sulfonic acid
IPTG	isopropyl-β-D-thiogalactopyranoside
IR	infrared
K <sup>+</sup>	potassium ion
KAc	potassium acetate
kDa	kilodaltons
KNF	Koshland-Nemethy-Filmer model of allostery
LB	Luria-Bertani broth
LDH	lactate dehydrogenase (bovine milk)
mAmps	milliamps
MDH	malate dehydrogenase (pig heart mitochondrial)
MES	2-(N-Morpholino)ethanesulfonic acid hydrate
mg	milligram
MgAc	magnesium acetate
ml	milliliter
MRT	mean residence time
mS	milliSiemens/centimeter
ms	milliseconds
MWC	Monod-Wyman-Changeux model of allostery
NaAc	sodium acetate

NADH	nicotinamide adenine dinucleotide
NEM	N-ethylmaleimide
Ni-NTA	nickel-nitrilotriacetic acid
nm	nanometers
OD	optical density
PAGE	polyacrylamide gel electrophoresis
PCR	polymerase chain reaction
PEP	phosphoenolpyruvate
PK	pyruvate kinase (bovine)
PK117	pyruvate kinase E117K (rabbit)
PMSF	phenylmethylsulfonyl fluoride
pmol	picomoles
R	<b>R</b> elaxed state in MWC terminology
RuBisCo	Ribulose biphosphate carboxylase
SDS	sodium dodecyl sulfate
SP	substrate protein
SP Sepharose	Sulfopropyl sepharose resin (strong cationic exchanger)
SR1	single-ring mutant of GroEL (R452E, E461A, S463A, and V464A)
SR1 <sup>IAX</sup>	SR1 D83C/K327C (intra-subunit double cysteine pair)
T	<b>T</b> ense state in MWC terminology
Tris	Tris (hydroxymethyl) aminomethane
TMA	tetramethylammonium chloride
UV/Vis	ultraviolet/visible

## **Chapter 1**

### **Introduction and Specific Aims**

The journey from a nascent polypeptide to a native, fully folded conformation can be a hazardous one. The rugged energy landscape for such a journey is full of pitfalls and false minima, and the energy required to escape such a disaster may not be available on the biologically significant timescale of 20 to 40 minutes [1]. To overcome this problem, nature has developed molecular guides known as chaperones. Chaperones are proteins that assist in the folding of other proteins, during nonpermissive conditions such as heat shock as well as under normal growth conditions, and are absolutely essential to cellular growth [2, 3]. In addition to their role as protein folders, chaperones also appear to have antigenic properties in a wide variety of infectious diseases [4, 5]. There are several classes of chaperone proteins, but perhaps the best studied for their structure and function are the chaperonins, typified by GroEL and its co-chaperone GroES, from *E. coli*. The primary role of chaperonins is to bind non-native proteins and then sequester them in a protective environment that allows for repeated attempts at the folding process. Although most of the individual steps in this process are well understood, there are still many aspects of GroEL function that remain controversial.

### ***1.1 GroE Architecture***

GroEL is a homo-oligomer of 14 subunits, each 57 kDa in size with 547 amino acids [6]. The 14-mer is composed of two rings, 7 subunits each, which are arranged back to back to form two central chambers. The crystal structure of GroEL was determined in 1994 to 2.8 Å [7]. The structure is highly symmetrical; a two-fold symmetry exists between the rings [8]. This unique structure is ideally suited to support the conformational changes necessary for binding and encapsulating non-native proteins. The domains of a GroEL subunit are distinguished as follows (Figure 1-1A):

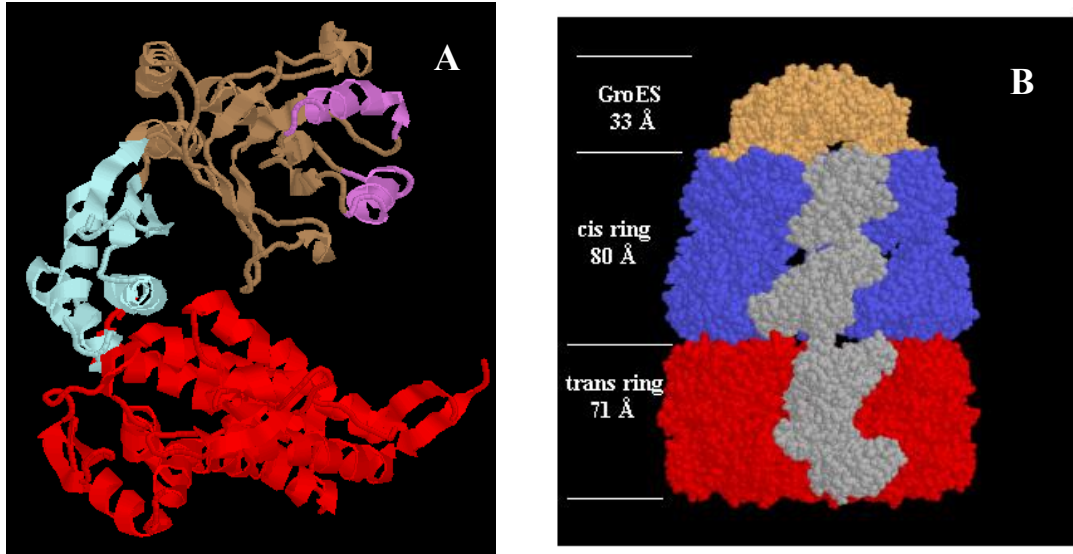


**Figure 1-1: Crystal Structures of GroEL and the Asymmetric Complex.** **A)** An isolated subunit of GroEL in the absence of nucleotide (pdb file 1oel) [9]. The equatorial domain is shown in red, the intermediate domain in blue, and the apical domain in brown. Helices H and I, which contain the residues primarily responsible for substrate protein and GroES binding, are highlighted in purple. **B)** The asymmetric complex of GroEL and GroES (pdb file 1aon) [10]. The *trans* ring of GroEL is shown in red, while the *cis* ring is shown in blue. A single subunit is highlighted in each ring (in gray) to underscore the dramatically different conformations. GroES (shown in gold) caps the *cis* ring, preventing escape of any encapsulated substrate protein and committing the seven ATP to hydrolysis.

1) The *equatorial domain* is a highly helical, solid foundation at the median of the 14-mer that serves to stabilize the structure during domain movements. It provides inter-ring contact, most of the intra-ring contacts, and contains a site for  $Mg^{2+}$ -ATP binding and hydrolysis [11]. The residues involved in ATP binding and hydrolysis are among the most conserved residues in GroEL homologs from several different species [12]. The equatorial domains also block the channel between the two rings [8].

2) The *apical domain* surrounds the opening of the cavity and is responsible for substrate protein and GroES binding [13]. It is inherently flexible, due to a more disordered structure.

3) The *intermediate domain* connects the equatorial and apical domains through two hinge regions that provide flexibility for conformational movements. These hinge regions allow for the transmission of allosteric signals (discussed in detail in section 1.3), tightly coupling the binding of nucleotide and GroES binding.

The co-chaperonin, GroES, is essential to GroEL function [2, 14]. It contains 7 identical subunits, each is 10 kDa with a core  $\beta$ -barrel and two hairpin loops [15]. GroES normally binds to GroEL with a 1:1 stoichiometry (1 GroES<sub>7</sub> per 1 GroEL<sub>14</sub>). In this way, it serves as a dome over the central cavity during protein sequestration until ligand release (Figure 1-1B). This complex is referred to as the asymmetric complex, or “bullet”, where mobile loops in GroES associate with helices H and I in the apical domain of GroEL [10]. The ring of GroEL that is complexed with GroES is referred to as the *cis* ring, in order to distinguish it from the other ring of GroEL, which is termed the *trans* ring. Electron microscopy has also revealed symmetric complexes, or “footballs” (GroES<sub>7</sub>-GroEL<sub>14</sub>-GroES<sub>7</sub>), under a variety of conditions [16-18]. It is still unclear if these structures exist *in vivo* or what role they play in the chaperone cycle, although they are possibly intermediates in the normal cycle [19]. This topic will be discussed in detail in Chapter 5.

### ***1.2 The Chaperonin Reaction Cycle***

The two rings of GroEL have been said to function as a “two-stroke motor,” since they alternatively undergo identical cycles [20, 21]. Thus, a single ring is often considered the fundamental unit, as the cycle of one ring fully describes the process by which a substrate protein is refolded [22]. The reaction cycle can be divided into five

basic steps: substrate binding, nucleotide binding, encapsulation, *cis* ligand release, and ATP hydrolysis (Figure 1-2).

*Substrate binding* The exact targets of GroEL function *in vivo* are unknown. *In vitro*, GroEL can interact with ~40% of the soluble proteins of *E. coli*, provided they are presented to GroEL in a denatured state [23]. However, kinetic considerations make it improbable that GroEL interacts *in vivo* with more than 5% of the proteins folding in the cell [24]. Even under normal cellular conditions, the extremely high concentration of RNA and protein in the cytoplasm, estimated to be about 340 g/L in *E. coli* [25], can lead

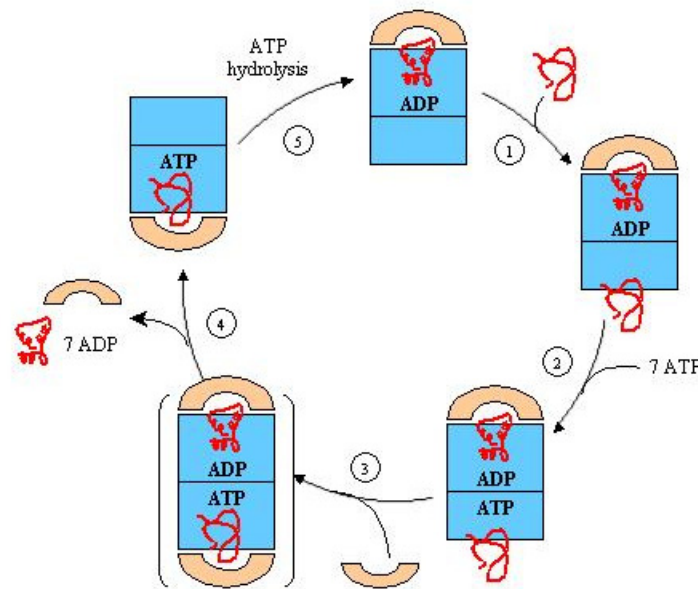


**Figure 1-2: Cartoon of the GroEL Reaction Cycle.** This shows the passage of GroEL as it proceeds through one round of substrate binding and release. GroEL is shown in blue, GroES in tan, and SP in red. The resting state, at the top of the cycle prior to step 1, is an asymmetric complex with substrate protein and ADP trapped inside the *cis* ring. The volume of the internal cavity of the *cis* ring is nearly twice that of the *trans* ring. In step 1, substrate protein binds to the *trans* ring of the asymmetric complex. Once ATP binds (step 2), the *cis* ligands are primed for release. The chaperone may or may not proceed through an intermediate, symmetric complex, as indicated by the brackets. Once the protein is encapsulated and the *cis* ligands are released (steps 3 and 4), ATP hydrolysis (step 5) returns the complex to the original resting state.

to aggregation. Other factors such as temperature increases, osmotic imbalances, and pH changes can greatly increase the number of misfolded states for proteins [26, 27].

GroEL-GroES can rescue nearly 80% of misfolded or aggregated proteins that would barely escape the energy barrier of a misfolded state without the presence of the chaperone [14]. Some proteins, while capable of interacting with GroEL *in vitro* in an unfolded state, most likely fold spontaneously under normal conditions. Based on the fact that GroEL is essential to the growth of *E. coli*, other proteins, as yet unidentified, appear to be fully dependent on GroEL to achieve their native conformation [3, 28].

Because GroEL evolved to interact with a wide variety of proteins, it would seem necessary that the recognition of substrate not be dependent on sequence or secondary structure, but instead on something more universal to misfolded or unfolded proteins: exposed hydrophobic residues which would normally be buried in the native state [29, 30]. Nine residues on helices H and I in the apical domain of GroEL, consisting of eight hydrophobic side chains plus one serine (Figure 1-1A), have been implicated in peptide binding through site-specific mutagenesis [13]. There has been some suggestion that GroEL preferentially recognizes  $\alpha\beta$ -folds [31], however this work was based on an analysis of proteins in their native state, with which GroEL does not interact [32].

Substrates shown to bind GroEL range from all  $\alpha$ -helical peptides to all  $\beta$ -structures [33].

A sequence based analysis of proteins with similar residues to the mobile loop of GroES and multiple, putative binding sites revealed approximately 3% of *E. coli* proteins serve as natural substrates and yet have no preferred secondary structure [34]. Other work demonstrated that GroEL bound several synthesized peptides, whose sequence was random and displayed no propensity for any particular type of secondary structure [35].

The hydrophobic binding sites of GroEL are repeated seven-fold around the inside of the central cavity, forming a complete ring. The volume of the cavity, as measured in the crystal structure, is  $\sim 85,000 \text{ \AA}^3$  and can accommodate a protein from 70 to 100 kDa in size [7, 36]. This is certainly reasonable if it is assumed the protein protrudes from the top of the cavity like the cork on an opened wine bottle, as confirmed by cryo-electron microscopy and small-angle neutron-scattering [37, 38]. Additionally, the substrate does not necessarily need to contact all seven binding sites; as few as 3 to 4 could be sufficient [39]. Indeed, since GroES binds to the same sites, binding of SP at all 7 sites would preclude GroES binding [22].

*Encapsulation* The binding of ATP to GroEL (Figure 1-2, step 2) is a prerequisite for the subsequent binding of GroES (Figure 1-2, step 3). By following pyrene-labeled GroEL through a folding cycle, it was discovered that the binding of ATP triggers a conformational change that precedes the binding of GroES [8, 40]. Upon binding ATP, each intermediate domain shifts inwards by about  $20^\circ$  towards the equatorial domain in a concerted fashion, moving about the hinges Pro137 and Gly410 [41]. This brings residue D398 within coordination of the  $\text{Mg}^{2+}$ -ATP and closes the nucleotide binding site. With the addition of GroES, the domains undergo even larger *en bloc* movements, where the apical domain shifts upwards  $60^\circ$  from the horizon and completes a  $90^\circ$  anti-clockwise twist, resulting in the dispersal of the peptide binding sites (Figures 1-3 and 1-4) [41]. The sum of these conformational changes has two very important consequences. First, the volume of the cavity expands almost two-fold [10]. Secondly, as the subunits pivot, affinity for the substrate dramatically decreases as the hydrophobic binding sites become buried within the interior of the cavity wall. The

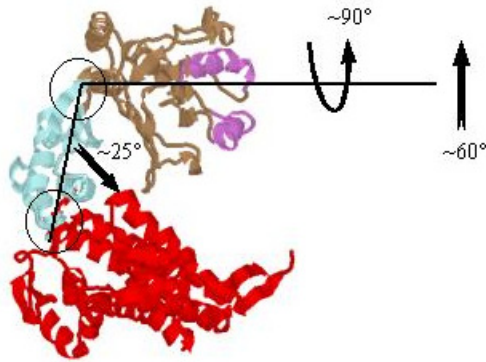


**Figure 1-3: Conformational Changes Induced Upon Ligand Binding.** Upon binding ATP and GroES, GroEL monomers within a ring undergo concerted movements, twisting and rotating about two hinge regions (indicated by circles). The first transition occurs upon ATP binding, where the intermediate domain (blue) moves towards the equatorial domain (red) by about 25°. The binding of GroES precipitates even larger movements, where the apical domain (brown) moves up 60° and twists in a anti-clockwise direction 90° about the horizontal axis.

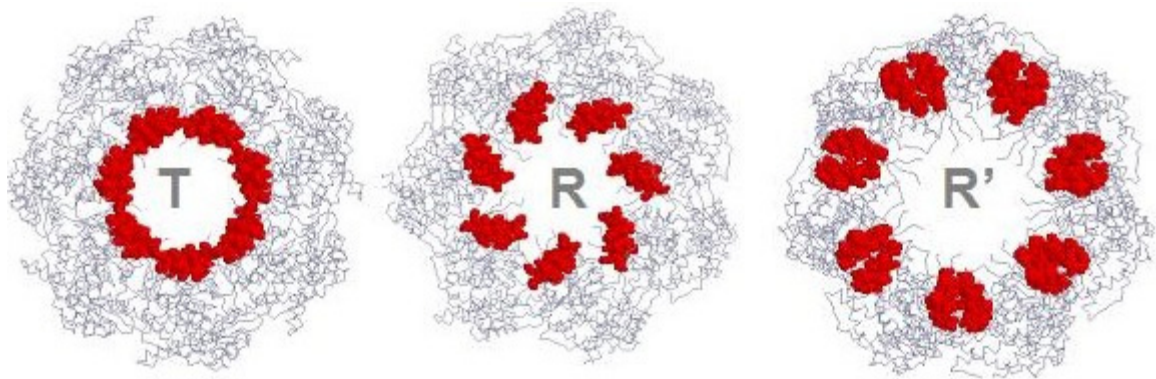


**Figure 1-4: Movement of SP Binding Sites in the Transition from T to R'.** The allosteric transitions that occur upon ATP binding (T to R) and subsequently GroES binding (R to R') cause the substrate binding sites to move apart from one another. The first transition is thought to actively unfold the substrate protein while the second transition encapsulates it. The T and R' states were determined by x-ray crystallography [9, 10], and the R state structure was determined by cryo-EM [41]. (Figure kindly provided by Dr. John Grason.)

effect is the dislodgment of the substrate into the GroEL cavity, with access to the surrounding media blocked by GroES [42]. The act of encapsulation is critical to the process of refolding because it is this step that introduces the substrate to an isolated, essentially infinitely diluted environment [36]. This is sometimes referred to as the “Anfinsen cage,” since it is believed that all the information needed to achieve the correct three dimensional structure is contained within the amino acid sequence of the protein [43]. This accomplishes a “bait and switch” mechanism: whereas the initial binding of the substrate was primarily through hydrophobic interactions, the encapsulated substrate is now surrounded by mostly hydrophilic residues [10, 36]. This new microenvironment gives the substrate protein a new chance to fold into the correct state while reducing the propensity for off-pathway aggregation [44]. It is not known if encapsulation proceeds via the symmetric complex shown in brackets in Figure 1-2, or if the *cis* ligands are released (step 4) prior to encapsulation.

*Cis Ligand Release* The  $\beta$ - $\gamma$  phosphoanhydride bond of the bound ATP is known to stabilize the asymmetric complex [45]. The presence of ADP in the *cis* ring weakens the interaction between GroEL and GroES, and primes the complex for ligand release. However, this is insufficient to cause dissociation. It is the binding of ATP to the *trans* ring, and the subsequent conformational changes that occur upon binding, that communicate the signal for ligand release [46-48]. The joint presence of substrate protein and ATP on the *trans* ring has been shown to greatly increase the rate of ligand release in the *cis* ring [20, 49]. Ligand release is presumed to be the reversal of the binding order: GroES leaves first, followed by the substrate protein (folded or not), whereby the apical and intermediate domains relax and the ADP is allowed to diffuse

away [22]. Because ADP release follows release of the substrate protein, a natural consequence is that the SP must be ejected from the GroEL cavity with each round of ATP hydrolysis in order for the process to continue [48].

*ATP Hydrolysis* The process of encapsulation (Figure 1-2, step 3) commits the trapped nucleotide to hydrolysis, where all seven ATP molecules are hydrolyzed in a quantized nature in the presence of GroES (Figure 1-2, step 5) [48]. While the inorganic phosphate is free to diffuse away from GroEL, the ADP remains trapped until primed for release by subsequent steps on the distal ring. When a GroEL mutant capable of binding ATP, but not hydrolyzing it, was employed in encapsulation experiments, the cycle was halted after initial formation of the asymmetric complex [20]. Thus, ATP hydrolysis is an essential step in the continued operation of the cycle. The same may be said of the release of the *cis* GroES.

### ***1.3 Allosteric Effects***

The above discussion of the chaperonin hemicycle has been described without mention of allosteric effects, and yet allosteric interactions are an essential part of the hemicycle. Allosteric considerations in large, oligomeric proteins such as the chaperonins are complex, and have been described using a model of nested cooperativity [50, 51]. Here, Monod-Wyman-Changeaux (MWC) interactions [52] within a ring of GroEL are nested inside Koshland-Nemethy-Filmer (KNF) interactions [53] between the rings (Figure 1-5). Another model that has not received wide spread acceptance in the field is a nested MWC model [54], which will be discussed in detail in chapter 4.

In the absence of GroES and ATP, the resting state of GroEL is described as each ring residing primarily in the T state, i.e.  $T_7T_7$ , where T refers to a tense state or one with

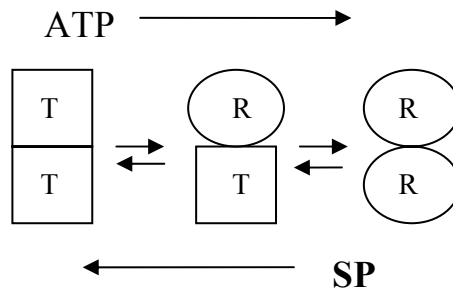


**Figure 1-5: The Model of Nested Cooperativity as Applied to GroEL.** In the model developed by Yifrach and Horovitz [50], MWC interactions are nested inside KNF interactions. With no ligands bound, both rings of GroEL exist primarily in the T state. Cooperative binding of ATP induces an “all or none” transition in the first ring (MWC transition), where subunits within a ring are either in the T state or the R state, but do not exist as a mixture of both. Once the first ring has transitioned to the R state, additional ATP binds to the second ring, inducing a second “all or none” transition. The sequential transition from TT to TR to RR is governed by KNF interactions. ATP shifts the equilibrium toward the R states, while unfolded SP shifts the equilibrium toward the T states.

low affinity for ATP. Conversion to the R state (relaxed, high affinity) is concerted in nature, where the binding of ATP at low concentrations ( $<100 \mu\text{M}$ ) shows positive cooperativity within one ring [51, 55]. A second level of allostery exists between the two rings. Due to inter-ring negative cooperativity, the RR state only exists at higher ATP concentrations ( $>100 \mu\text{M}$ ) [51]. Thus the conversion from TT via TR to RR is sequential in nature. When GroES is present, two more allosteric states may be defined: the R' state, where GroES is bound to the *cis* ring but ATP hydrolysis has not occurred, and the R'' state, where hydrolysis has taken place but the *cis* ligands have not yet departed [22].

Evidence for the above allosteric transitions is considerable. Kinetic measurements of ATP hydrolysis at various ATP concentrations revealed two allosteric transitions, which initially suggested the nested cooperativity model [50]. Structures of

the TT, TR and RR states, based on cryo-electron micrographs, are available at 28Å [56]. Crystal structures of the TT and TR'' states have also been determined [7, 10]. Various experiments have probed the nature of the concerted, rigid-body conformational changes within a ring. Normal mode analysis and molecular dynamic simulations suggest that steric interactions between the apical domain of one subunit and its neighbor may be the primary cause for the positive cooperativity within a ring [57]. Additionally, a E155A mutation in GroEL which eliminates an essential intra-subunit interaction, leads to destabilized allosteric intermediates and a sequential, rather than concerted, mechanism, suggesting that tertiary conformational changes govern the allosteric transitions [58].

Interactions between the equatorial domains of the two rings contribute most strongly to the negative cooperativity, although they are less well understood. During the T to R' transition, equatorial domains in the *cis* subunit push down on the *trans* ring, and in an effort to maintain structural contacts, the *trans* ring must slightly buckle by moving approximately 2° away from the horizontal axis [10, 20]. Thus, the binding of ATP and GroES to one ring transmits a signal to the other that opposes formation of a similar complex. However, this describes an attempt to dock one GroES-ADP-GroEL ring with another to make a truly symmetric complex [57]. However, “footballs” are not symmetric with respect to nucleotide[59].

Besides ATP, it is known that GroES, ADP, Mg<sup>2+</sup>, K<sup>+</sup>, and substrate protein can all have allosteric effects on GroEL [51, 56, 60, 61]. These allosteric effectors may work in concert or antagonistically to one another, making GroEL allostery rather complicated. For example, the positive cooperativity of ATP binding is reduced with increasing K<sup>+</sup> concentrations [62], presumably because K<sup>+</sup> influences the equilibrium between the T

and R states [61, 63]. In contrast, GroES binding to the *cis* ring of the asymmetric complex reduces the affinity for substrate in the *trans* ring and shifts the  $T \rightleftharpoons R$  equilibrium in the *trans* ring to the right [20, 64]. Perhaps the most important effector is substrate protein, which can alter the time it takes to complete the GroEL reaction cycle (as shown in Figure 1-2, also called the mean hemicycle time) as much as 20-fold [49]. The exact role of each of these effectors, and how they interact with each other *in vivo*, is still largely a mystery.

#### ***1.4 Active versus Passive Models for Folding***

Although the steps in the chaperonin cycle are fairly well understood, questions remain as to the actual mechanism of substrate re-folding. The allosteric effects caused by SP binding relate directly to the controversy. A subunit in the T state has a low affinity for ATP, but a high affinity for non-native SP, whereas R state affinities are reversed [65]. The affinities for non-native SP exhibited by the two states can be understood by remembering that in the T to R transition, the apical domains twist with respect to the equatorial domain in a concerted fashion, and the substrate binding sites move apart from one another (Figure 1-5) [42, 50]. The binding of substrate protein stimulates ATPase activity [65], where the activity of a subunit in the T state is thought to be nearly 4 times greater than one in the R state [22]. Moreover, a chemical cross-link inserted into one subunit locks the entire ring in the T state, giving rates of ATP hydrolysis comparable to those with saturating substrate protein present [49]. Taken together, these data imply that SP resists the T to R transition, and work is performed on the SP through rotation of the subunits. This model of GroEL function has been likened to substrate proteins getting stretched on the rack [66].

This explanation is not fully accepted however, and some hold that the mechanism for refolding by GroEL is purely passive [25, 67, 68]. In this model, the “Anfinsen cage” provided by the GroEL cavity prevents intermolecular, hydrophobic interactions between non-native peptides that can lead to aggregation. Folding of substrate protein occurs solely inside the cavity, in an infinitely diluted environment. It is noted that all the substrates normally used in refolding assays *in vitro* can fold spontaneously under permissive conditions, usually when protein concentrations and temperatures are low [22, 25]. Unlike enzyme catalysts, the chaperonin system *usually* only enhances the yield of re-folded substrate protein, and only rarely (and modestly) enhances the rate [22, 33].

The active unfolding proposal suggests substrate proteins are subjected to mechanically-induced unfolding during the GroEL allosteric transitions [69]. This idea is often tied to the iterative annealing model [70], which is based on data that show the substrate protein is ejected from the GroEL cavity whether or not it has completed its refolding [48, 71]. Incompletely folded proteins are quickly recaptured by the chaperonin, and iterative annealings are performed until the substrate can reach its native conformation. This supposes that the slow step in protein folding is the intramolecular reorganization of misfolded or trapped segments, which are assisted in achieving the correct conformation through the forced unfolding [70]. In this case, the substrate may fold into the correct conformation either inside or outside the GroEL cavity. The classic substrate used to demonstrate iterative annealing is RuBisCO, which can be rescued only by the GroEL-GroES system under nonpermissive conditions [14]. In its denatured form, RuBisCo can exchange all but a small core of amide hydrogens with solvent. But upon

interaction with GroEL, GroES, and ATP, almost a full exchange is observed, suggesting the protein is indeed unfolded [69]. This result was also achieved when AMP-PNP was used, which can bind in the GroEL nucleotide site, but cannot be hydrolyzed, further suggesting that the binding of nucleotide, or the T to R transition, is responsible for the results. Importantly, a single interaction with GroEL is sufficient to support full or partial unfolding of the substrate.

Other studies provide important substantiation for the active unfolding model. Fedorov and Baldwin used the bacterial luciferase system to show that GroEL may release intermediates that resemble the transition state, a form capable of achieving the native conformation faster than the originally bound form of the protein [33]. This acceleration in the rate of folding strongly suggests GroEL can actively lower the free energy barrier to folding, at least in some cases [46]. Theoretical modeling confirms that a passive mode of function should have little effect on folding kinetics [44], although some groups have used molecular dynamics simulations to suggest that encapsulation can smooth the energy landscape, thereby increasing refolding rates approximately two-fold [72]. However, this study did not consider the effect of “confinement” on folding rates.

The critical dependence of timing in GroE folding reactions was confirmed with dimeric citrate synthase (CS) [17]. Under nonpermissive conditions, unfolded CS monomers,  $M_1$ , can be trapped by GroEL and refolded to an assembly competent state,  $M_2$ . This form can degrade over time to an intermediate  $M_3$ , which is misfolded and can again be trapped and rescued by GroEL. Interestingly, if the  $M_3$  form is sequestered in a GroEL cavity incapable of turn over, either due to the use of nonhydrolyzable analogs of ATP or the GroEL mutant SR1, it irreversibly misfolds to a state  $M_4$ , which can no longer

be rescued under any conditions [17]. Since the act of sequestration is supposed to be the driving force for folding in a passive model, it is difficult to reconcile such irreversible misfolding. Because the conversion of  $M_3$  to  $M_4$  is slow, it appears the ATP-controlled release of ligands is critical to GroEL function. Moreover, both in the case of CS and luciferase, it appears the assembly competent form resides in a higher energy state, and thus misfolds could only be rescued if work was performed on the substrate protein.

The importance of timing was also highlighted in a recent study using biotinylated GroEL which showed that when rebinding of a RuBisCo substrate was blocked after a single turn-over, folding rates were comparable to the slow, spontaneous rates of folding observed in GroEL's absence [67]. Surprisingly, folding in the single-ring version of GroEL, SR1, produced a significant rate enhancement. The authors concluded that the rate enhancement could solely be explained by a passive confinement of the substrate and what they termed "a smoothing of the energy landscape" due to the hydrophilic environment of the cavity. However, this ignores that even one cycle by GroEL can actively unfold the substrate [22, 44]. Additionally, rate enhancement via a passive mechanism is not anticipated by the Anfinsen model, as acknowledged by the authors themselves [43, 67].

It should be noted that while the passive model excludes the possibility of an active mechanism, the reverse is not true. An explanation of the above results that seems more likely is that both models are viable: folding of RuBisCo depends on iterative annealing *in vivo*, but folding in a sequestered, hydrophilic environment is also crucial to the process. The dependence on encapsulation is only true for certain substrate proteins; it has been demonstrated that aconitase, an 82 kDa protein too large to fit inside the

GroEL chamber, can refold solely through interactions with the trans ring [73, 74]. Because GroEL is promiscuous in its substrate specificity, and the mechanism for folding seems to vary between systems, it is easy to find examples where not all aspects of the GroEL mechanism are required for refolding. As Betancourt and Thirumalai suggest, although GroE appears at first glance to be a “one size fits all” system, probably many mechanisms are possible depending on kinetic requirements [44].

### ***1.5 Specific Aims***

The goal of this work was to better understand the allosteric mechanisms involved in GroEL function. The various projects can be summarized as follows:

- 1) Although many groups have utilized the single ring mutant, SR1, for a variety of single turnover experiments [17, 46, 47, 75], a full characterization of the allosteric and functional properties of SR1 has not been completed. Because the nested cooperativity model is inherently complex, the goal of this project was to exploit the single ring in simplifying the allosteric mechanisms under study. Previous work in our lab analyzed a GroEL double cysteine mutant, D83C/K327C, which replaces an intra-subunit salt bridge and can be used to lock a ring in the T state [49]. This mutation was introduced into the single ring for further study.
- 2) The original model for nested cooperativity made two assumptions; a) the T state does not bind or hydrolyze ATP (termed the exclusive binding assumption), and b) the activity of an R subunit in the RR state is less than the activity of an R subunit in the TR state [50]. This was necessary to explain negative cooperativity and the loss of ATPase activity as higher ATP concentrations. Based on previous work in our lab and the single ring studies above, it is clear the exclusive binding assumption is not

valid [49]. Here, a coupled enzyme assay is employed to examine the effects of potassium and substrate protein on the initial rates of ATP hydrolysis by both GroEL and SR1. The data were then fit to an equation describing a new model of nested cooperativity in which exclusive binding was not assumed.

3) Previous studies in this lab and others used fluorescence resonance energy transfer (FRET) to examine the dissociation of ligands from the *cis* ring of GroEL [20, 49]. These studies demonstrated how exquisitely sensitive the GroEL hemicycle is to the presence of substrate protein and ADP on the *trans* ring. Due to the controversy over symmetric complex formation, it was not known if association would mirror dissociation kinetics under all the conditions previously studied. This project extends the results of the dissociation work by examining the kinetics of GroES association to the *trans* ring of GroEL. The effects of potassium and substrate protein are explored in detail.

## **Chapter 2**

### **General Methods and Experimental Procedures**

This chapter will describe laboratory methods and procedures that are common to the studies presented in this dissertation. Techniques and procedures specific to certain studies will be detailed in the appropriate chapter.

### ***2.1 Protein Concentrations***

Unless otherwise stated, all protein concentrations are listed as monomer concentrations. Wherever oligomer concentrations are used, they will be designated with a subscript, indicating the number of subunits included in the concentration. For example, GroEL<sub>14</sub> refers to the concentration of GroEL tetradecamers and GroES<sub>7</sub> refers to the concentration of GroES rings.

### ***2.2 Bradford Assay***

The Bradford reagent, Coomassie Brilliant Blue G-250 (CBBG), changes its absorbance maximum when bound to arginine and aromatic residues in various proteins and can be used to detect microgram quantities of protein in a sample [76]. This method is ideal for determining total protein concentration of an unpure sample, such as the intermediate steps of a protein purification. To generate a standard curve, 800 µl of a bovine serum albumin (BSA) sample, prepared from a BSA standard solution at 1.44 mg/ml (BioRad), was mixed with 200 µl of Bradford Dye Reagent (BioRad). After waiting five minutes, the absorbance at 595 nm was measured for each of six samples having a final BSA concentration ranging from 2.5 to 12.5 µg/ml. The data were fit to a linear regression with an  $R^2$  value of 0.993. The regression equation was then used to determine the total protein concentration in an unknown sample.

### ***2.3 Polyacrylamide Gel Electrophoresis (PAGE)***

Gel solutions were prepared according to standard recipes [77, 78] using a pre-mixed 30% acrylamide/bis-acrylamide (29:1) solution from Bio-Rad. Gels were poured using 10 x 8 cm glass plates and either 0.75 or 1 mm spacers. Gels were loaded into the Hoefer SE250 Mini-Vertical apparatus and run at 15 mAmps per gel using a Tris/glycine buffer. Under nondenaturing conditions, gels were prepared as described except the sodium dodecyl sulfate (SDS) was omitted from all steps (loading buffer, gel solutions and running buffers). Protein bands were visualized by first staining with PhastBlue (a Coomassie Blue variant from Amersham), and then destaining with 30% methanol/10% acetic acid solution followed by a 10% methanol/10% acetic acid solution.

Protein bands on SDS denaturing gels could be quantitated by densitometry using the PDSI hardware and ImageQuant software from Molecular Dynamics. Special care was taken with gels that needed quantitation to ensure they were dust-free and gel plates were clean. The first and last lanes were not used due to band curvature. In order to determine protein concentration from a gel, standards of the same protein at known concentrations were loaded on the same gel, typically three to five samples containing 20 to 80 pmol total protein. These bands were quantitated and a standard curve generated. In other cases, the relative amount of different proteins or protein forms within one sample was needed. In this case, no standards were necessary and the relative densitometry values were used to compute the ratio.

### ***2.4 Purification of GroEL***

GroEL was purified with several modifications to the existing protocols [79]. Glycerol stocks of *E. coli* JM105 cells harboring the pGEL1 plasmid (a gift of Dr. Ed

Eisenstein) were streaked onto LB plates containing 100 µg/ml ampicillin (Amp) and grown at 37°C overnight. A starter culture was prepared from a single colony in LB media with 100 µg/ml Amp and grown at 37°C until suspension was cloudy. This was used to inoculate 6 L of LB media plus 100 µg/ml Amp. Cultures were grown for two hours at 37°C with shaking at 200 rpm, at which time protein over-expression was induced with 0.5 mM IPTG. The cultures continued to grow for another 12-15 hours at 30°C.

Cells were harvested by centrifugation and resuspended in lysis buffer (50 mM Tris pH 8, 1 mM EDTA, 1 mM DTT and 1 tablet per 50 ml buffer of complete protease inhibitor cocktail tablets from Roche). The cells were lysed in 50 ml portions by sonication using a Branson sonicator for 75 seconds (power level 5, 50% duty cycle). Following centrifugation to remove cell debris, the nucleic acid was precipitated using streptomycin sulfate at a final concentration of 1 mg/ml. The precipitate was then removed by centrifugation at 32,500xg for 60 minutes at 4°C. This is referred to as the crude lysate.

The crude lysate, usually around 150 ml, was loaded onto a 500 ml DEAE Sepharose Fast Flow column (Amersham) which had previously been equilibrated with 400 ml of 200 mM Tris pH 8 followed by 1800 ml of Buffer A (50 mM Tris pH 8, 5 mM MgCl<sub>2</sub>, 1 mM EDTA, 1 mM DTT). The GroEL was eluted using a 0 to 0.5 M gradient over 2 L. The fractions containing GroEL normally eluted at a conductivity of 28 mS, with a total volume of 170 ml. These fractions were concentrated using saturated ammonium sulfate to a final concentration of 65% and allowed to sit overnight at 4°C. The solution was centrifuged the following day at 10,000xg for 25 minutes at 4°C. The

supernatant was removed and the pellet resuspended in 20 ml of S300 buffer (50 mM Tris pH 7.5, 10 mM MgCl<sub>2</sub>, 1 mM DTT). The protein was desalted on a 300 ml S300 Sephacryl gel filtration column (Amersham) that was previously equilibrated with 300 ml of S300 buffer. The protein was collected and concentrated using Centriplus centrifugal filter devices (Millipore, 50 kDa cut-off) to approximately 10 mg/ml, as determined by a Bradford assay. The GroEL was stored as 1 ml aliquots at -80°C until the next step.

Removal of the remaining contaminants is a key step. Most are denatured proteins which are tightly bound to GroEL and cannot be separated by normal chromatographic methods. However, the importance of eliminating as many contaminants as possible cannot be overstated. Because substrate protein is a significant allosteric effector of GroEL function, contaminating protein can obscure or complicate results. We have found the acetone precipitation method, modified from Voziyan and Fisher [80], to be the best way of removing the remaining contaminants. The principle behind this method rests on the idea that because GroEL can bind hydrophobic, unfolded proteins, it should be stable in the presence of a hydrophobic solvent. Pure acetone was added drop-wise to a vigorously stirred solution of GroEL until the acetone was 45% by volume. This causes all of the proteins, GroEL and contaminants alike, to precipitate. The protein was pelleted by centrifugation at 32,500xg for 20 minutes at room temperature. The supernatant was removed, and the pellet resuspended in 10 mM Tris pH 7.5, 10 mM MgAc. GroEL goes back into solution, whereas the contaminating proteins mostly remain as precipitates and can be removed by centrifugation (32,500xg, 60 minutes). Pure GroEL is now contained in the supernatant and was concentrated through addition of saturated ammonium sulfate to 65%. Any remaining acetone was

removed after desalting the protein on a PD-10 column equilibrated in 10 mM Tris pH 7.5, 10 mM MgAc. The final product was concentrated and the purity confirmed by SDS-PAGE (Figure 2-1) and tryptophan fluorescence (Figure 2-2). To measure the fluorescence, GroEL samples, pre- and post-acetone treatment, were diluted to a final concentration of 9  $\mu\text{M}$  in 10 mM Tris, 10 mM MgAc, and 6 M guanidinium HCl (GdnHCl). Fluorescence was measured from 300 to 400 nm, exciting at 295 nm. The area under the curve was corrected based on the signal of buffer alone, and compared to a fluorescence standard curve made with bovine serum albumin (BSA). Although the signal is significantly decreased after the acetone treatment, it is possible that up to 10% of the GroEL rings are still occupied with contaminating SP. The GroEL concentration was confirmed by measuring the absorbance at 280 nm, using an extinction coefficient of  $9600 \text{ M}^{-1}\text{cm}^{-1}$ .

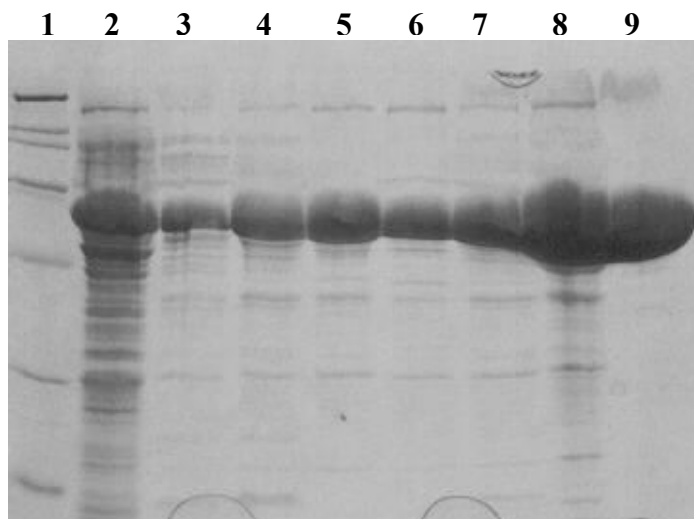


**Figure 2-1: GroEL<sup>wt</sup> Purification.** 12% SDS polyacrylamide gel of GroEL purification steps. The lanes are identified as follows: molecular weight standards (lane 1), crude lysate (lane 2), DEAE fractions (lanes 3-7), pool from S300 desalt (lane 8), pure GroEL following acetone treatment (lane 9). Figure kindly provided by Dr. John Grason.

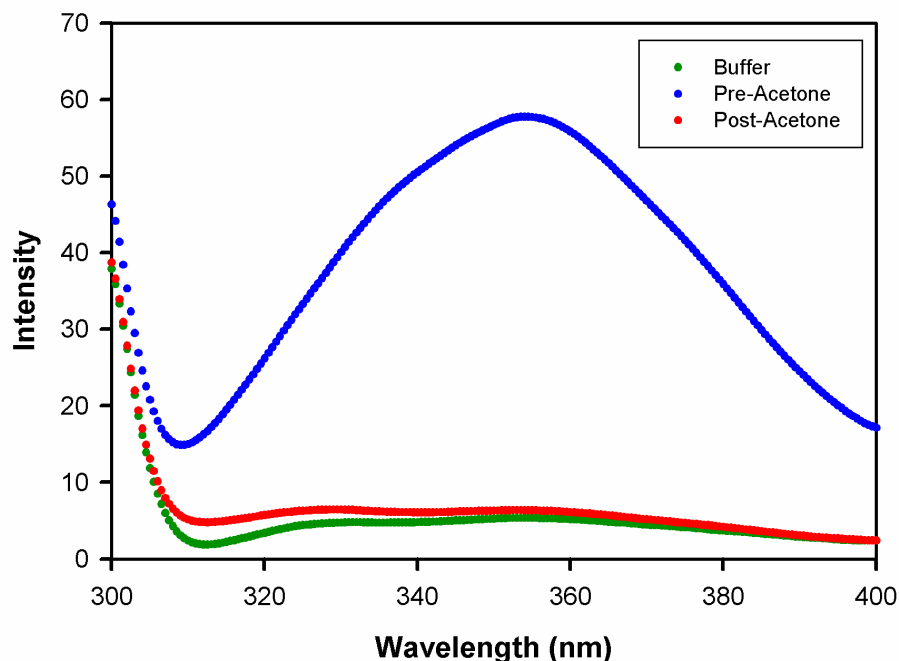


**Figure 2-2: Tryptophan Fluorescence of GroEL, Pre- and Post-Acetone Treatment**  
GroEL samples, taken before and after the acetone treatment, of the same concentration were diluted into a 10 mM Tris, 10 mM Mg, 6 M GdnHCl solution. Fluorescence was measured by exciting at 295 nm.

### ***2.5 Purification of SR1***

SR1 was purified as previously described with a few modifications [81]. A crude lysate was prepared from 4.5 L of JM105 cells containing the pSR1 plasmid (a gift of Dr. Art Horwich) as described in section 2.4, except that the lysis buffer contained 20 mM Tris pH 7.4, 1 mM EDTA, 50 mM KCl. The lysate was loaded onto a 25 ml Q Sepharose Fast Flow column (Amersham) previously equilibrated with Buffer A (50 mM Tris pH 8.0, 1 mM EDTA, 5 mM MgCl<sub>2</sub>, 1 mM DTT). Following passage of the flow through, SR1 was eluted using a 0 to 750 mM NaCl gradient over 300 ml. The SR1 eluted at approximately 35 mS. Fractions containing SR1 were pooled and then concentrated in Centriplus centrifugal filter devices (50 kDa cut-off) to approximately 10 mg/ml, as determined by a Bradford assay. The protein was stored as 1 ml aliquots until further

purified by the acetone precipitation described in section 2.4. Assessments regarding the purity and properties of SR1 will be discussed in detail in Chapter 3.

## ***2.6 Purification of GroES<sup>wt</sup>***

GroES was purified using the previously published methods, but with modifications [82]. Crude lysate was prepared from 4.5 L of JM105 containing the pGES1 plasmid (a gift of Dr. Ed Eisenstein) using the procedure described for GroEL in section 2.4. The lysate was then subjected to a heat treatment, where the lysate is immersed in an 80°C water bath and constantly stirred until the lysate reaches a temperature of 70°C for 10 minutes. Precipitated proteins were removed by centrifugation at 32,500xg for 25 minutes at 4°C. Saturated ammonium sulfate was added to a final concentration of 65% and the solution was stored, with stirring, overnight at 4°C. The following day, the protein was collected by centrifugation (10,000xg, 25 minutes, 4°C) and resuspended in 15 ml of G25 buffer (10 mM Tris pH 7.5, 0.1 mM EDTA, 0.1 mM DTT). This was then desalted on a 150 ml G25 column (Amersham) which was previously equilibrated with 300 ml G25 buffer. The flow-through, at pH 7.5, was then jumped to approximately pH 5.0 through the addition of 50 mM NaOAc, pH 5.0. One third of this solution was loaded onto a 75 ml SP Sepharose HP column (Amersham) equilibrated with 400 ml of 50 mM NaAc pH 5, 0.1 mM EDTA, 0.1 mM DTT. Following elution of the flow-through, GroES was eluted using a 750 ml gradient from 0 to 200 mM NaCl. Fractions were analyzed by SDS-PAGE for the presence of GroES, pooled, and brought to 65% ammonium sulfate. Another third of the protein was loaded on the column and the process repeated until all the protein had been collected. Ammonium sulfate precipitates from the three runs were then pooled and stored

overnight at 4°C. The protein was collected by centrifugation (10,000xg, 25 minutes, 4°C) and resuspended in 5 ml 10 mM Tris pH 7.5. This was then desalted on PD-10 columns equilibrated in the same buffer and concentrated in Centricon centrifugal filter devices (Millipore, 10,000 Da cutoff). The final concentration was determined by measuring the absorbance at 280 nm using an extinction coefficient of 1200 M<sup>-1</sup>cm<sup>-1</sup>. Purity was assessed by SDS-PAGE (Figure 2-3).

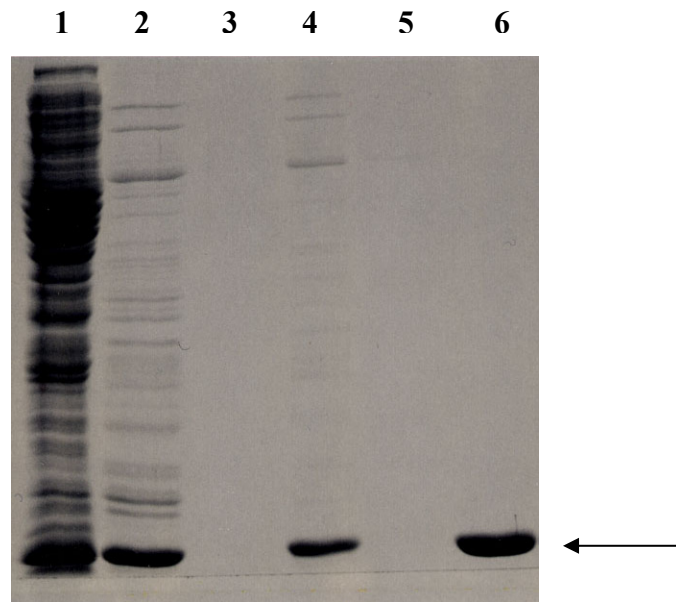


**Figure 2-3: GroES<sup>wt</sup> Purification.** 12% SDS polyacrylamide gel of GroES purification. The lanes are identified as follows: crude extract (lane 1), post heat treatment (lane 2), empty (lane 3), post pH jump and G25 desalting (lane 4), flow through of SP Seph column (lane 5), final pool of pure GroES after SP Seph column (lane 6). Arrow indicates the position of the GroES on the gel.

### **2.7 Purification of His-tagged GroES**

JV 30 cells containing the pGES1His plasmid (a gift of Dr. Ed Eisenstein) were grown and lysed as previously described in section 2.4. The crude lysate obtained from 1 L of cells was combined with 4 ml of Ni-NTA resin (Qiagen), which had been previously equilibrated with 10 mM imidazole, 20 mM Tris pH 8.0, and 300 mM NaCl. The lysate

was mixed with the resin in batch process for 30 minutes on ice. The mixture was then loaded into a syringe barrel and washed with 3 column volumes of 60 mM imidazole, 20 mM Tris pH 8.0, 300 mM NaCl. This removed any proteins that did not bind, or were weakly bound, to the resin. A final wash with 60 mM imidazole, 20 mM Tris pH 8.0 was then performed to eliminate any residual contaminants. The GroES<sup>his</sup> was then eluted with 3 column volumes of 250 mM imidazole, 20 mM Tris pH 8.0. The eluant was concentrated in a Centriplus centrifugal filter device (10 kDa cut-off) and exchanged into 10 mM Tris pH 7.5 on a PD-10 column. Purity was assessed by SDS-PAGE (data not shown) and concentration measured by absorbance at 280 nm using the extinction coefficient given in section 2.5.

### ***2.8 Coupled Enzyme ATPase Assay***

In order to measure the rate of ATP hydrolysis by GroEL, we employed a coupled enzyme assay which ties the production of ADP by GroEL to the oxidation of NADH by lactate dehydrogenase (LDH) [83], as shown in Figure 2-4. The last step in the process can be measured spectrophotometrically by monitoring the change in absorbance at 340 nm over time (Figure 2-5). The enzymes and reagents used, pyruvate kinase (PK), lactic dehydrogenase (LDH), NADH, and phosphoenol pyruvate (PEP), must be in excess to ensure complete coupling of the system.

This system provides a number of benefits over the single time point assays used by other researchers [50, 75]. It provides real time data, using an ATP regeneration system that ensures constant ATP concentration over time. Moreover, each rate measurement is calculated from the slope of a line that includes up to 450 individual data

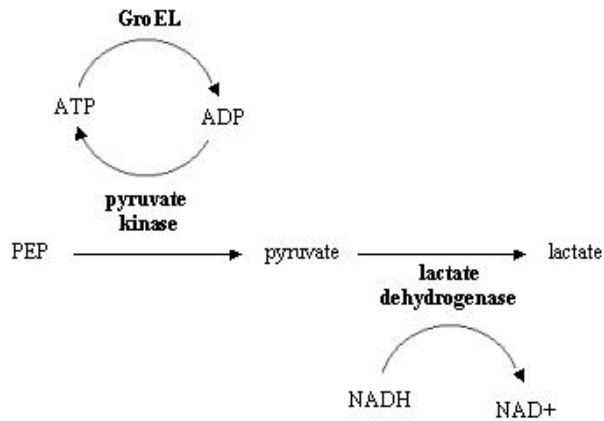


**Figure 2-4: Coupled Enzyme ATPase Assay.** In order to monitor ATP hydrolysis by GroEL, a coupled enzyme assay was employed. Each ATP hydrolyzed by GroEL is coupled to the oxidation of a NADH by lactate dehydrogenase (LDH) through the intermediary, pyruvate kinase (PK). The PK also keeps the ATP concentration constant over the course of the assay (usually 3 minutes). Oxidation of NADH can be measured spectrophotometrically since NADH absorbs light at 340 nm while NAD<sup>+</sup> does not.

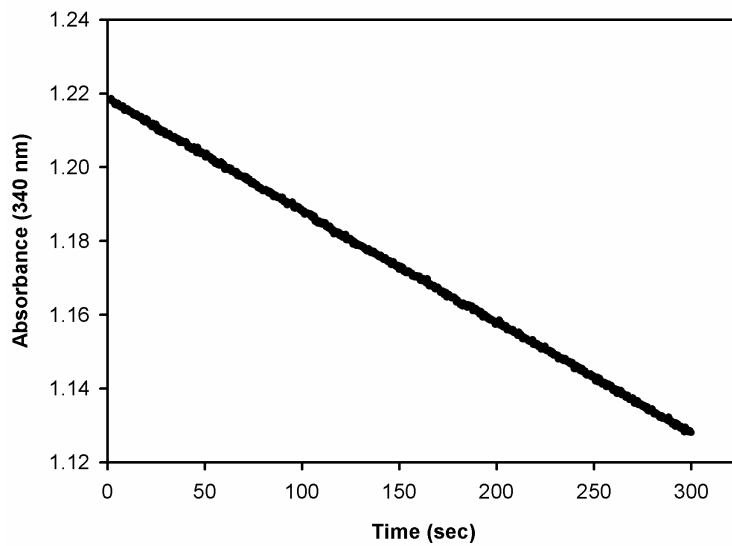


**Figure 2-5: Monitoring ATP Hydrolysis in Real Time.** An example of a kinetic trace monitoring ATP hydrolysis by GroEL over time. The absorbance at 340 nm decreases as ATP is hydrolyzed via NADH oxidation using the coupled enzyme assay. The rate of hydrolysis is found by exporting the data to Microsoft Excel (or similar graphing program) and taking a linear regression of the data. The slope of the regression is used to calculate the turnover at each ATP concentration. Typically, R<sup>2</sup> values were greater than 0.99.

points. For most experiments, a Hewlett Packard 8453 UV/Vis spectrophotometer was used. Absorbance data was collected every second and the cuvette holder was connected to a circulating water bath (VWR) to maintain a constant temperature (37°C). It was possible to add reagents, such as GroES or denatured substrate protein, partway through a run to measure differences in rate with a minimum of error.

Final concentrations used in the assay, unless otherwise stated, were 2  $\mu$ M GroEL, 50 mM Tris pH 7.5, 10 mM MgAc, 100 mM KAc, 0.2 mM PEP, 0.2 mM NADH, 4 units LDH and 5 units PK at 37°C. The rate of ATP hydrolysis was calculated from the change in absorbance over time by fitting each data set with a linear regression. Traces that yielded  $R^2$  values less than 0.99 when fit with a linear regression were discarded.

The equations for calculating turnover are as follows:

According to Beer's Law:  $\Delta[NADH] = \frac{\Delta A_{340}}{\epsilon}$  where  $\epsilon = 6.22 \text{ mM}^{-1} \text{ cm}^{-1}$  for NADH.

The slope of the linear regression line equals  $\Delta A_{340}$  per second. Converting to minutes, and taking into account the stoichiometry (1 NADH = 1 ADP = 1 ATP; Figure 2-3), the nmol of ATP consumed per minute is represented by:

$$\frac{\Delta[ATP]}{\text{min}} = \frac{\text{slope}(\text{sec}^{-1})}{6.22 \text{ mM}^{-1}} \times \frac{60 \text{ sec}}{1 \text{ min}} \times \frac{10^6 \text{ nmol}}{1 \text{ mmol}} \times \frac{1 \text{ L}}{10^6 \mu\text{l}} \times 900 \mu\text{l}$$

Turnover is calculated by dividing the nmol of ATP hydrolyzed per minute by the nmol of GroEL subunits used in the assay.

$$\text{Turnover} = \frac{\Delta[ATP]}{\text{min}} \div \text{nmol GroEL}$$

The turnover values can be plotted against ATP concentration to examine the cooperativity under various conditions.

## ***2.9 Preparing Unfolded Substrate Proteins***

Two proteins were utilized throughout these studies: mitochondrial malate dehydrogenase (MDH) from pig heart (Roche) and  $\alpha$ -lactalbumin ( $\alpha$ -LA) from bovine milk (Sigma). Unfolded  $\alpha$ -LA is a stable species in the presence of DTT and the absence of  $\text{Ca}^{2+}$  [65, 84]. It can therefore be denatured in large quantities and stored at  $-80^{\circ}\text{C}$ , as long as the DTT is refreshed prior to use. MDH, on the other hand, will refold spontaneously [85, 86] and must be denatured just prior to use. To unfold both of these proteins, a concentrated aliquot of the protein was diluted into 1 mM Tris, pH 7.5, 2 mM DTT and allowed to react for 10 minutes. The solution was diluted 2-fold with 0.01 N HCl and allowed to denature for 1 hour on ice. MDH was used as is;  $\alpha$ -LA was buffer exchanged into 10 mM Tris, pH 7.5, 1 mM DTT and stored at  $-80^{\circ}\text{C}$  until needed. Concentrations were determined using extinction coefficients of  $28,400 \text{ M}^{-1}\text{cm}^{-1}$  and  $6880 \text{ M}^{-1}\text{cm}^{-1}$  at 280 nm for  $\alpha$ -LA and MDH, respectively.

## ***2.10 Computer Software***

Protein structures were obtained from the free Protein Explorer software package, found at [www.proteinexplorer.org](http://www.proteinexplorer.org) [87]. Data plotting and fitting were accomplished with SigmaPlot, version 8.0 (SPSS Inc.).

## **Chapter 3**

### **Probing Allosteric Interactions with the Single Ring Variant, SR1**

### 3.1 Introduction

The two rings of GroEL are held together by electrostatic and hydrophobic interactions between residues in their equatorial domains [7]. As shown in Figure 3-1, each subunit interfaces with two subunits in the opposing ring, forming two sets of contact sites. Residues E102, K105, E434 and R445 compose the so-called “left site” whereas residues R452, E461, S463 and V464 compose the “right site” [7]. A single ring variant of GroEL, SR1, was created by mutating residue 452 to glutamate and the other right site residues to alanine [81]. Other than the disrupted inter-ring contacts, SR1 is

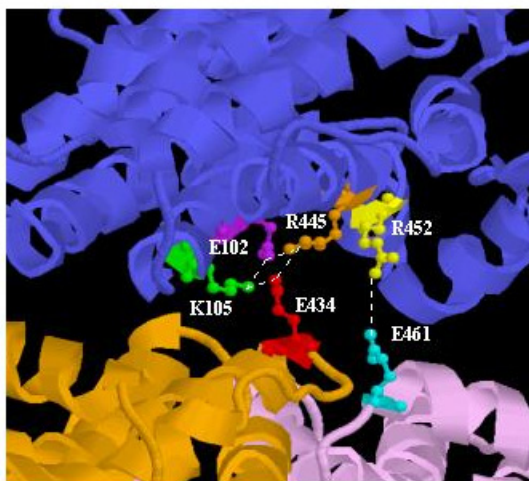


**Figure 3-1: Contact Sites at the Inter-Ring Interface of GroEL.** The two rings are held together primarily through ionic and hydrophobic interactions at the equatorial interface. Each subunit of GroEL interacts with two subunits in the opposing ring, forming two sets of contact sites known as the left and right sites. The left site consists of an ionic tetrad including residues E102, K105, E434 and R445. The right site consists of the ionic interaction between residues R452 and E461, as well as contacts between residues S463 and V464 (not shown). Taken from the crystal structure of the asymmetric complex (pdb file 1aon)[10], the subunit in blue resides in the *cis* ring while the orange and pink subunits are in the *trans* ring. The GroEL<sup>LSM</sup> mutations (discussed later in this chapter) include E102A, K105A, and M11A. The SR1 mutations include R452E, E461A, S463A, and V464A [81].

structurally very similar to GroEL, as shown by infrared spectroscopy (IR) [88]. Thus, the mutations which create the single ring do not otherwise significantly disturb the chaperonin's structure.

SR1 can stably bind GroES in the presence of ATP, although it cannot release its ligands (GroES, ADP or any encapsulated substrate protein) due to the absence of a signal sent by the second ring [46]. For this reason, SR1 is unable to substitute for GroEL *in vivo* [46, 89]. It was originally believed that the mammalian mitochondrial homolog of GroEL, Hsp60, existed as a single ring and was capable of binding and releasing its co-chaperonin, Hsp10, without transitioning through a double-ring intermediate [90]. It was thought that Hsp60 could function as a single ring due to a weak interaction with Hsp10 in the presence of ADP, which allowed for dissociation on a biologically relevant timescale [91]. This view seemed to be supported by the fact that mutations introduced into SR1 that reduced, but did not eliminate, GroES binding produced chaperones that were as efficient *in vivo* as GroEL [92]. However, more recent studies with Hsp60 indicated that the presence of ATP and Hsp10 favored formation of a double ring, although no negative cooperativity was apparent in its ATPase activity [93].

SR1 has been employed in numerous studies, most of which address the question of active versus passive refolding of denatured substrate proteins. Because SR1 undergoes only one round of ATP hydrolysis and encapsulation, it is well suited to these types of experiments. However, such studies are complicated by the fact that even a single turnover event may induce active unfolding as the subunits pivot upon ATP binding and the substrate protein becomes encapsulated [22, 94]. Other groups have

investigated the nature of the inter-ring contacts, suggesting they serve as a thermostat that allows the chaperonin to sense physiological from stress temperatures [88].

ATP-induced allosteric transitions play a key role in chaperonin function, and yet many GroEL studies fail to even invoke an allosteric model. This chapter probes the allosteric properties of GroEL by taking advantage of the more simplified case of the single ring. Both of the nested cooperativity models that have been applied to GroEL rely on a MWC, all-or-none, model to describe the T to R transitions within a ring [50, 54]. Thus, initial conclusions can be drawn from single ring studies without having to select a fully, nested cooperativity model. This will be examined in detail in the following chapter.

A common method for studying cooperativity in GroEL is the ATPase assay, described in section 2.8, where initial rates of ATP hydrolysis are measured as a function of ATP concentration. However, deconvoluting the GroEL ATPase profile is complicated; as shown in Figure 3-2, there is an initial increase in activity at low ATP concentrations, followed by a decrease and then a leveling off at higher ATP concentrations. The initial rise has been attributed to the positive cooperativity within a ring as it progresses from the TT to the TR state, with a Hill coefficient of 2.75 ( $\pm 0.12$ ) at 10 mM  $K^+$  [50]. The decrease in activity is widely attributed to be the result of negative cooperativity between the rings as they proceed from the TR to the RR state, where the RR state is thought to have significant less activity than the TR or TT states [50]. Ideally, studies with the single ring could experimentally constrain the deconvolution of GroEL ATPase properties.

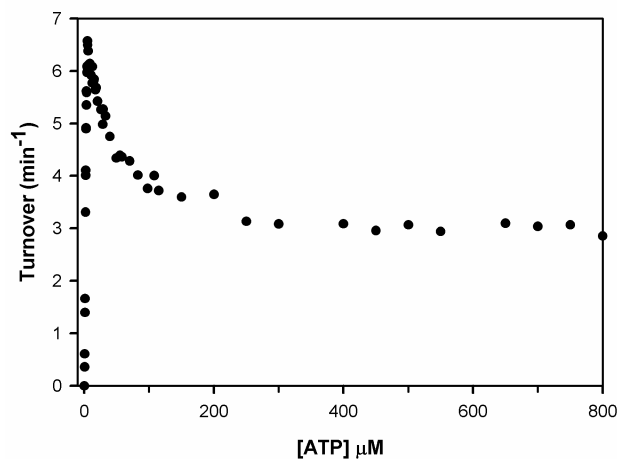


**Figure 3-2: Initial Velocities of ATP Hydrolysis by GroEL.** The initial rates of ATP hydrolysis are plotted versus ATP concentration at 100 mM  $K^+$  and 37°C. Two different models have been suggested to explain the shape of the curve: one where MWC interactions are nested inside KNF interactions, and another which includes only nested MWC interactions.

Previous work in our lab with a GroEL double cysteine mutant, D83C/K327C [95], addressed the concerted nature of the allosteric transition within a ring (G. Curien, unpublished results). Normally, this intra-subunit salt bridge connects the equatorial and apical domain and stabilizes the T state (Figure 3-3A). Upon transitioning to the R and R' states (Figure 3-3B), the salt bridge is broken [41]. By introducing a cysteine pair in place of the salt bridge, it was possible to lock a subunit in the T state with chemical cross-linkers or disulfide bonds via oxidation. Moreover, it was possible to control the extent of cross-linking or oxidation such that 0 to 100% of the subunits were modified. Under these conditions it was shown that a single cross-link was capable of locking an entire ring in the T state, thereby preventing the binding of GroES (G. Curien and G. Lorimer, unpublished results). This demonstrated that the transition from the T to R state

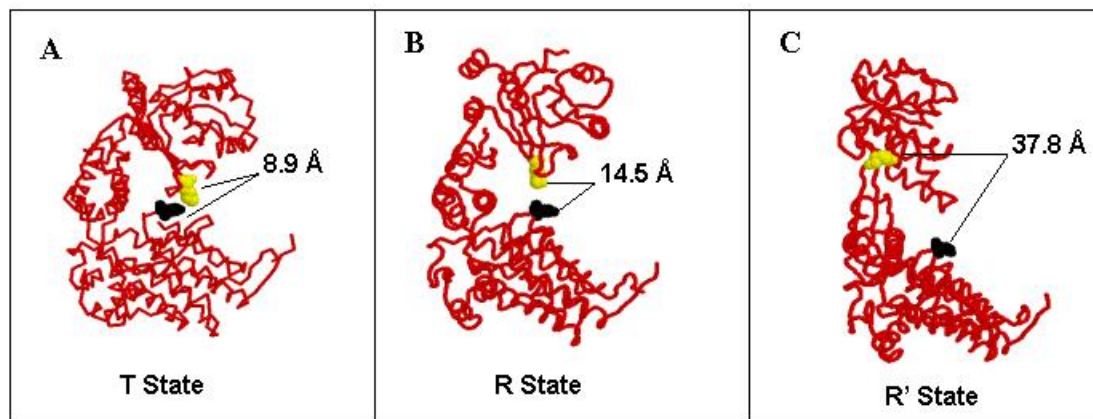


**Figure 3-3: An Intra-Subunit Salt Bridge Is Replaced with Two Cysteines.** Two residues, D83 (black) and K327 (yellow), connect the apical and equatorial domains through an inter-subunit salt bridge which stabilizes the T state (panel A, pdb file 1grl [9]). Upon progressing to the R (panel B, pdb file 1gr6 [41]) and R' state (panel C, pdb file 1aon [10]), this salt bridge is broken. Site directed mutagenesis replaced each residue with a cysteine, allowing for precise and controlled oxidation by diamide.

within a ring was concerted, as predicted by the current models for nested cooperativity in GroEL [50, 54]. Here, the same mutations are inserted into the single ring for further study.

### 3.2 Methods Specific to Chapter 3

#### 3.2.1 Assaying GroES Release and SP Encapsulation in SR1 Using His-tagged

**GroES** This assay was originally developed by Mark Uebel in our lab [96]. To assay GroES release, a 300  $\mu$ l solution containing 20 mM Tris pH 7.5, 10 mM MgAc, 5 mM KAc, 70  $\mu$ M ATP, 35  $\mu$ M GroES<sup>his</sup> and 14  $\mu$ M GroEL<sup>wt</sup> or SR1 was incubated for 10 minutes at room temperature, allowing the GroEL/SR1 to complex with GroES<sup>his</sup> and exhaust the ATP. This solution was then loaded onto a column containing 1 ml Ni-NTA resin (Qiagen) equilibrated with 20 mM Tris pH 7.5, 10 mM MgAc. After the sample was loaded, the column was rinsed three times with 0.8 ml of the equilibration buffer to

elute any flow through. A challenge solution containing 20 mM Tris pH 7.5, 10 mM MgAc, 5 mM KAc, 50  $\mu$ M ATP and 14  $\mu$ M GroES<sup>wt</sup> was added in three 0.8 ml portions. This was followed by two 0.8 ml washes of equilibration buffer. Elution of any remaining material was accomplished with three 0.8 ml washes of 250 mM imidazole. Aliquots from each eluate were loaded on a 15% SDS-PAGE gel. To check for substrate encapsulation, the same procedure was followed except 2  $\mu$ M denatured MDH was included in the initial solution.

**3.2.2 Gel Filtration Using HPLC** To test the oligomeric structure of GroEL mutants, 30  $\mu$ l of a 30  $\mu$ M sample was loaded onto a 800 x 7.80 mm BioSep-SEC-S gel filtration column (Phenomenex) equilibrated with 50 mM Tris pH 7.5, 10 mM MgAc, 10 mM KAc,  $\pm$  25  $\mu$ M ATP. Elution was monitored by absorbance at 280 nm.

**3.2.3 Site Directed Mutagenesis** The D83C and K327C mutations were introduced into a plasmid containing SR1 (a gift of Dr. Art Horwich) using the Stratagene Quik-Change kit. This mutant is referred to as SR1<sup>IAX</sup> (intra-subunit x-linked) since the cysteine pair replaces an intra-subunit salt bridge. The mutagenic primers were as follows: D83C: 5'-GCCTCTAAAGCAAAGTGCCTGCAGGCGACGGTACC-3' and K327C: 5'-CGTGTTGTGATCAACTGTGACACCACCTATCATCGATGGC-3'. For the mutagenesis, 15 ng of template was combined with 125 ng of primer, and the remaining ingredients from the kit (dNTP mix, reaction buffer, Pfu DNA polymerase). PCR was performed in a Techne Progene thermocycler with the cycling parameters shown below.

Segment	Cycles	Temperature	Time
1	1	95°C	30 seconds
2	16	95°C	30 seconds
		55°C	1 minute
		68°C	12 minutes

**Table 3-1: Thermocycler Conditions for PCR-based Mutagenesis**

Amplified DNA was cut with Dpn I (Stratagene) to eliminate wild type plasmids and then transformed by heat shock into *E. coli* XL1-Blue cells (Stratagene). Small scale plasmid preps (3 ml) were performed using the Qiagen Qiaprep Spin Miniprep Kit. Because XL1-Blue cells grow slowly and are not ideal cell lines for protein purification preps, DNA from each mini-prep was then transformed into *E. coli* JM105 cells (Amersham) using a BTX electroporator. Large scale plasmid preparations (100 ml) were obtained using the Qiagen Hi-Speed Plasmid Midi Kit. Mutations were confirmed by DNA sequencing using the University of Maryland DNA sequencing facility.

**3.2.4 Oxidation of SR1<sup>IAX</sup> with Diamide** In order to control the degree of oxidation in these experiments, samples of SR1<sup>IAX</sup> were freshly reduced prior to use. This was accomplished by bringing a sample of SR1<sup>IAX</sup> to 20 mM DTT and incubating at 37°C for 30 minutes. The DTT was removed by buffer exchange on a PD-10 column equilibrated with 10 mM Bis-Tris pH 7.0, 10 mM MgAc. The protein was then concentrated on a Centricon YM-50 (Millipore). To minimize oxidation by contaminating metal ions in buffers, all buffers used in these experiments were treated

with chelex resin (Sigma) prior to use. Those buffers that contained MgAc were treated before the MgAc addition.

Disulfide bonds were introduced between the two mutated cysteines by adding stoichiometric amounts of diamide, a reagent which oxidizes thiols non-catalytically via a double displacement mechanism [97]. Previous work in our lab demonstrated that the three native GroEL cysteines were essentially unreactive [49]. Oxidation was initiated by incubating a solution containing 10 mM Tris pH 8.0, 10 mM MgAc, and 40  $\mu$ M SR1<sup>IAX</sup> with a stoichiometric amounts of diamide (with respect to subunits) for 30 minutes at 37°C. Before loading samples on a gel for quantitation, unreacted cysteines were blocked with the addition of 40 mM N-ethylmaleimide (NEM) and by dropping the pH with 100 mM Tris pH 6.8.

**3.2.5 Gel Quantitation of the Reaction Coordinate** The extent of oxidation in a sample of SR1<sup>IAX</sup> can be quantitated. Subunits containing an intra-subunit disulfide bond will run with reduced mobility on a SDS-PAGE gel, as shown in Figure 3-4. Thus, the fraction of subunits oxidized is calculated by simply dividing the intensity of the top band

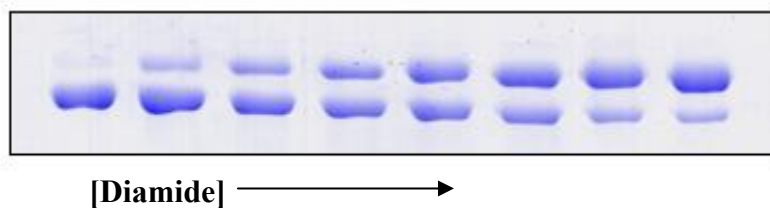


**Figure 3-4: SDS Gel of SR1<sup>IAX</sup> with Increasing Amounts of Diamide.** Subunits which have been oxidized run with reduced mobility compared to reduced subunits. The degree of oxidation in a sample can be determined by quantitating the intensity of the bands in a single lane; the intensity of the upper band is divided by the total intensity of the upper and lower bands to yield the fractional oxidation.

by the total intensity of the upper and lower bands. Since this is a ratio, the measurement of each lane is independent of the next. Therefore, it is not necessary for the sample load to be standardized.

The information from the gel provides a global view of the fraction of subunits oxidized. Each subunit is able to exist in one of two states, reduced (R) or oxidized (O). Initially, all 7 subunits are in the reduced state, designated  $R_7O_0$ . Previous work has shown that diamide converts reduced subunits to oxidized subunits in a purely stochastic manner, meaning that oxidation of one subunit in a ring does not increase the likelihood for other subunits in the ring to be modified (G. Curien, J. Grason, and G. Lorimer, unpublished results). As the oxidation proceeds, the starting material,  $R_7O_0$ , disappears and the intermediate species ( $R_6O_1$ ,  $R_5O_2$ ,  $R_4O_3$  etc.) become progressively populated as a consequence of oxidation, until the seventh oxidation step in a ring yields the end product  $R_0O_7$ . At any point along the reaction coordinate, it is possible to define the population of species in the mixture by a simple binomial distribution function (Figure 3-5). The mole fraction,  $F(x)$ , of each 7-mer containing  $x$  oxidized subunits is given by the expression:

$$F(x) = \frac{7!}{x!(7-x)!} \times p^x (1-p)^{7-x}$$

where  $p$  is the global fraction of subunits oxidized as obtained from the gel quantitation.

### **3.3 Results**

**3.3.1 Verifying the Oligomeric Structure of SR1** To confirm that SR1 exists as a 7-mer, samples of purified SR1 along with a GroEL standard were run on a 6% native gel (Figure 3-6A). Three bands were visible in the lane for SR1: a faint band at the top corresponding to a 14-mer, a primary band with increased mobility, presumably

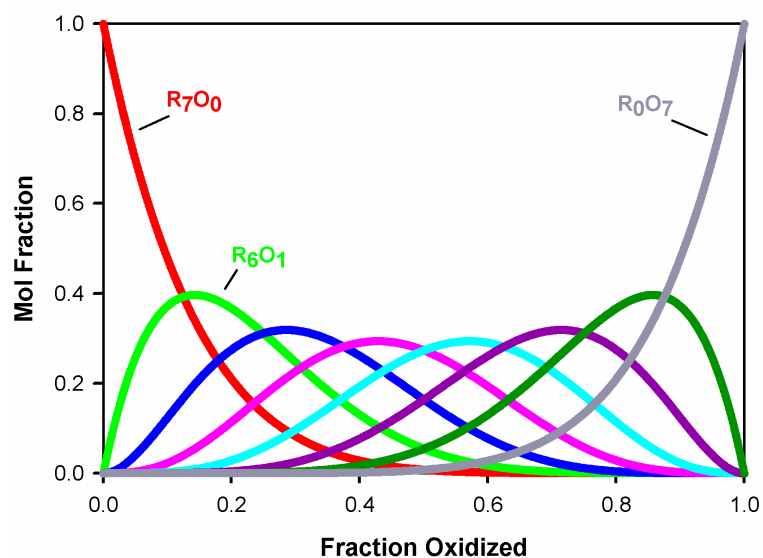


**Figure 3-5: Binomial Distribution for SR1<sup>IAX</sup>.** Using the information from the quantitated SDS gel (x-axis), the mole fraction for each oxidized species can be predicted. Initially, all subunits are in the fully reduced state, represented by R<sub>7</sub>O<sub>0</sub>, where R stands for a reduced subunit in a ring, and O is an oxidized subunit in the same ring. As the amount of oxidant increases, the population shifts towards the more oxidized species, starting with R<sub>6</sub>O<sub>1</sub> (1 disulfide bond) and continuing until the all the subunits in a ring are oxidized, R<sub>0</sub>O<sub>7</sub>.

corresponding to a 7-mer, and a third band with even greater mobility, most likely representing a monomer. Since the faint bands are difficult to see, a Western blot was performed on the gel with anti-GroEL antibodies according to standard procedures in our lab (Figure 3-6B) [96]. It is not surprising that a small population of 14-mers was present. Since *E. coli* cells contain a genomic copy of the GroEL gene, some wild type production is expected. These subunits are likely mixed with over expressed SR1 subunits, although other experiments performed in this lab suggest that only two GroEL<sup>wt</sup> subunits in a ring are required to produce a 14-mer (data not shown). The 14-mer oligomeric structure, whether it be GroEL<sup>wt</sup> or a mixture, is essential to the viability to the cell; SR1 cannot substitute for GroEL in vivo [89, 92]. Based on quantitation of the

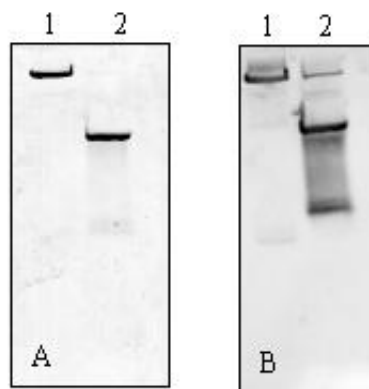


**Figure 3-6: Native Gel and Western Blot of GroEL<sup>wt</sup> and SR1** A 6% native gel of GroEL<sup>wt</sup> (lane 1) and SR1 (lane 2) reveals the mutant is a 7-mer, as previously reported [81]. Although it is difficult to see in the Coomassie stained gel (A), a band corresponding to a 14-mer is clearly present in the SR1 sample in the western blot (B), indicating that some wild type subunits are present. Quantitation of the native gel indicates the contamination by GroEL<sup>wt</sup> is less than 1%. The other faint band below the 7-mer probably represents monomers. This may imply that SR1 is inherently less stable than its wild type counterpart.

native gel, the amount of contaminating 14-mers is estimated to be less than 1%. The original purification protocol of SR1 called for the use of a gel filtration column (7.8 x 300 mm TSK4000SW<sub>xl</sub>) to solve this contamination problem [81]. However, because this did not provide baseline separation between the 14-mer and 7-mer, and the population of 14-mers is so small, this step was deemed unnecessary. The presence of a monomer band may indicate that SR1 is inherently less stable than its wild type counterpart.

To confirm the oligomeric structure of SR1 under aqueous conditions that mimic the *in vitro* assays employed here, samples of SR1 and GroEL<sup>wt</sup> were run on a 800 x 7.80 mm BioSep-SEC-S analytical gel filtration column (Phenomenex) equilibrated with 50 mM Tris pH 7.5, 10 mM MgAc, 100 mM KAc, ± 25 μM ATP. The retention times,

shown in Figure 3-7, substantiate the native gel results, suggesting that SR1 is a 7-mer both in the absence and presence of nucleotide. This is in agreement with a previous study in which the presence of double ring structures was investigated over a wide range of SR1 protein concentrations (0.25  $\mu$ M to 2.5  $\mu$ M) in the presence of ATP [98].

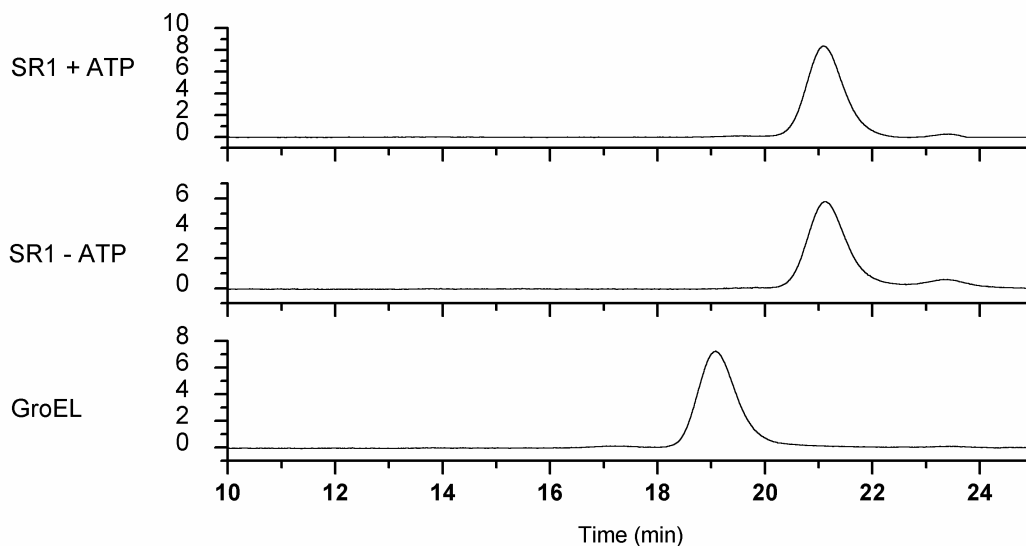


**Figure 3-7: SR1 Remains a 7-mer in the Presence of Nucleotide** Samples of GroEL<sup>wt</sup> and SR1 were run on a gel filtration column in the presence and absence of nucleotide in order to confirm the oligomeric structure of the mutant under conditions that mimic the ATPase assay. GroEL eluted with a retention time of 19.1 min, while SR1 eluted at 21.1 min, both in the absence and presence of ATP. A small peak is visible at 23.4 min in both SR1 samples. This most likely represents the monomer population that was also present in the native gel analysis. Using the area of the peaks, the fraction of monomers present in the sample is approximately 5%.

### 3.3.2 The Effect of Unfolded Substrate Protein and GroES on SR1 ATPase

**Activity** Previous work with SR1 showed it underwent a T to R transition similar to GroEL, with a reported Hill coefficient of 2.87 ( $\pm$ 0.16) at 10 mM K<sup>+</sup> [75]. ATPase measurements performed in our lab gave similar results, with a resolved Hill coefficient

of  $3.35 (\pm 0.20)$  (Figure 3-8A). A value for the Hill coefficient was obtained by fitting the data to the equation:

$$V_o = \frac{V_{\max} K_{app} [S]^n}{(1 + K_{app} [S]^n)}$$

where  $V_o$  and  $V_{\max}$  are the initial and maximal ATPase velocities,  $K_{app}$  is the apparent binding constant and  $n$  is the Hill coefficient [50]. As expected, only positive cooperativity is evident; the curve is sigmoidal at low ATP concentrations and then quickly levels off at concentrations above  $10 \mu\text{M}$  ATP. Moreover, in the presence of GroES, the rate of ATP hydrolysis essentially goes to zero, as previously reported [98]. The value for  $V_{\max}$  ( $\sim 10 \text{ min}^{-1}$ ) is greater in SR1 than it is for GroEL, presumably due to the lack of negative cooperativity.

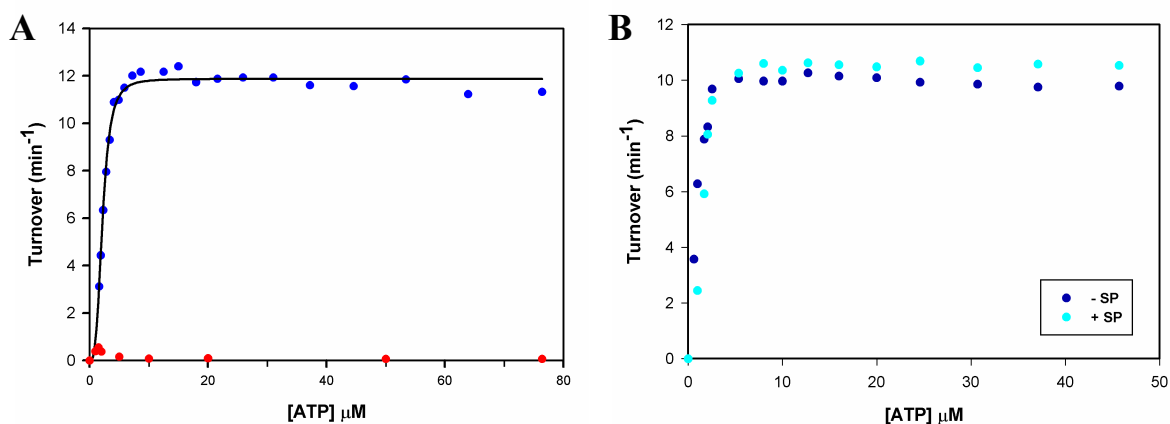


**Figure 3-8: ATPase Assays of SR1.** **A)** ATPase of SR1 at  $10 \text{ mM K}^+$ ,  $\pm$  GroES. The data without GroES (blue) was fit to the Hill equation (solid line). The value for the Hill coefficient was estimated to be  $2.87 (\pm 0.16)$ , similar to previously reported values. GroES almost completely inhibits ATP hydrolysis by SR1 (red). This result is expected, since GroES cannot be released after the first turnover, but is at odds with previous studies which report an inhibition of only 85% (ref). **B)** Unfolded MDH has little effect on the rate of ATP hydrolysis by SR1 at  $100 \text{ mM K}^+$ . This is in stark contrast to the stimulatory effects observed with GroEL under similar conditions, which is stimulated nearly 7-fold at high ATP concentrations (greater than  $500 \mu\text{M}$ ). A mild inhibition of activity is seen at low ATP concentrations, indicating that SP increases apparent cooperativity by shifting the equilibrium toward the T state.

Experiments in this lab and others have shown the presence of unfolded substrate protein stimulates the rate of ATP hydrolysis by GroEL 6 to 7-fold [49, 65]. The ATPase activity of SR1 was measured in the presence of acid-denatured malate dehydrogenase (MDH) at 100 mM  $K^+$  (Figure 3-8B). Only a slight stimulation of activity was seen at the higher ATP concentrations, while a slight inhibition is visible at low ATP concentrations. In the absence of SP, there is a very slight decline in the activity at higher [ATP]. This may be due to the contaminating GroEL<sup>wt</sup>. This effect disappears in the presence of SP, which would stimulate the activity of any contaminating 14-mers to 18 turnovers per minute. In fact, the mild stimulation of SR1 activity at high ATP concentrations may be due to the 14-mer population.

The simplest explanation for why substrate protein does not stimulate the ATPase activity of SR1 is that, for some reason, it can't bind to SR1. However, previous studies indicate that unfolded MDH can bind and be encapsulated by SR1 [94]. To substantiate these results, we utilized a functional assay previously developed in our lab [96], where GroEL was allowed to form an asymmetric complex with GroES<sup>his</sup>. This was then run on a Ni-NTA column, which traps his-tagged material and anything complexed to it. As shown in Figure 3-9A, GroEL is released upon addition of an ATP/GroES<sup>wt</sup> challenge, which initiates turnover and release from the GroES<sup>his</sup> still bound to the column. The GroES<sup>his</sup> is eluted with 250 mM imidazole. An identical experiment was performed using SR1, with and without a 2-fold excess of unfolded MDH (Figure 3-9, B and C, respectively). SR1 was not released from GroES<sup>his</sup> with the ATP/GroES<sup>wt</sup> challenge, but instead eluted with the imidazole wash. Since SR1 does not have a second ring to transmit the release signal, this result was expected. When MDH was included,

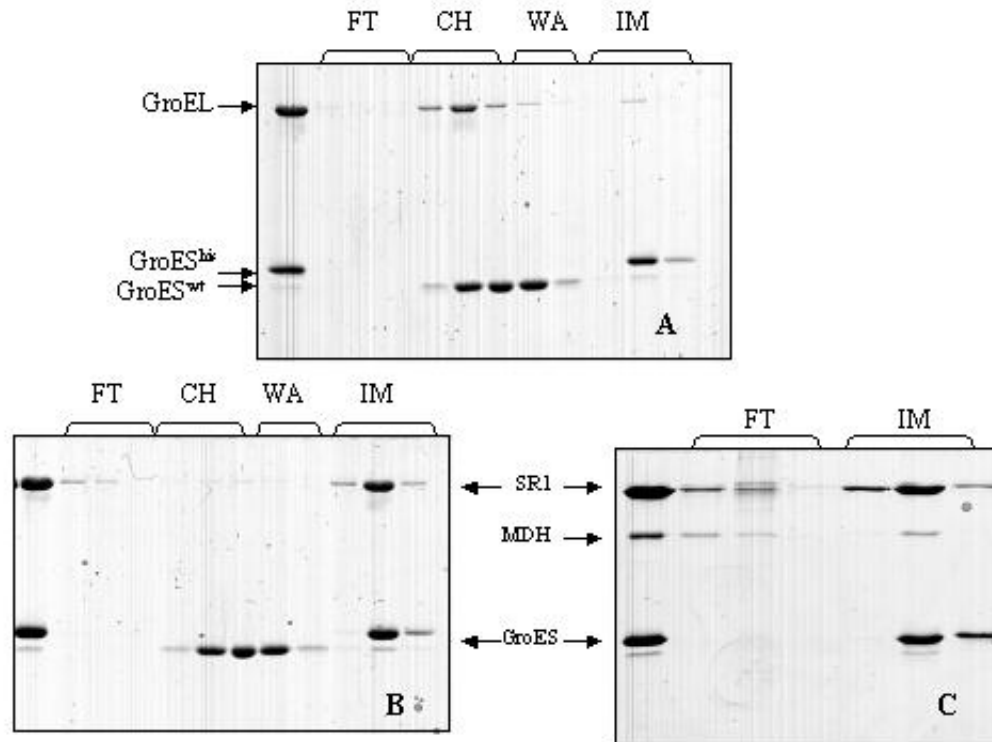


**Figure 3-9: SR1 Can Bind and Encapsulate SP.** Functional assays test SR1's ability to bind and release his-tagged GroES, and in the process, encapsulate unfolded MDH. **A)** GroEL<sup>wt</sup> control. GroEL<sup>wt</sup> was incubated with GroES<sup>his</sup> and ATP. After allowing the ATP to exhaust, the asymmetric complex was loaded onto a Ni-NTA resin, which binds the GroES<sup>his</sup>. The first lane represents the material loaded on the column. The complex was not eluted in the flow through (lanes labeled FT), but was released when challenged with buffer containing ATP and GroES<sup>wt</sup> (lanes CH). The column was washed again with Tris/Mg buffer (lanes WA). His-tagged material was eluted with 250 mM imidazole (lanes IM). GroES<sup>his</sup> has reduced mobility compared to GroES<sup>wt</sup>, and can be distinguished in the CH and IM lanes. Nearly all of the GroEL is released with the challenge, indicating it can bind GroES<sup>wt</sup> on the *trans* ring and while releasing GroES<sup>his</sup> on the *cis* ring. **B)** An identical experiment was performed with SR1. A small amount of material was eluted with the flow-through, most likely monomers unable to form a complex. SR1 was not released with the ATP/GroES<sup>wt</sup> challenge or wash, but instead eluted with the GroES<sup>his</sup> in the imidazole wash. This indicates SR1 is a 7-mer and cannot release the GroES<sup>his</sup>, even in the presence of competing GroES<sup>wt</sup>, due to the absence of a signal from the opposite ring. **C)** The same experiment as in B, but without a challenge or wash, in the presence of a 2-fold excess of acid denatured MDH over SR1 rings. Gel quantitation indicated approximately 50% of the MDH eluted with the SR1 in the imidazole wash, showing that the substrate protein could be bound and encapsulated by SR1.

approximately 50% of the substrate protein eluted with the SR1, as determined by gel quantitation. Thus, the lack of ATPase stimulation is not due to a deficiency in substrate binding.

**3.3.3 Response of SR1<sup>IAX</sup> ATPase Activity to Oxidation** To confirm that SR1 serves as an appropriate allosteric substitute for GroEL, a mutant was created where an intra-subunit salt bridge (D83 and K327) was replaced with two cysteine residues (SR1<sup>IAX</sup>). Previous work in our lab with GroEL<sup>IAX</sup> demonstrated that only one disulfide bond per ring was needed to hold a ring in the T state and prevent its transition to the R' state (G. Curien and G. Lorimer, unpublished results). This is a particularly straightforward experiment with SR1<sup>IAX</sup> since GroES eliminates the ATPase activity of SR1 when bound. Thus, GroES binding can be measured by its fractional inhibition of SR1<sup>IAX</sup> ATPase activity, given by the equation:

$$\text{Fractional Inhibition} = 1 - \frac{\text{Turnover}(+GroES)}{\text{Turnover}(-GroES)}$$

Hence, a fractional inhibition value of 1 means that GroES is bound by all the SR1 rings in the population and no turnover is detected. A fractional inhibition value of zero means that GroES has no effect on the rate of ATP hydrolysis and therefore is not bound. A graph of fractional inhibition versus fractional oxidation of SR1<sup>IAX</sup> (as determined by gel quantitation, described in section 3.2.5) is shown in Figure 3-10. The data coincide with the population of fully reduced rings, R<sub>7</sub>O<sub>0</sub>, confirming that the SR1<sup>IAX</sup> system behaves similarly to GroEL<sup>IAX</sup> and that only one disulfide bond per ring is needed to prevent the concerted transition from the T to R' state.

**3.3.4 Modeling the Effects of Oxidation in SR<sup>IAX</sup>** Previous work with GroEL<sup>IAX</sup> utilized a model in which each cross-link or disulfide bond introduced was thought

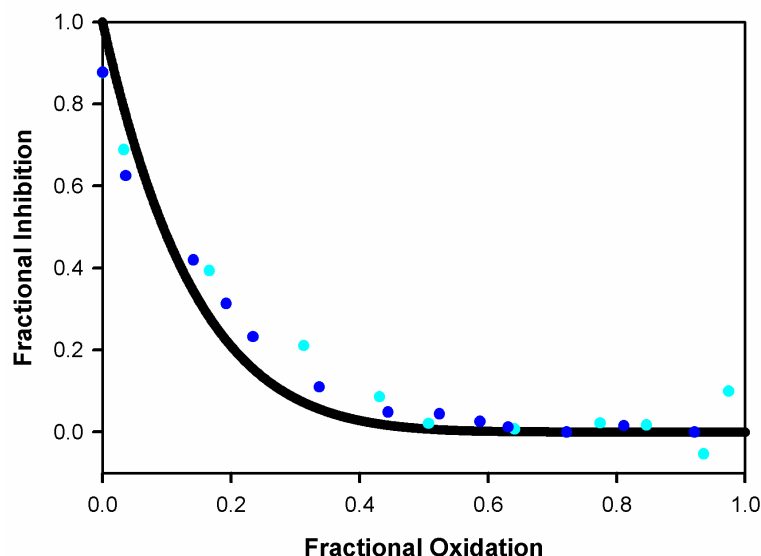


**Figure 3-10: Inhibition of Fractionally Oxidized SR1<sup>IAx</sup> by GroES** When GroES is bound to SR1, ATP hydrolysis is halted. Fractional inhibition of variously oxidized samples can be used to determine the number of disulfide bonds per ring necessary to lock a ring in the T state and prevent transitioning to the R' state. The circles represent the actual data collected, and the solid black line is the theoretical population of fully reduced rings. Circles are colored either blue or cyan, to indicate experiments performed on different days. The fractional inhibition data maps to population of fully reduced rings, indicating that, as with previous experiments utilizing GroEL<sup>IAx</sup>, only one disulfide bond per ring is required to prevent GroES binding.

to eliminate the ATPase function of the modified subunit (G. Curien and G. Lorimer, unpublished results). This was combined with the result from the GroES binding experiments that showed only one cross-link was necessary to lock a ring in the T state. Using these constraints, the predicted rate of ATP hydrolysis was calculated as follows:

$$Rate = V_R x_0 + \sum_{n=1}^7 [V_T - \frac{n}{7}(V_T)] \times x_n$$

where  $V_R$  and  $V_T$  represent the maximal rates of hydrolysis for a subunit in the R and T states, respectively,  $n$  is the number of disulfide bonds in a ring (from 1 to 7), and  $x_n$  is the mole fraction of rings with  $n$  number of disulfide bonds. The first term in the

equation ( $V_R \times x_0$ ) represents the rate contribution of fully reduced rings, in which all subunits are in the R state. Rings with one or more disulfide bonds are in the T state, but have the activity of any tethered subunits subtracted. Experimental results of GroEL<sup>IAX</sup> ATPase activity versus fractional oxidation (G. Curien and G. Lorimer, unpublished results) seemed to match well with this theoretical model (Figure 3-11A). Of note is the rise in activity at low levels of oxidation, followed by a sharp decrease at the higher levels. The rise in activity was explained by saying the activity of a subunit in the T state was much higher than a subunit in the R state. Thus, as the rings were progressively locked in the T state, the activity increased until all the rings in the population contained at least one cross-link, at which point the activity decreased as in an active site titration. In this model, the activity of the TT state was not the apex of the fractional oxidation curve, since by that point half the subunits were no longer turning over. The  $V_{\max}$  of the TT state was therefore computed by extrapolating the data back to the y-axis, yielding a turnover value of 25 min<sup>-1</sup>. The highest value observed experimentally is approximately 18 min<sup>-1</sup> in the presence of saturating, unfolded substrate protein. Further, it has been shown that SP stimulates GroEL<sup>IAX</sup> only when there is a population of rings in the R state remaining [49].

It was assumed this model would also explain the effects of oxidation in SR1<sup>IAX</sup>. However, when the same model was applied to the 7-mer, it did not fit the data at all (Figure 3-11B). One distinguishing feature of the SR1<sup>IAX</sup> data is that there is very little change in the ATPase activity at the low oxidation levels. This seemed to suggest that, at least in the single ring, there is very little difference between the T and R state activities. Since the GroES binding data confirmed that only one disulfide bond was required to

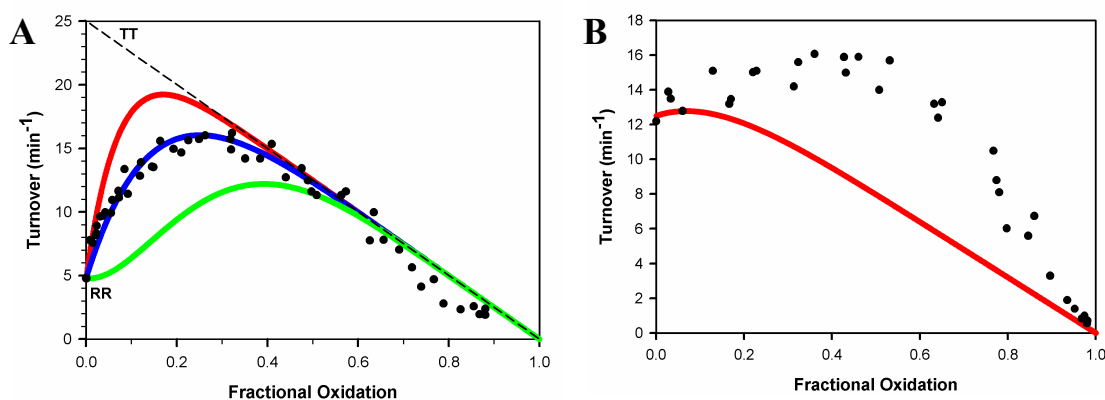


**Figure 3-11: Modeling the Effects of Oxidation Using the Model for GroEL<sup>IAX</sup>**  
 Previous work with GroEL<sup>IAX</sup> fit the ATPase data of fractional oxidized samples to models which assumed that each disulfide bond introduced eliminated the activity of the subunit modified (G. Curien and G. Lorimer, unpublished data). Three different variations were plotted where: one disulfide bond per 14-mer (green), one disulfide bond per ring (blue), or two disulfide bonds per 14-mer (red) were required to lock a ring in the T state. The data fit best to a model to the “1 in 7” model, shown in **A**. The same model is applied to the SR1<sup>IAX</sup> data in **B**.

lock a ring in the T state, we tried fitting the SR1<sup>IAX</sup> data to a new model that assumed no activity was lost until a certain number of disulfide bonds had been introduced into a single ring. That is, one disulfide bond effectively locks a ring in the T state, but does not abolish or alter activity in that subunit. Instead, a ring must accumulate a number of disulfide bonds, at which point, the entire ring loses activity. We modeled the data to assume that 5, 6, or 7 disulfide bonds per ring eliminated activity (Figure 3-12A), as given by the following equation:

$$Rate = V_R x_0 + \sum_{n=1}^y V_T x_n + \sum_{n=y+1}^7 0 x_n$$

Here, the first term represents the rate contribution of fully reduced rings. The second term represents rings locked in the T state by one or more disulfide bonds, but have not accumulated enough tethers to affect activity. The third term reflects those rings which have lost activity due to the presence of a certain number of disulfide bonds within the

ring. Values for  $V_T$  and  $V_R$  can be set as appropriate and, after trial and error, were assumed to be 15.4 and 12.2  $\text{min}^{-1}$ , respectively. Clearly, the data fit best to a “six strikes” model, where six disulfide bonds must accumulate in a ring before activity of a ring is abolished. When this model was applied to the GroEL<sup>IAX</sup> data, it also fit very well (Figure 3-12B). Significantly, when this model is used with GroEL<sup>IAX</sup>, a value for  $V_{\text{max,TT}}$  of 18  $\text{min}^{-1}$  produces the best fit, matching the value obtained with unfolded substrate protein. The model was subsequently applied to another double cysteine mutant in our lab, GroEL R197C/E386C, which also fit well to the “six strikes” model [49].

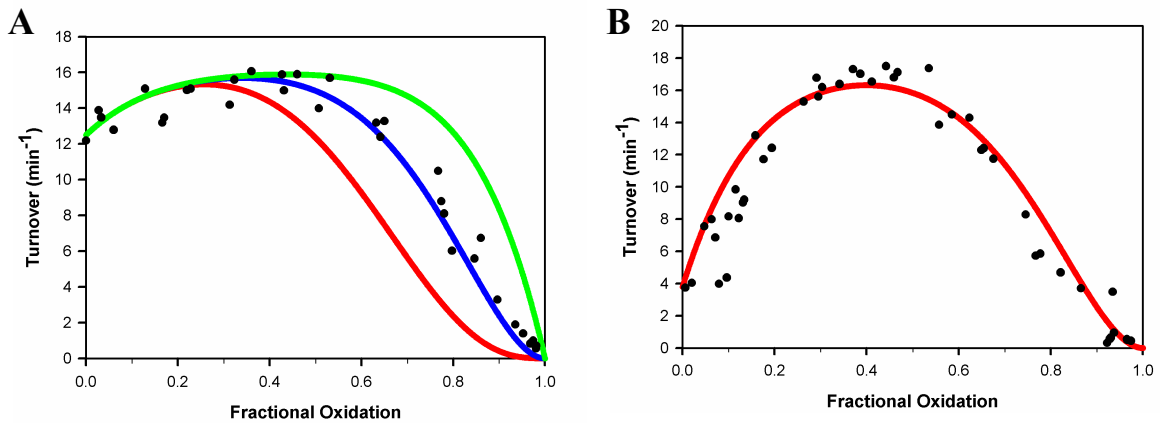


**Figure 3-13: Applying the New Model to SR1<sup>IAX</sup> and GroEL<sup>IAX</sup>** **A)** All models assume that one disulfide bond per ring locks the ring in the T state, as suggested by the GroES binding data presented earlier (Figure 3-11).  $V_{\text{max,T}}$  and  $V_{\text{max,R}}$  were set to 15.4  $\text{min}^{-1}$  and 12.2  $\text{min}^{-1}$ , respectively. Three models were plotted beside the data: where five (red), six (blue), or seven (green) disulfide bonds per ring are required to eliminate the activity of the entire ring. The data fit best to the “6 strikes” model. **B)** The GroEL<sup>IAX</sup> data was also fit to the “6 strikes” model. In this model,  $V_{\text{max,TT}}$  was set to 18  $\text{min}^{-1}$ , a value observed experimentally with unfolded substrate protein.

**3.3.5 The Effect of Left Site versus Right Site Mutations** When we first made SR1<sup>IAX</sup>, the original DNA sample sent from Yale was transformed into *E. coli* JM105 and a plasmid purification was performed for use in the mutagenesis. However, when the



**Figure 3-13: Native Gel Reveals that GroEL<sup>LSM</sup> is a 14-mer** A native gel of SR1 (lane 1), GroEL<sup>wt</sup> (lane 2) and GroEL<sup>LSM</sup> (lane 3) demonstrated that mutations to the left contact sites do not separate the two rings, as might be expected.

mutant protein was run on a native gel as before, the primary band corresponded to a 14-mer rather than a 7-mer (Figure 3-13). After several transformations and induction trials, it became apparent the DNA provided was a mixed sample, which sometimes produced 7-mers and sometimes produced 14-mers. The template for each of these species was isolated and sent for DNA sequencing. The template which produced 7-mers contained the right site mutations R452E, E461A, S463A and V464A, those originally reported for SR1 [81]. However, the 14-mer species, which we termed GroEL<sup>LSM</sup>, contained left site mutations at E102A, K105A, and M111A.

The ATPase profile for GroEL<sup>LSM</sup>, with and without GroES, has properties of both GroEL and SR1 (Figure 3-14). In the absence of GroES, only a small degree of negative cooperativity is evident, with a  $V_{max}$  around  $16 \text{ min}^{-1}$ . This rate approaches the maximum value seen with GroEL<sup>wt</sup> in the presence of unfolded substrate protein. Upon addition of GroES, the rate is reduced by approximately 65%. The inhibition by GroES

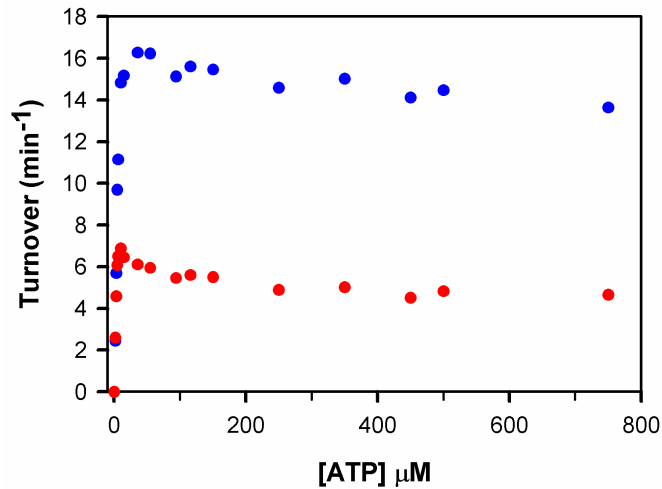


**Figure 3-14: ATPase Activity of GroEL<sup>LSM</sup>, ±GroES** The ATPase profile of GroEL<sup>LSM</sup> in the absence of GroES (blue) reveals that the mutant is deficient in inter-ring communication, as evidenced by lack of negative cooperativity at higher ATP concentrations. The  $V_{max}$  approaches the maximal value seen in GroEL<sup>wt</sup> with substrate protein, which may also indicate the two rings are turning over independently of each other. In the presence of GroES (red), negative cooperativity is increased slightly and the rate of hydrolysis is reduced approximately 65%.

is similar to that seen with GroEL<sup>wt</sup> [62]. However, like SR1, GroEL<sup>LSM</sup> was not significantly stimulated by unfolded MDH, either in the presence or absence of GroES.

The high rate of ATP hydrolysis suggested that GroEL<sup>LSM</sup> might separate into 7-mers in the presence of ATP, but came back together as a 14-mer in the presence of GroES, much like Hsp60 [93]. 30 μl samples of 30 μM GroEL<sup>LSM</sup> were run on a gel filtration column as described in section 3.3.1, both in the absence and presence of 25 μM ATP. Although the concentration loaded on the column was 30 μM, by the time it elutes from the column, it should approximate the concentration used in the ATPase assay. The observed retention time was 19.7 minutes, both in the absence and presence of ATP, indicating that the high rate of hydrolysis seen in steady state measurements is not due to the rings coming apart in the presence of nucleotide (data not shown).

Gel filtration was also used to study GroES release from GroEL<sup>LSM</sup>. Complexes were made with 60  $\mu$ M GroEL<sup>LSM</sup>, 20  $\mu$ M GroES 98C labeled with fluorescein-5-maleimide (F5M) and 300  $\mu$ M ATP in a 20 mM Tris pH 7.5, 10 mM MgAc, 100 mM KAc, 2 mM DTT buffer (see section 5.2.1 for a full description of the labeling process of GroES 98C). The complex was diluted with buffer to a final concentration of 30  $\mu$ M GroEL<sup>LSM</sup> and run on a gel filtration column equilibrated with 20 mM Tris pH 7.5, 10 mM MgAc, 100 mM KAc, 2 mM DTT and 30  $\mu$ M ADP. ADP was included in the buffer to stabilize the complex as it migrated down the column. Elution was monitored both by absorbance at 280 nm and fluorescence emission at 515 nm (excitation at 473 nm). Surprisingly, the GroEL<sup>LSM</sup> and GroES-F5M elute separately (retention times of 19.7 and 23.9 minutes, respectively), indicating that the complex fell apart before elution (data not shown). This was surprising since GroES clearly inhibits ATPase activity in the steady state assay (Figure 3-14). Previous experiments in our lab with GroEL<sup>wt</sup> show that nearly all of the GroES-F5M elutes with the GroEL as an asymmetric complex (J. Grason, unpublished results).

### **3.4 Discussion**

**3.4.1 Implications for the Allosteric Model** This work provides support for two conclusions reached through previous studies in our lab (G. Curien and G. Lorimer, unpublished results). First, it supplies further experimental evidence that the movement of subunits within a ring is concerted, as predicted by the current allosteric models. Second, the exclusive binding assumption used to simplify the mathematics of the nested cooperativity model, which states ATP only binds to the R state [50], is not justified. Clearly the T state is capable of binding and hydrolyzing ATP. Both of these conclusions

support those initially reached in previous studies with GroEL<sup>IAX</sup> (G. Curien and G. Lorimer, unpublished results).

The effect of substrate protein on SR1 ATPase activity was initially difficult to understand. Previous explanations for the effect of unfolded substrate protein suggested it shifts the allosteric equilibrium toward the T state, which was thought to have a higher  $V_{\max}$  than the R state [22, 65]. Since SR1 can bind SP and also undergoes a cooperative transition from the T to the R state, stimulation would be anticipated. Here, we see that the lack of stimulation can be explained by the observation that, in the absence of negative cooperativity, the  $V_{\max}$  of the T and R states is nearly the same. This is true both for SR1, which lacks negative cooperativity because of the missing opposing ring, and GroEL<sup>LSM</sup>, which has impaired ring to ring communication. Thus, substrate protein appears to have the effect of overcoming the negative cooperativity in the double ring.

Experimental evidence with substrate protein and cross-linked GroEL<sup>IAX</sup> puts the activity of subunits in the TT state around  $18 \text{ min}^{-1}$  at  $37^\circ\text{C}$ . Why, then, is the  $V_{\max}$  of SR1 only  $10 \text{ min}^{-1}$ ? One factor could be the small contamination of 14-mers, which would have considerably lower activity at high ATP concentrations. Although the degree of contamination is small, a weighted average ( $18 \text{ min}^{-1}$  versus  $3 \text{ min}^{-1}$ ) might decrease  $V_{\max}$  by approximately 1 to 2 turnovers. However, this still doesn't come close to explaining the  $10 \text{ min}^{-1}$  observed. A population of monomers also exists in the SR1 sample, as seen by both native gel electrophoresis and HPLC. Perhaps the monomers are not hydrolyzing ATP, again bringing the average turnover per subunit down. A final possibility, and probably the most likely, is that the mutations themselves are influencing the rate of ATP hydrolysis. Other seemingly innocuous mutations, such as

D83C/K327C, have been known to influence the rates of ATP hydrolysis [49]. In the end, it is difficult to know which of these factors contributes to the lower than expected  $V_{\max}$ .

**3.4.2 A New Oxidative Model from  $SR1^{IAX}$**  When the original model was proposed to explain the oxidative effects in GroEL<sup>IAX</sup>, it made logical, structural sense that a disulfide bond or chemical cross-linker would eliminate the ATPase activity of the subunit modified. The data also fit very well to the model (Figure 3-11A). The only issue was the theoretical  $V_{\max}$  for the TT state, which extrapolated from the data back to 25 turnovers per minute, much higher than the experimentally observed value in the presence of unfolded substrate protein. Even this could be explained by theorizing that substrate protein, while influencing the equilibrium, could not shift it *entirely* to the TT state, and thus the experimental value would fall short of the theoretical value. It was only when the  $SR1^{IAX}$  data clearly did not fit the model that the original model was called into question. The “6 strikes” model assumes that there is no change in activity until a ring accumulates 6 disulfide bonds, at which point the entire ring shuts down. Unlike the other model, this one is difficult to explain structurally. What is it about the sixth tether that suddenly eliminates ATP hydrolysis, when tethers one through five have no effect besides locking the ring in the T state? Unfortunately, such a model cannot be proved, but exists until a better one is proposed. However, the “6 strikes” model does have a number of advantages. The predicted TT state  $V_{\max}$  now agrees with the experimentally observed value of 18 min<sup>-1</sup>. It also supports the result that the  $V_{\max}$  of the T and R states are very similar in the single ring. The model has been successfully applied to three different mutants: GroEL<sup>IAX</sup> and  $SR1^{IAX}$ , as well as an inter-subunit double cysteine

mutant, GroEL R197C/E386C [49]. This lends a certain amount of credibility to the model, even if we don't yet understand the structural basis for the observed results.

**3.4.3 The Nature of Inter-Ring Communication** The contamination of the SR1 plasmid DNA sample with plasmid encoding GroEL<sup>LSM</sup> turned out to be a fortuitous frustration. To our knowledge, this mutant has not been studied before, but offers interesting insights into the nature of the allosteric signal transmitted across the rings. A similar mutant, GroEL E434K, was determined to be a 14-mer by electron microscopy, and displayed decreased negative cooperativity in ATP hydrolysis compared to wild type [88]. However, it was also noted in the same paper that a SR1-like mutant, GroEL E461K, was also a 14-mer, and none of the chaperonins studied, including wild type, exhibited much negative cooperativity to speak of [88]. This is most likely due to a significant contamination by substrate protein, which is not uncommon throughout the literature [49]. Work with the E434K and E461K mutants also stated the two mutants were inhibited by GroES similarly to SR1; all three were reported to be inhibited by GroES to approximately 85% at 37°C [88]. Work here shows that GroEL<sup>LSM</sup> exhibits very little negative cooperativity, but is inhibited by GroES similarly to GroEL<sup>wt</sup>. Furthermore, in our hands, SR1 is inhibited nearly 100% by GroES, as would be expected for a single ring. It is difficult to explain the discrepancies between the two studies.

It is somewhat surprising that GroEL<sup>LSM</sup> exists as a 14-mer; differential scanning calorimetry experiments indicate the E434-K105 salt bridge contributes more to inter-ring stability than the E461-R452 salt bridge [88]. Moreover, the left site contains a tetrad of ionic interactions compared to the single right site E461-R452 salt bridge

(Figure 3-1). The lack of negative cooperativity, combined with the lack of stimulation by substrate protein, both in the presence and absence of GroES, suggests the two rings of GroEL<sup>LSM</sup> are deficient in their inter-ring communication and are turning over independently of each other. Since elimination of the right contact sites produces a 7-mer, it is therefore tempting to speculate that the right site contacts are the glue that holds the rings together, while the left site contacts transmit the allosteric signal across the rings. Cryo-EM studies have suggested as much. Alpha-helix 4 (residues 89-108) connects lysine 105 (involved in the left site inter-ring salt bridge) with threonine 91 (located in the ATP binding site) [56]. Thus, the binding of ATP can influence the dipole of the  $\alpha$ -helix, weakening the balance of charges at the contact site. The distance between the rings is known to increase upon binding of ATP to one of the rings [56].

Since communication between the rings of GroEL<sup>LSM</sup> is inhibited or maybe even abolished, it may make sense that GroES only binds weakly; otherwise it could not be released, much like SR1. Thus, GroEL<sup>LSM</sup> behaves similarly to Hsp 60 in the presence of GroES. The lack of communication between the rings is supported by the value of  $V_{\max}$  (16 min<sup>-1</sup>) and the lack of stimulation by substrate protein. However, more work is needed to fully characterize this mutant and make definitive conclusions about its properties. First, like with SR1, it would be necessary to show conclusively that GroEL<sup>LSM</sup> can bind substrate proteins such as MDH. It would be interesting to see if GroEL<sup>LSM</sup> can refold stringent substrates, such as RuBisCo, and if it can substitute *in vivo* for GroEL<sup>wt</sup>. Further, the kinetics of GroES binding and release should be examined.

## **Chapter 4**

### **Examining the Effects of Potassium on the Allosteric Properties of GroEL: A New Equation for Nested Cooperativity**

## **4.1 Introduction**

Understanding the allosteric effects in a large macromolecule is complicated. The study of allostery in hemoglobin, only a tetramer, is still ongoing after nearly a century [99]. However, the study of allosteric properties in large assemblies such as GroEL is worth the effort, since it may offer invaluable insights into the workings of other complicated allosteric systems, such as the cytoplasmic eukaryotic chaperonin, CCT [100]. The key to selecting one model as opposed to another is often having enough accurate data to distinguish between them. In the case of GroEL, this has been an issue since its allosteric properties are governed by a number of factors (i.e. the amount of unfolded SP present, the concentration of ADP and  $K^+$ ) which have not always been fully considered.

The first model to describe the allosteric properties of GroEL proposed MWC interactions were nested inside KNF interactions (Figure 4-1) [50]. Nested models arrange interactions hierarchically in terms of the protein's structure; in this case, the heptameric ring is considered the allosteric unit. This means that subunits within a ring undergo a concerted transition from the T state to the R state in response to ATP binding in accordance with MWC allosteric theory [52]. The allosteric transitions between the rings is sequential, in accordance with KNF-type interactions [53]. Thus, the 14-mer must progress from the TT state to the RR state via the TR state (Figure 1-4). Two allosteric constants define the equilibrium between the various states:  $L_1 = [TR]/[TT]$  and  $L_2 = [RR]/[TR]$ . The Yifrach and Horovitz model makes two assumptions [50]. First, it assumes that ATP binds only to the R state, which is known as the exclusive binding principle. This eliminates a number of terms from the mathematical representation of the

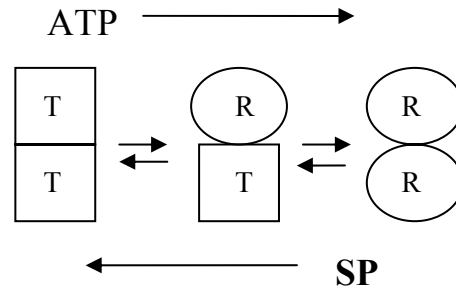


**Figure 4-1: The Original Model for Nested Cooperativity in GroEL** Developed by Yifrach and Horovitz [50], the model nests MWC interactions inside KNF interactions. With no ligands bound, both rings of GroEL exist primarily in the T state. Cooperative binding of ATP induces an “all or none” transition in the first ring (MWC transition), where subunits within a ring are either in the T state or the R state, but do not exist as a mixture of both. Once the first ring has undergone the transition to the R state, additional ATP binds to the second ring, inducing a second “all or none” transition. The sequential transition from TT to TR to RR is governed by KNF interactions. ATP shifts the equilibrium toward the R states, while unfolded SP shifts the equilibrium toward the T states.

model, simplifying the fitting of the equation to real data. The second assumption says the activity of a R subunit in the RR state is lower than the activity of a R subunit in the TR state. This is an effect of the negative cooperativity and is used to explain the decrease in the rate of ATP hydrolysis at higher ATP concentrations [50].

A nested MWC model was recently proposed which described the ATPase activity of GroEL without invoking negative cooperativity [54]. Here, the heptameric ring is considered the *smallest* allosteric unit, which can exist in one of two conformations, t or r (Figure 4-2). The two heptamers interact with each other to form a *higher* allosteric unit, the 14-mer, which may exist in the T or R state. The allosteric equilibrium is defined for the 14-mer as  $L = [T]/[R]$ . Within each of these states, the heptameric rings may also adopt two different conformations: (rT) and (tT) in the T state

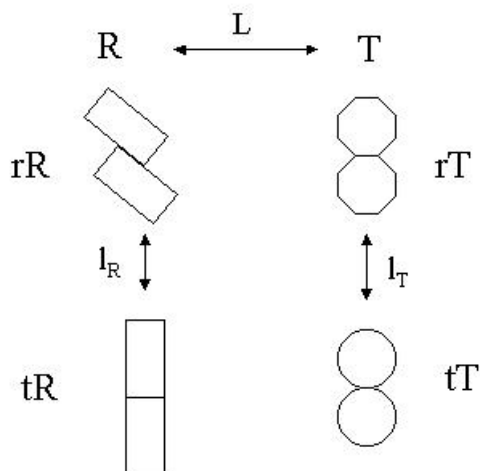


**Figure 4-2: Nested MWC Model for Cooperativity in GroEL** Here, the heptameric ring is considered the smallest allosteric unit, which is nested inside a larger allosteric unit, the 14-mer [54]. Thus, the individual rings may adopt either a t or r conformation, and the 14-mer also exists as either T or R. This allows for a total of four states, each symbolized by a different conformation.

or (rR) and (tR) in the R state. Thus, equilibria can further be defined for the different quaternary states:  $l_R = [tR]/[rR]$  and  $l_T = [tT]/[rT]$ . The difficulty with this model is that the various conformational states have not been described structurally. Moreover, the number of dependent variables is huge; for each of the four conformations, there is an ATP binding constant,  $K_{\alpha\beta}$ , and a rate of hydrolysis,  $v_{\alpha\beta}$ , where  $\alpha\beta$  represent rR, tR, rT, and tT. There are also three allosteric constants, making for a total of 11 variables.

There is considerable experimental evidence to support intra-ring positive cooperativity, as detailed in chapters 1 and 3. Negative cooperativity between the rings is less well understood, and is supported mainly by mutants, including the work with SR1 and GroEL<sup>LSM</sup> in chapter 3, which lack ring-to-ring communication and also the sharp decrease in steady state ATPase activity seen at the higher ATP concentrations with wild type. The original paper describing nested cooperativity in GroEL relied on the mutant

R197A, which had impaired inter-ring communication, the structural basis of which was not understood [50]. Structural studies and molecular dynamic simulations also support the idea of negative cooperativity between the rings. Cryo-EM has provided images of the TT, TR, and RR states at 28 Å resolution [42, 56]. In order to preserve the inter-ring interface, the equatorial plate of the trans ring moves away from the horizontal axis by 2° [10], preventing steric clashes at the left contact sites of the equatorial interface [57].

The rate of ATP hydrolysis by GroEL, and the degree of cooperativity displayed, are related to the  $K^+$  concentration used in the assay [62, 63]. However, it is not clear if this effect is due to potassium's ability to shift the allosteric equilibrium [63], or if it simply influences the affinity for which ATP binds to the T and R states [62]. Results from previous studies (G. Curien and G. Lorimer, unpublished results), and those presented in chapter 3, indicate that the exclusive binding assumption is not justifiable. The work presented in this chapter attempts to fit ATPase data at three different potassium concentrations to a more expansive equation, one which recognizes that ATP can be bound and hydrolyzed by both the T and R states.

## ***4.2 Methods Specific to Chapter 4***

***4.2.1 Purification of Recombinant Rabbit Pyruvate Kinase*** The activity of the pyruvate kinase normally used in our coupled enzyme ATPase is dependent on the potassium ion concentration. This makes measurements below approximately 10 mM  $K^+$  problematic. Previous studies demonstrated that rabbit pyruvate kinase with the mutation E117K worked in our steady state assay (described in section 2.8) and did not depend on potassium for its activity [63, 101]. For the sake of consistency, this enzyme was used in

all the ATPase assays presented in this chapter, even where the potassium concentration did not dictate its use.

Purification of PK E117K was performed as previously described with a few modifications [101]. BL21(DE3) cells harboring the pET-E117K plasmid (a gift of Dr. George Reed) were streaked onto LB plates containing 0.2 mg/ml amp and grown at 37°C overnight. One colony was inoculated into 50 ml of LB with 0.5 mg/ml amp as a starter culture. The starter culture was grown at 37°C until the OD<sub>600</sub> reached 0.3, at which point 15 ml was transferred to two 1.5 L cultures also containing 0.5 mg/ml amp. Cultures were grown until the OD<sub>600</sub> reached 0.8, at which point protein over-expression was induced with lactose (20 g/L). Cultures were incubated overnight at 30°C, with replenishment of antibiotic after approximately 10 hours. The maintenance of antibiotic concentrations is crucial to prevent the loss of plasmid. Cells were harvested by centrifugation and resuspended in lysis buffer (10 mM TrisCl pH 8.0, 1 mM DTT, 10 mM PMSF). Cells were lysed by sonication in 25 ml portions, on ice, using a 30 second burst, a 2 minute rest, and then another 30 second burst (50% duty cycle, power level 5). Cell debris was removed by centrifuging the suspension in a Beckman Optima LE-80K ultracentrifuge at 27,400xg for 15 min. DNA was precipitated by addition of streptomycin sulfate to a final concentration of 1 mg/ml and spun again at 42,800xg for 30 minutes. An initial purification was accomplished through addition of ammonium sulfate, which was brought to 37% saturation (220 g/L). After stirring on ice for 1 hour, the suspension was centrifuged at 20,000xg for 20 minutes at 4°C. The supernatant was transferred to a new container and brought to 55% saturation (140 g/L). Again, this was allowed to stir on ice for 1 hour and centrifuged as before. The supernatant was

discarded, and the pellet was resuspended in 20 ml of 10 mM TrisCl, pH 8.0 and loaded onto a 150 ml G-25 desalting column (Amersham) equilibrated with 400 ml of the same buffer. Protein fractions with low salt (<7 mS) were pooled and loaded on a 25 ml DEAE column (Amersham) equilibrated with 50 ml of 200 mM TrisCl, pH 8.0 followed by 150 ml 10 mM TrisCl, pH 8.0. The pyruvate kinase elutes in the flow through, which is collected and brought to pH 6.3 and 1 mM MgCl<sub>2</sub> with 1 M MES, pH 6.3 and 2 M MgCl<sub>2</sub>. The protein was then loaded onto a 25 ml CM-Sepharose column (Amersham) equilibrated with 100 ml 200 mM MES pH 6.3 followed by 150 ml 10 mM MES pH 6.3, 1 mM MgCl<sub>2</sub>. Following elution of the flow through, pyruvate kinase was eluted using a 0 to 400 mM NaCl gradient over 200 ml. The PK117 elutes at approximately 20 mS. Fractions with the most activity (described below) are pooled, desalted into 10 mM Tris pH 7.5, 10 mM MgAc, and concentrated to the desired activity. Concentration is determined at 280 nm in 6 M GdnHCl ( $\epsilon = 0.54 \text{ mg/ml}^{-1} \text{ cm}^{-1}$ ). Purity was assessed on a 12% SDS gel (Figure 4-3). The activity assay for PK117 is very similar to the ATPase assay previously described (section 2.8) except that ADP is substituted for the ATP (final concentration 1 mM) and no potassium is included. The specific activity of the material purified was 13.5 U/mg.

**4.2.2 ATPase Assay Using the Cary 100 Bio UV Spectrophotometer** For the experiments in this chapter, where the data were eventually fit to various equations, every effort was made to acquire extremely accurate values for turnover. Extinction coefficients for ATP were determined at 282 nm and 285 nm ( $1.4 \text{ mM}^{-1} \text{ cm}^{-1}$  and  $0.537 \text{ mM}^{-1} \text{ cm}^{-1}$ , respectively), which enabled us to directly determine the concentration of all the ATP solutions used in the assay with final concentrations up to 120  $\mu\text{M}$ . Absorbance

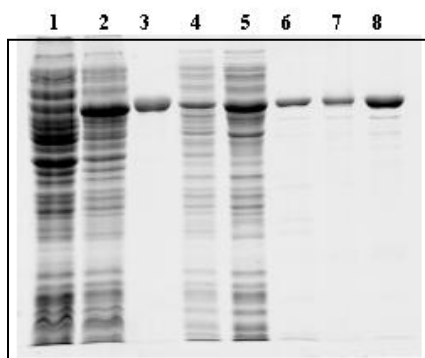


**Figure 4-3: Purification of Rabbit Pyruvate Kinase E117K** Rabbit pyruvate kinase with the mutation E117K has an activity that is independent of potassium concentration. This makes it ideal for studying the ATPase activity of GroEL at various potassium concentrations in the coupled enzyme assay. GroEL and PK are nearly the same size and migrate to the same place on a 12% SDS gel. It was used here as a molecular weight marker for PK. The other lanes are as follows: uninduced crude extract (lane 1), induced crude extract (lane 2), purified GroEL (lane 3), lysate after DNA precipitation (lane 4), lysate after second ammonium sulfate precipitation (lane 5), DEAE flow through (lane 6), final pool from CM-Sepharose (lane 7), concentrated PK (lane 8).

data was collected on a Cary Bio 100 UV/Vis dual beam spectrophotometer every 0.4 seconds while a heat block (set to 38°C) maintained the temperature of the cuvettes at 37°C. The reference cell contained water. In most cases, the GroEL concentration was 0.5  $\mu$ M. When measurements were needed at low ATP concentrations (<1  $\mu$ M), the subunit concentration was lowered to 0.2  $\mu$ M. There was no detected difference in rates determined at the two GroEL concentrations. When the potassium concentration varied from 100 mM, the ionic strength was kept constant using tetramethylammonium chloride (TMA). In all other respects, the assay was performed as previously described in section 2.8.

**4.2.3 ATPase of GroEL and SR1 at Variable Potassium Concentrations** The rate of ATP hydrolysis was measured for GroEL (J. Grason, unpublished results) and SR1 at variable potassium concentrations. The ATP concentration was held constant at 1

mM. Potassium and TMA were added such that the combined concentration was always 100 mM. The final SR1 concentration was 0.8  $\mu$ M and the ATPase activity was measured at 37°C. The final GroEL concentration was 2  $\mu$ M and activity was measured at 30°C.

**4.2.4 Fitting Data to the Nested Cooperativity Equations** The equations used to fit the data, both with and without the exclusive binding assumption, have been previously described [50]. A full explanation of the theory and mathematics used to develop these equations is presented in Appendix A. Equations were fit to the data using SigmaPlot 8.0 (SPSS Inc.), which uses a Levenberg-Marquardt algorithm. Fits were performed using 1000 iterations, with a step size of 1 to 10 and a tolerance of  $1 \times 10^{-5}$ . The equations for nonexclusive binding used for fitting data from SR1 (Equation 1) and GroEL (Equation 2) are shown below.

$$V_o = \frac{V_R \alpha (1 + \alpha)^6 + V_T L c \alpha (1 + c \alpha)^6}{(1 + \alpha)^7 + L(1 + c \alpha)^7} \quad (1)$$

where  $V_o$  and  $V_R$ , and  $V_T$  are the initial and maximal ATPase velocities in the R and T states, respectively. The allosteric constant,  $L$ , is defined as  $[T]_o/[R]_o$ , where the subscripts indicate the equilibrium is in the absence of ligand.  $\alpha$  is the  $[ATP]$  divided by the microscopic dissociation constant,  $k_R$ . The constant,  $c$ , represents the ratio  $k_R/k_T$ . When  $c$  is less than zero, the ligand (ATP) binds more strongly to the R state than the T state. The exclusive binding equation can be obtained by setting  $c$  equal to zero.

For GroEL, the nonexclusive binding equation is:

$$V_o = \frac{V_{TT} c \alpha (1 + c \alpha)^{13} + 0.5 V_{TR} \alpha L_1 (1 + \alpha)^6 (1 + c \alpha)^7 + 0.5 V_{TR} c \alpha L_1 (1 + \alpha)^7 (1 + c \alpha)^6 + V_{RR} \alpha L_1 L_2 (1 + \alpha)^{13}}{(1 + c \alpha)^{14} + L_1 (1 + \alpha)^7 (1 + c \alpha)^7 + L_1 L_2 (1 + \alpha)^{14}} \quad (2)$$

where  $V_o$ ,  $V_{TT}$ ,  $V_{TR}$ ,  $V_{RR}$  represent the initial and maximal velocities in the TT, TR and RR states, respectively. The terms  $c$  and  $\alpha$  are as described for equation 1. Here,  $L_1 = [TR]/[TT]$  and  $L_2 = [RR]/[TR]$ , also in the absence of ligand. It is important to note the difference in the definition of  $L_1$  and  $L_2$  for GroEL compared to the definition of  $L$  for the single ring. In the case of the single ring, the exponent should be positive (i.e. the T state is favored in the absence of ligand). For the same reason, exponents for  $L_1$  and  $L_2$  will be *negative*. The exclusive binding equation, as presented and used to fit the data in the original paper on GroEL nested cooperativity [50], is obtained by setting  $c$  equal to zero.

### 4.3 Results

#### 4.3.1 Examining the Effects of Potassium Concentration on the ATPase

**Activity of SR1** ATPase assays were performed using 0.5  $\mu\text{M}$  SR1 at 37°C and 1, 10, and 100 mM potassium (Figure 4-4). In order to better visualize the effects at lower ATP concentrations, the data is shown out to 50  $\mu\text{M}$  ATP, after which the rate of turnover is relatively constant. As reported previously with GroEL [62], the apparent cooperativity

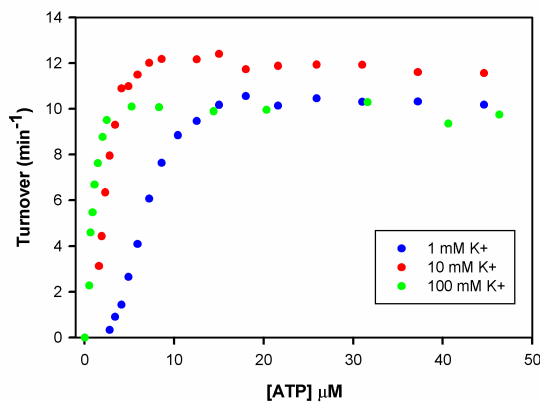


**Figure 4-4: ATPase of SR1 at Various Potassium Concentrations** ATP hydrolysis was measured for 0.5  $\mu\text{M}$  SR1 at 37°C at three different potassium concentrations. The apparent cooperativity increases as the potassium concentration decreases, but there is little to no effect on  $V_{\text{max}}$ .

increases as the potassium concentration decreases. There does not appear to be any effect on the  $V_{\max}$  due to changing the potassium concentration. Although the  $V_{\max}$  at 10 mM is slightly higher than at 1 mM or 100 mM, this is within the error of the experiment. To address whether the difference in  $V_{\max}$  at 10 mM was an anomaly, we tested the ATPase activity at various potassium concentrations and 1 mM ATP using the same SR1 protein solution (Figure 4-5). The differences observed in the 10 mM  $K^+$  data in Figure 4-4 are within the error observed in Figure 4-5. Thus, potassium does not appear to affect the  $V_{\max}$  in SR1.

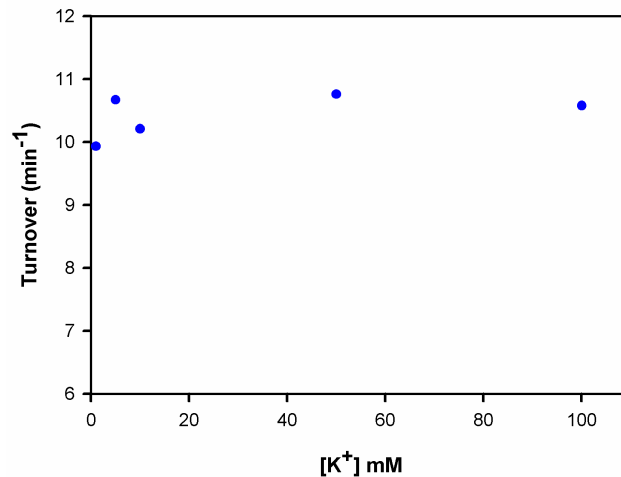


**Figure 4-5: The  $V_{\max}$  for SR1 is Not Affected By Changing Potassium Concentrations** ATP hydrolysis was measured using 0.8  $\mu$ M SR1 at 37°C with variable potassium concentrations. The ionic strength was held constant with TMA. The ATP concentration was held constant at 1 mM.

#### ***4.3.2 Fitting SR1 ATPase Activity to the Exclusive and Nonexclusive Binding***

**Equations** To further understand how potassium affects the ATPase activity of SR1, the data were fit to Equation 1 for each potassium concentration (Figure 4-6, A-C).

Exclusive binding was assessed by simply setting  $V_T$  and  $c$  equal to zero. Fits to the exclusive binding form of the equation are shown in red, while fits to the full equation are

shown in black. The residuals from the fit are plotted below each graph. Fitted parameters, the associated errors, and the dependency of the fit are displayed inside the respective graph.

Fits to SR1 ATPase data assuming exclusive binding to the T state are not very different from fits to the full equation. Both are visually reasonable, although the nonexclusive form of the equation seems to represent the data slightly better, particularly as the value for turnover begins to plateau, supported by the slightly higher values for  $R^2$ . Relatively large variations from both fits are evident in the residuals at low ATP concentrations. This is most likely due to the fact that at low ATP concentrations, the overall change in the raw absorbance data is quite small, meaning there is greater scatter and increased error in these measurements.

Since work from previous studies (G. Curien and G. Lorimer, unpublished data) and from Chapter 3 indicates that the exclusive binding assumption is not valid, only the values obtained from the fits to the nonexclusive binding equation are presented in Table 4-1. The value for  $k_T$  was calculated from the fitted parameters  $c$  and  $k_R$ . The absolute error in  $k_T$  was calculated by propagating the percent relative uncertainty ( $\%e$ ) for  $c$  and  $k_R$  as follows:

$$Error = \sqrt{(\%e_1)^2 + (\%e_2)^2} \times 100 \times k_T$$

A few points can be made evaluating the data in Table 4-1. First, at all potassium concentrations, there are large errors associated with the value of  $V_T$ . This is contrasted with the errors in  $V_R$ , which range between 1 and 3%. The difference is most likely due to the fact that the T state in the single ring is virtually unpopulated; due to positive

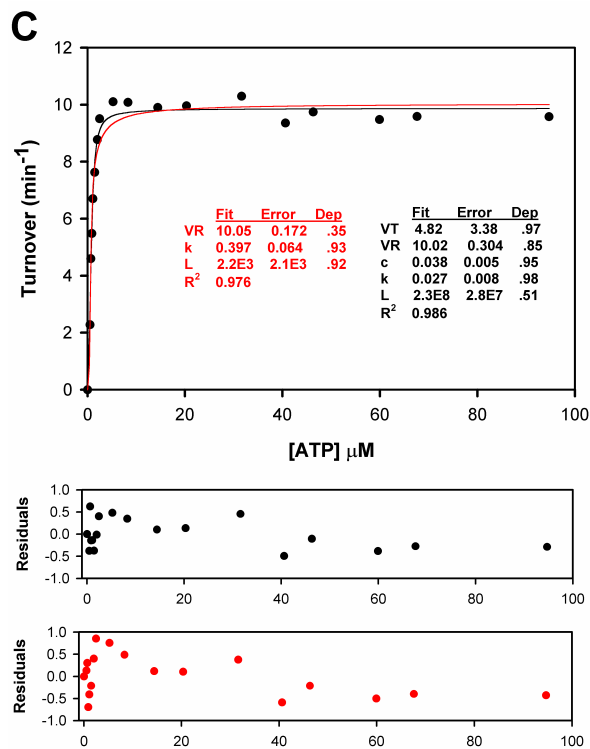
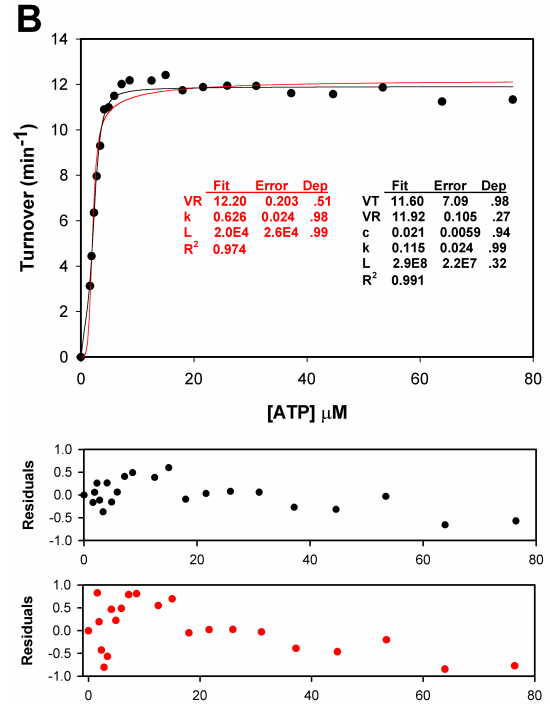
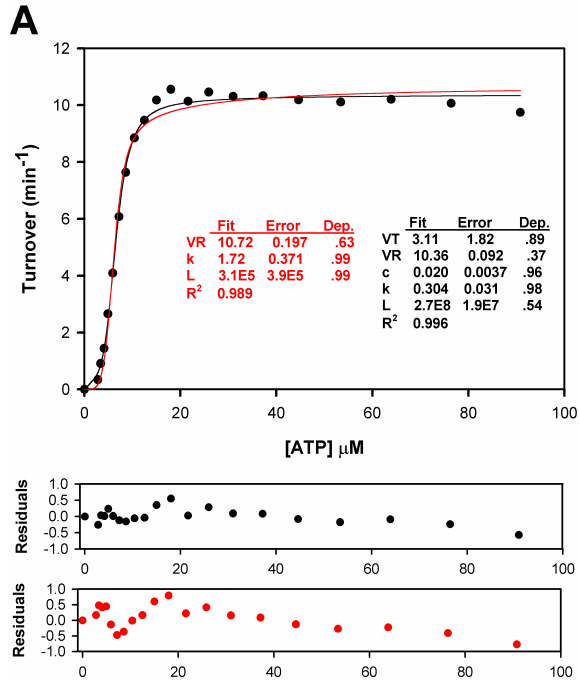


**Figure 4-6: Evaluating the Exclusive Binding Assumption in SR1 ATPase** experiments were performed using 0.5  $\mu\text{M}$  SR1 at 37°C and three different potassium concentrations. The data at each potassium concentration were fit to Equation 1. Fits and the derived parameters shown in **red** utilized the exclusive binding assumption, where  $V_T$  and  $c$  are set to zero. Fits and parameters shown in **black** allowed all variables to float. Residuals are plotted for each fit below the graph in the corresponding color. Although the nonexclusive form of the equation fit the data slightly better (higher  $R^2$ , better residuals), the fits are visually very similar. **A)** 1 mM  $\text{K}^+$ , **B)** 10 mM  $\text{K}^+$ , **C)** 100 mM  $\text{K}^+$ .

	1 mM K <sup>+</sup>	10 mM K <sup>+</sup>	100 mM K <sup>+</sup>
V <sub>T</sub> (min <sup>-1</sup> )	3.1 ± 1.8	11.6 ± 7.1	4.8 ± 3.4
V <sub>R</sub> (min <sup>-1</sup> )	10.4 ± 0.1	11.9 ± 0.1	10.0 ± 0.3
c (k <sub>R</sub> /k <sub>T</sub> )	0.02 ± 0.004	0.02 ± 0.006	0.04 ± 0.005
k <sub>R</sub> (μM)	0.30 ± 0.03	0.11 ± 0.02	0.03 ± 0.008
k <sub>T</sub> (μM)	15.2 ± 3.4	5.5 ± 1.9	0.71 ± 0.23
L ([T]/[R])	2.7E8 ± 2E7	2.9E8 ± 2E7	2.3E8 ± 3E7

**Table 4-1: Parameters Derived from Fits of SR1 ATPase Data to the Nonexclusive Binding Equation**

cooperativity, as soon as ATP is added, rings flip to the R state. States that are not well represented in the data cannot be fit well, regardless of how accurate or abundant the data is [54]. Thus, large errors are also expected for k<sub>T</sub>, for the same reasons. For the most part, however, the values obtained from the fit (within error) support the data obtained from Chapter 3, where V<sub>T</sub> and V<sub>R</sub> were very similar. Second, the average value for c obtained from the fits was 0.03, indicating roughly a 25 to 50-fold difference in the binding affinities for the T and R state. Third, as the potassium concentration increases, the value for both k<sub>T</sub> and k<sub>R</sub> decreased while L remained relatively constant. This suggests that potassium increases the binding affinity for ATP to both the T and R states, but does not affect the equilibrium between the states in the absence of ATP. This is in direct contrast to the assumptions used in the Nested MWC model, where potassium was treated as an allosteric effector which could only modulate the value of L [54]. These observations were then used to constrain the variables in the double ring system (Equation 2).

**4.3.3 Examining the Effects of Potassium on the ATPase Activity of GroEL** As before, ATPase assays were performed using 0.5 μM GroEL at 37°C and 1, 10, and 100 mM potassium (Figure 4-7). The rates obtained at the three potassium concentrations

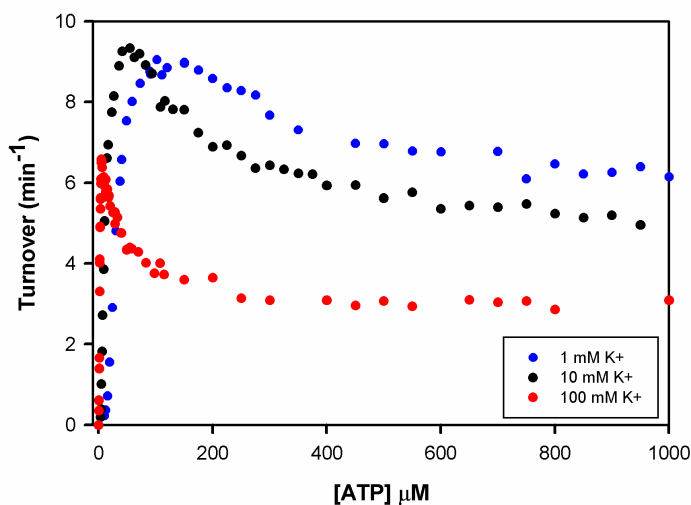


**Figure 4-7: Potassium Affects both  $V_{\max}$  and  $k_R$  in GroEL** ATPase experiments were performed at 37°C using 0.5  $\mu\text{M}$  GroEL at three potassium concentrations. The GroEL concentration was lowered to 0.2  $\mu\text{M}$  to collect data at ATP concentrations less than 1.5  $\mu\text{M}$ . The data obtained here are similar to that previously collected in our lab [63].

agree very well with those obtained previously in our lab [63]. As with SR1, the degree of positive cooperativity increases as the potassium concentration decreases. Unlike SR1, however, the  $V_{\max}$  obtained at the highest ATP concentrations (i.e. the  $V_{\max}$  for the RR state) increases as the potassium concentration decreases. ATPase assays performed at a single ATP concentration with variable potassium indicate the reciprocal nature of the two ligands (Figure 4-8); the shape of the curve obtained with GroEL and variable potassium is similar to the one with variable ATP (J. Grason, unpublished results). This suggests that potassium directly influences the binding of ATP and vice versa, which is supported by fits of the SR1 data.

#### 4.3.4 Fitting the GroEL ATPase Data to the Exclusive and Nonexclusive

**Binding Equations** GroEL ATPase data at the three potassium concentrations were fit to Equation 2 (Figure 4-9, A-C). As before, fits to the exclusive binding form of the equation were obtained by setting  $V_{\text{TT}}$  and  $c$  equal to zero, shown in red. The rates

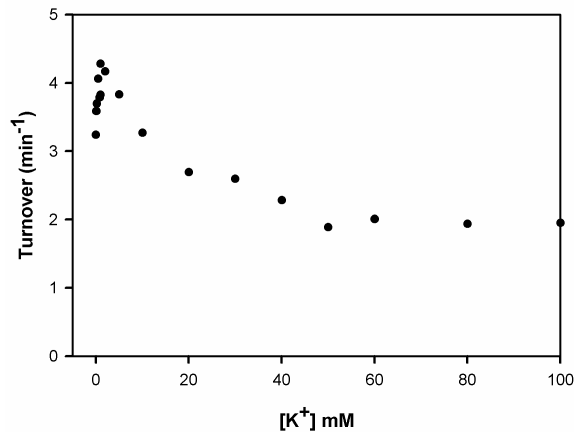


**Figure 4-8: The Reciprocal Nature of the Allosteric Ligands ATP and K<sup>+</sup>** ATPase data was collected with variable potassium using 2  $\mu$ M GroEL at 30°C (J. Grason, unpublished results). The ATP concentration was held constant at 1 mM. Unlike the SR1 data (Figure 4-5), the data with variable potassium looks very similar to that obtained with variable ATP concentrations. With no added potassium, there is still significant turnover. However, it is not known how much contaminating potassium may be present.

predicted for the TR state using the exclusive binding equation are somewhat misleading, since the reported values are per subunit. However, with exclusive binding, only one ring (the one in the R state) is assumed to be hydrolyzing ATP, and so the rates must be doubled to obtain the rate per functional subunit.

In order to limit the number of variables that must be fit to the nonexclusive form of the equation, some of the variables were constrained using experimentally derived values. First, the rate of turnover in the presence of saturating substrate protein, which is thought to shift the allosteric equilibrium towards the TT state, is approximately 18 min<sup>-1</sup> [49]. Moreover, the rate is independent of the potassium concentration used in the assay [63]. Secondly, fitting results from the single ring suggested that terms  $c$ ,  $L_1$ , and  $L_2$  should not change with potassium concentration. Thus, the values for  $V_{TT}$  and  $c$  can be fixed for the first potassium concentration, while the other variables are allowed to float.

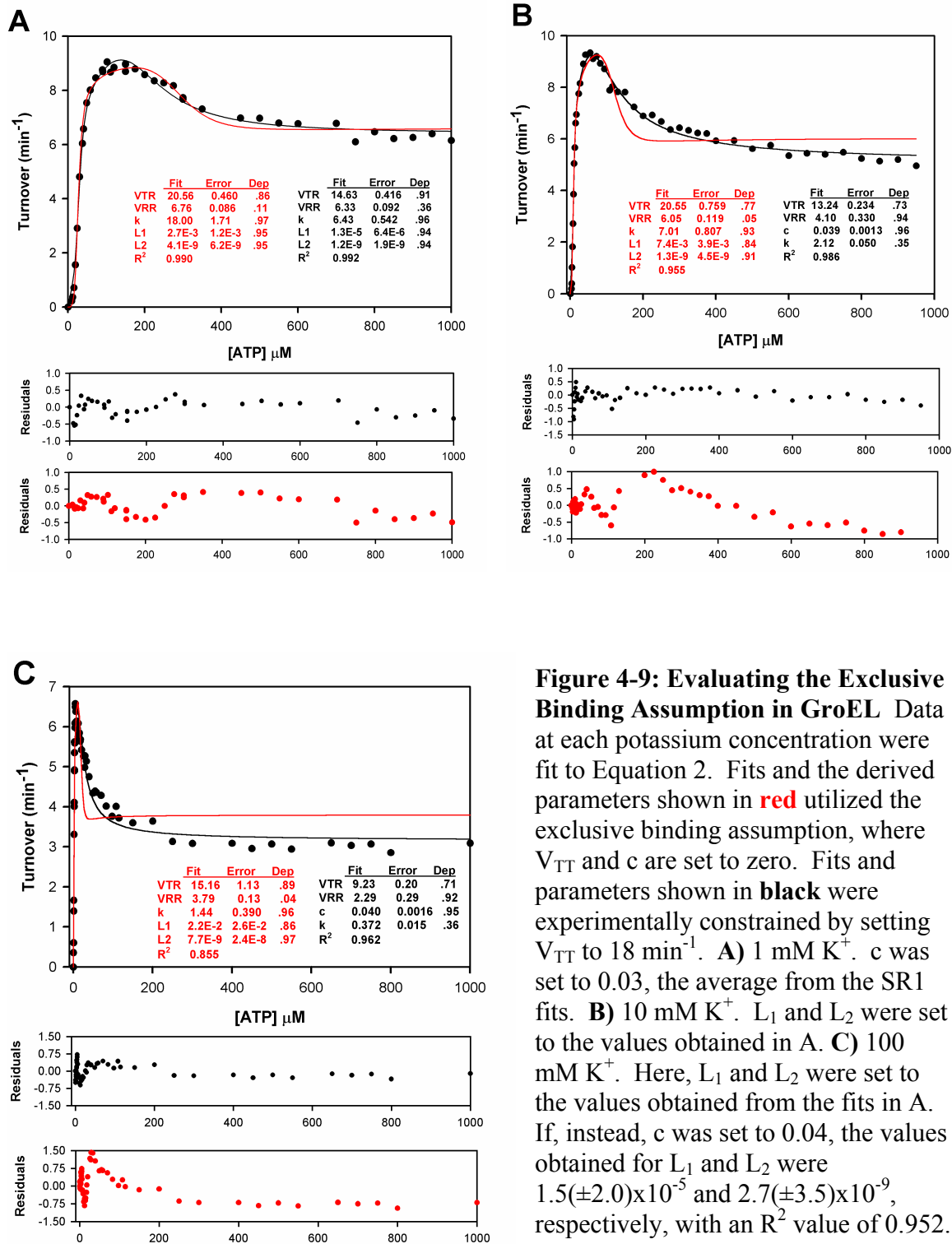


**Figure 4-9: Evaluating the Exclusive Binding Assumption in GroEL Data** at each potassium concentration were fit to Equation 2. Fits and the derived parameters shown in **red** utilized the exclusive binding assumption, where  $V_{TT}$  and  $c$  are set to zero. Fits and parameters shown in **black** were experimentally constrained by setting  $V_{TT}$  to  $18 \text{ min}^{-1}$ . **A)**  $1 \text{ mM K}^+$ .  $c$  was set to  $0.03$ , the average from the SR1 fits. **B)**  $10 \text{ mM K}^+$ .  $L_1$  and  $L_2$  were set to the values obtained in A. **C)**  $100 \text{ mM K}^+$ . Here,  $L_1$  and  $L_2$  were set to the values obtained from the fits in A. If, instead,  $c$  was set to  $0.04$ , the values obtained for  $L_1$  and  $L_2$  were  $1.5(\pm 2.0) \times 10^{-5}$  and  $2.7(\pm 3.5) \times 10^{-9}$ , respectively, with an  $R^2$  value of  $0.952$ .

Once values for  $L_1$  and  $L_2$  are determined, they can be fixed for the other potassium concentrations, reducing the number of dependent variables from seven to four. Specifically, this approach was used by fitting the data at 1 mM  $K^+$  with  $V_{TT}$  fixed at 18  $\text{min}^{-1}$  and  $c$  fixed at 0.03 (an average of the values obtained with SR1). A fit performed on the 1 mM data fixing only  $V_{TT}$  yielded a value for  $c$  of  $0.033 \pm 0.004$ . Fits to the other two potassium concentrations were performed with  $V_{TT}$ ,  $L_1$  and  $L_2$  fixed, while the other variables were allowed to float (Table 4-2). This can also be performed in reverse. Fixing  $V_{TT}$  to 18  $\text{min}^{-1}$  and  $c$  to 0.04 for the 100 mM  $K^+$  data yields similar values for  $L_1$  and  $L_2$  compared to those obtained at 1 mM  $K^+$ . This indicates that this method for fitting the double ring data is fairly robust, even though the errors for the values of  $L_1$  and  $L_2$  are relatively high.

	<b>1 mM <math>K^+</math></b>	<b>10 mM <math>K^+</math></b>	<b>100 mM <math>K^+</math></b>
$V_{TT}$ ( $\text{min}^{-1}$ )	<i>18</i>	<i>18</i>	<i>18</i>
$V_{TR}$ ( $\text{min}^{-1}$ )	$14.6 \pm 0.4$	$13.2 \pm 0.2$	$9.2 \pm 0.2$
$V_{RR}$ ( $\text{min}^{-1}$ )	$6.3 \pm 0.1$	$4.1 \pm 0.3$	$2.3 \pm 0.3$
$c$ ( $k_R/k_T$ )	<i>0.03</i>	$0.04 \pm 0.001$	$0.04 \pm 0.002$
$k_R$ ( $\mu\text{M}$ )	$6.4 \pm 0.54$	$2.1 \pm 0.05$	$0.37 \pm 0.01$
$k_T$ ( $\mu\text{M}$ )	$214 \pm 32$	$54 \pm 2$	$9.3 \pm 0.5$
$L_1$ ( $[TR]/[TT]$ )	$1.3\text{E-}5 \pm 6\text{E-}6$	<i>1E-5</i>	<i>1E-5</i>
$L_2$ ( $[RR]/[TR]$ )	$1.2\text{E-}9 \pm 2\text{E-}9$	<i>1E-9</i>	<i>1E-9</i>

**Table 4-2: Parameters Derived from Fits of GroEL ATPase Data to the Non-exclusive Binding Equation.** Parameters in italics were fixed, while the other values were allowed to float. The value for  $k_T$  was calculated from the two fitted parameters,  $k_R$  and  $c$ .

At the lowest potassium concentration, a good fit can be obtained using either form of the equation. However, at 10 mM and 100 mM potassium, the difference becomes much more obvious. Comparisons at 10 mM  $K^+$  are particularly interesting

since the original data used to develop the nested cooperativity model were collected at this concentration [50]. The data used by Horovitz contained only 18 data points. The 10 mM  $K^+$  data presented here has 45 data points. This may be the explanation for why the two data sets look so different; the data presented in the original paper simply did not have enough data to properly define the shape of the curve, particularly on the downward slope at the higher ATP concentrations ( $>100 \mu\text{M}$ ). The values obtained here for  $L_1$  and  $L_2$  are not drastically different than those initially reported:  $2.0 (\pm 1.0) \times 10^{-3}$  and  $6.0 (\pm 3.2) \times 10^{-9}$  for  $L_1$  and  $L_2$ , respectively [50].

#### **4.4 Discussion**

**4.4.1 Evaluating a New Equation for Nested Cooperativity** Under certain conditions, the exclusive binding assumption seems to work fairly well. Particularly with SR1, the fits using the two equations are virtually indistinguishable from a visual standpoint. Since only two states are present in the single ring, this is not entirely surprising. The T state is only barely populated in the presence of ligand (due to the absence of negative cooperativity) and has an affinity for ATP that is reduced 30-fold compared to the R state. Despite the fits being visually similar, the parameters obtained are very different. The values for  $k_R$  differ by 5-fold, and L differs by 3 to 4 orders of magnitude. In trying to evaluate what is a reasonable value for the allosteric constant in the single ring, one might expect that it would approximate the value for  $L_1$  in the double ring as it transitions from TT to TR. It is not clear, however, that this is necessarily the case. Certainly the values obtained here ( $3 \times 10^8$  in SR1 versus  $1 \times 10^5$  in GroEL, expressed as  $[T]/[R]$  and  $[TT]/[TR]$ , respectively) are not similar at all. Cryo-EM structures of GroEL have indicated asymmetry between the rings even in the absence of ATP [102].

Perhaps the presence of a second ring, in fact, influences the allosteric equilibrium of the first transition. However, the values obtained from the fits here would suggest that the equilibrium in the single ring is shifted more towards the T state than in the double ring. This is hard to rationalize structurally.

The exclusive binding assumption does not work nearly as well when applied to the double ring system, despite the fact that it was for this system that the assumption was first applied. This makes sense since there are now three states which are variously populated: TT, TR and RR. Although the TT state will not be very populated, the TR state makes a substantial contribution to the rate, and therefore must be considered as having two functional rings instead of just one. We believe that the data obtained here, which comes from a real time assay, monitored every 0.4 seconds over three minutes, with an ATP regeneration system, offers superior data for evaluation. The original data was obtained using a  $^{32}\text{P}$  fixed endpoint assay which allows for the build-up of ADP [50], a potent inhibitor of ATP hydrolysis by GroEL [49]. Moreover, the number of data points used here, sometimes more than twice as many points as used in the original paper, also provides a more accurate picture of the ATPase profile of GroEL. Thus, while the exclusive binding assumption appeared to fit the data in the original analysis [50], more likely the analysis was underdetermined and the shape of the curve was ill defined.

This does not mean, however, that the values for the allosteric constants derived here can be accepted at face value. The errors associated with the fitted parameters are quite high, 45% for  $L_1$  and 150% for  $L_2$ . Although the best fits are represented here after a variety of initial guesses and constraints, there is no way to know for sure that this fit represents the global, rather than a local, minima. That said, the trends observed are

consistent between the single and double ring and between the various potassium concentrations. Thus, it is reasonable to suggest that, contrary to previous conjectures [54, 63], that the allosteric constants are not affected by the potassium concentration.

**4.4.2 A Proposal for the Role of Potassium** X-ray crystal structures of GroEL in the presence of potassium have suggested that the monovalent ion binds to the same site as ATP and interacts with the  $\gamma$ -phosphate of the nucleotide [103]. This is supported by the work presented here, where potassium influences the binding affinity in both the T and R states, leaving the allosteric equilibrium in the absence of ATP unchanged. This role for potassium has been previously suggested [62] and accounts for the effects on positive cooperativity seen at low ATP concentrations. However, it is the effects of potassium on the negative cooperativity of GroEL that is novel; the  $V_{\max}$  for GroEL at the highest ATP concentration measured increases with decreasing potassium (Figure 4-7). The reciprocal nature of ATP and  $K^+$  binding in GroEL is demonstrated in Figure 4-8 (J. Grason, unpublished results), which indicates that the binding of one ligand directly influences the binding of the other, as dictated by allosteric theory. The explanation for this effect comes from previous FRET studies performed in our lab, where it was discovered that the dissociation of ADP from the *trans* ring of the asymmetric complex was the rate limiting step in GroES dissociation from the *cis* ring [49]. More recently, studies using fluorescently labeled phosphate binding protein, which changes fluorescence upon binding the  $P_i$  released from ATP hydrolysis, indicate that product release is also rate limiting in the absence of GroES (J. Grason, unpublished results). Thus, potassium influences the  $V_{\max}$  of the RR state by altering the affinity of the product ADP, which must be released before a new round of hydrolysis can occur. At low

potassium, the affinity for nucleotide is reduced, so ADP is released more quickly and the  $k_{\text{cat}}$  increases. At high potassium, the ADP is bound more tightly, and thus the rate of turnover is lower. This effect is visible with GroEL, but not SR1. Potassium and substrate protein are thought to have similar, but opposing, effects on the rate of ATP hydrolysis. The presence of unfolded substrate protein shifts the equilibrium towards the T state, which has a lower affinity for nucleotide and thus releases the bound ADP, allowing for faster turnover, similar to the explanation given here for the effect of potassium. Substrate protein also has no stimulatory effect on SR1 ATPase rates, suggesting that both SP and  $K^+$  play a role in negative, as well as positive, cooperativity.

## **Chapter 5**

### **Stopped Flow Analysis of GroES Association to the Asymmetric Complex: Looking at Inter-Ring Communication**

## 5.1 Introduction

As previously discussed in Chapter 1, the resting state of the GroEL reaction cycle can be thought of as the asymmetric complex, GroEL<sub>14</sub>-[ADP]<sub>7</sub>-(SP)-GroES<sub>7</sub>. The brackets indicate the ADP in the *cis* ring is not free to exchange with the surrounding solution, and the parenthesis indicate that SP may or may not be encapsulated in the *cis* ring, since it is not a requisite part of the chaperonin cycle. Although the asymmetric complex is primed for ligand release after hydrolysis of nucleotide in the *cis* ring, it is extremely stable in the absence of ATP, on the order of days [104]. It is only once ATP binds to the *trans* ring that GroES, ADP, and SP are released from the *cis* ring [47]. But the exact nature of the signal transmitted between the rings, and to what extent symmetric complexes may play a role, is not understood.

Previous work by Rye *et al.* examined the kinetics of GroES dissociation and association using two mutants, GroEL E315C and GroES 98C, which served as a FRET pair when labeled with donor and acceptor fluorophors [20]. Because the efficiency of energy transfer is directly related to the distance between the two probes, GroES binding and release are easily measured. When GroES is bound, the two probes are approximately 36Å apart, which provides for strong acceptor emission [10]. When GroES is released, the distance between the two probes is essentially infinite, and no energy transfer occurs. Performing a series of stopped-flow experiments measuring acceptor fluorescence, they found GroES release to be a two step mechanism in which ATP hydrolysis in the *cis* ring is the rate limiting step in the presence of substrate protein. However, when our lab performed dissociation experiments under slightly different conditions, it became apparent that the release of ADP from the *trans* ring of an

### Events in the Chaperonin Cycle

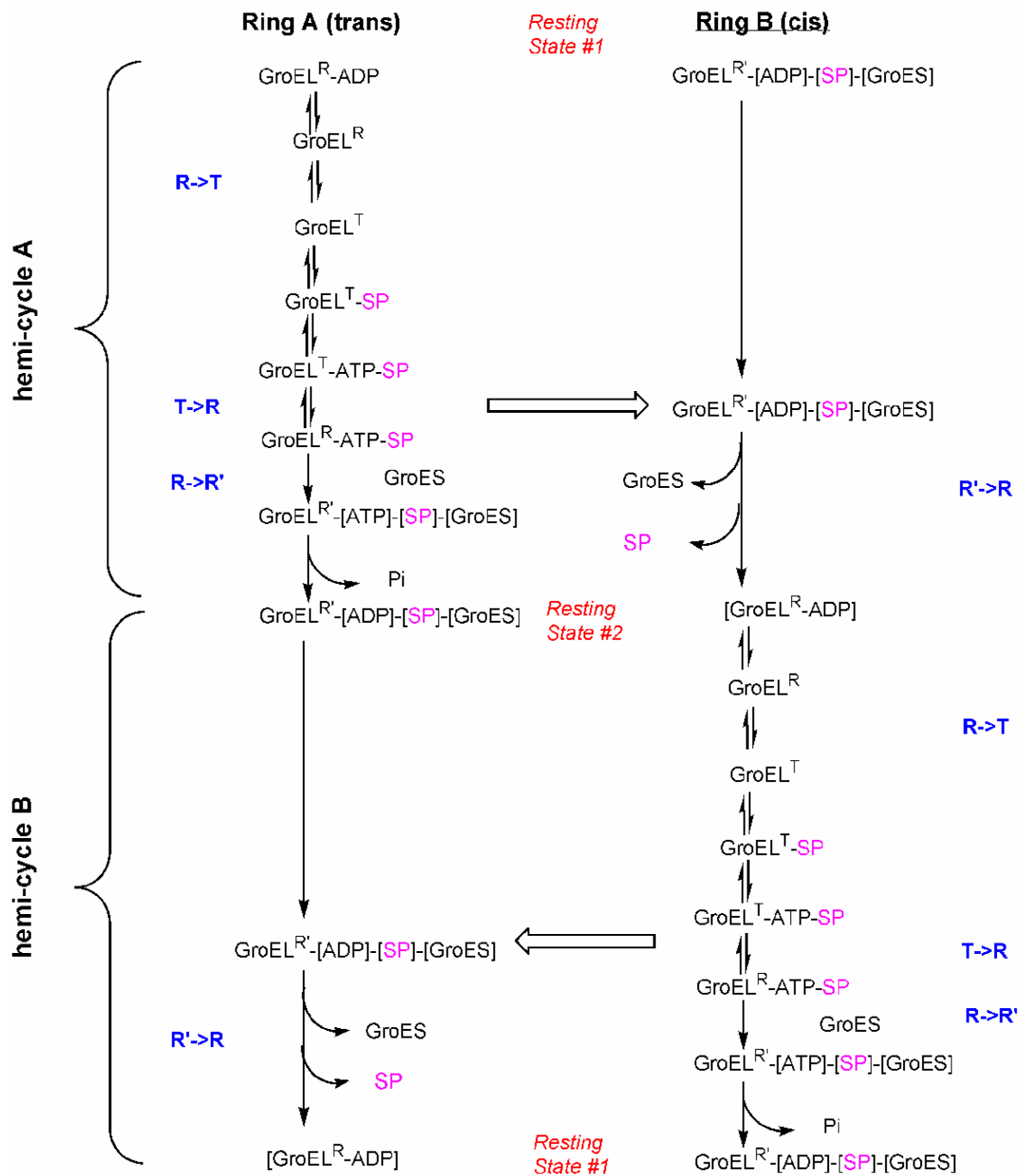


**Figure 5-1: The GroEL Reaction Cycle** GroEL has been described as a “two-stroke motor[21].” Each ring of GroEL (ring A and B) undergoes a complete cycle, out of phase with the other, such that a complete cycle is composed of two hemicycles. There are two resting states, which can be described as an asymmetric complex with ADP bound to the *trans* ring. Ligands which are not exchangeable with the solution are shown in brackets, e.g. [ADP]. The power stroke, represented by the block arrows, is the concerted T to R transition in the *trans* ring, which is believed to actively unfold the substrate protein just prior to encapsulation. The allosteric changes occurring within each ring are shown in blue. (Figure kindly provided by Dr. George Lorimer)

asymmetric complex, and/or a conformational change associated with it, was actually the rate limiting step [49]. Moreover, saturating amounts of substrate protein bound to the *trans* ring can speed the dissociation of *cis* ligands as much as 1000-fold, presumably by “locking” the ring in the T state, which has a lower affinity for ADP than the R state [49]. The Rye group also looked at the kinetics of GroES association to the *trans* ring [20]. However, in light of the numerous discrepancies with regards to the dissociation experiments, this project set out to re-examine the kinetics of GroES association to the *trans* ring.

There are two benefits to studying the association reaction kinetics. First, such experiments would flesh out the GroEL reaction cycle (Figure 5-1), where the two rings act as a “two-stroke motor” with identical, alternating cycles [21, 49]. Previous work indicates that, in the presence of SP, dissociation of ligands from the *cis* ring takes up less than 0.2 seconds of the 12 second cycle time [49]. Filling in the time for association would lend credence to the model and narrow the window available for encapsulation and passive folding within an isolated environment.

Secondly, comparison of association and dissociation data also speaks to the presence of symmetric complexes as intermediates in the normal reaction cycle. Various studies using electron microscopy and analytical ultracentrifugation have confirmed the existence of symmetric particles, or “footballs” [105-108]. Under conditions that mimic what are believed to be *in vivo* concentrations of salts such as  $Mg^{2+}$ , up to 58% of the complexes detected were symmetric [18]. The presence of “footballs” appears to be strongly dependent on the concentrations of  $K^+$  and ADP; high  $K^+$  and low ADP favor formation of the symmetric complex [16]. Negatively stained electron microscopy

revealed that substrate protein may be trapped inside the GroEL cavity of both rings simultaneously, although this may be an artifact of the staining [105]. Although such complexes appear symmetric, fluorescence anisotropy experiments with a pyrene-labeled GroES indicated that symmetric complexes are only formed when a mixture of ADP and AMP-PNP nucleotides are present [59]. This suggests that symmetric particles are actually asymmetric with regards to nucleotide: one ring of GroEL contains ATP, while in the other ATP has already been hydrolyzed to ADP. Despite overwhelming evidence for their existence, a stopped-flow kinetic analysis failed to show a requirement for GroES binding to the *trans* ring for *cis* ligand release [20]. For this reason, we decided to re-examine the experimental conditions for association to see if similar results were obtained.

## ***5.2 Methods Specific to Chapter 5***

***5.2.1 Purification and Labeling of Mutant Proteins*** The two mutants used in this study, GroEL E315C and GroES 98 C, were previously created in our lab by Dr. John Grason [49]. Changing GroEL residue 315 to cysteine and adding a cysteine residue to the C-terminus of GroES allowed us to label each protein with a fluorescent probe, thereby creating a FRET pair sensitive to GroES binding and dissociation [20]. Unlike the mutants used by the Rye group, the mutants used in this study were made in a wild type background with the three native cysteines intact. Previous work in our lab demonstrated that the native cysteines were not labeled to any significant extent [49]. GroEL E315C was purified as previously described in Chapter 2 for GroEL wild type. The GroES 98C purification was also identical to that previously described except for a

minor adjustment to the SP Sepharose conditions. The column was run at pH 4.8, as opposed to pH 5.0, and was eluted with a 150 ml gradient from 0 to 300 mM NaCl.

Donor and acceptor probes, IAEDANS and fluorescein-5-maleimide (F5M), were purchased from Molecular Probes. Stock solutions were made in anhydrous DMF to a final concentration of 20 mM. Immediately prior to labeling, mutant proteins were reduced with 20 mM DTT for 30 minutes at room temperature. The DTT was then removed by gel filtration on a PD-10 column equilibrated with chelexed 10 mM Tris, pH 7.5, 10 mM MgAc.

GroEL 315C was labeled at a concentration of 350  $\mu$ M, using a 1.5-fold excess of IAEDANS label over GroEL monomers. The reaction was carried out in the dark at room temperature for 40 minutes. Unreacted cysteines were quenched with a molar equivalent of NEM followed by 6 mM DTT. Excess label was removed by desalting on a PD-10 equilibrated with the same chelexed 10 mM Tris, pH 7.5, 10 mM MgAc. The extent of labeling was determined spectrophotometrically by comparing protein and label concentrations at 280 nm and 336 nm, respectively ( $\epsilon_{280}=9600 \text{ M}^{-1}\text{cm}^{-1}$  and  $\epsilon_{336}=5400 \text{ M}^{-1}\text{cm}^{-1}$ ). Conditions used here resulted in approximately 60% labeling. Labeled GroEL will hereafter be referred to as GroEL<sup>D</sup>, since it serves as the donor in the FRET pair.

GroES 98C was labeled at a concentration of 120  $\mu$ M, using a 3-fold excess of F5M over ES monomers. The reaction was carried out in the dark for 10 minutes at room temperature and then quenched with 5 mM DTT. Excess label was removed by desalting on a PD-10 equilibrated with chelexed 10 mM Tris, pH 7.5. Because the label interferes with the UV spectra at 280 nm, protein concentration was determined by both Bradford assay and quantitative SDS-PAGE, as described in Chapter 2. The label concentration

was determined by checking the absorbance at 491 nm ( $\epsilon=74,500 \text{ M}^{-1}\text{cm}^{-1}$ ). The extent of labeling under these conditions was 22%. Labeled GroES will hereafter be referred to as GroES<sup>A</sup>, since it serves as the acceptor of the FRET pair. Previous experiments in our lab determined that the kinetics of GroES<sup>A</sup> dissociation from the asymmetric complex were independent of the extent of labeling of either GroEL<sup>D</sup> or GroES<sup>A</sup> [49]. The  $R_0$  value for this pair, which represents the distance at which transfer efficiency is 50%, is approximately 40Å.

**5.2.2 Stopped-flow Fluorescence Measurements** All fluorescence measurements were made in an Applied Photophysics SX18MV-R stopped-flow apparatus. The instrument was configured with a 20  $\mu\text{l}$  flow cell with a pathlength of 2 mm and a 530 nm cutoff filter. The monochromator entry and exit slits were each set to 2 mm, which corresponds to a band pass of 9.3 nm. The syringes and flow cell were kept at a constant temperature of 30°C using a circulating water bath. The shot volume was set to approximately 170  $\mu\text{l}$ , consuming 85  $\mu\text{l}$  from each syringe for each shot. The excitation wavelength, 336 nm, was identical to that used in previous studies [20, 49].

Both dissociation and association experiments were performed in this study. The only difference in experimental set-up was the type of GroES used in each syringe. For dissociation experiments, GroES<sup>A</sup> was used to make the asymmetric complex and GroES<sup>wt</sup> was loaded in syringe B as a competitor. For association experiments, the reverse was true: GroES<sup>A</sup> was in syringe A and GroES<sup>wt</sup> was in syringe B. Both experiments used a 5-fold excess of GroES in syringe B. This had the consequence of using much more fluorescent material in the association experiments than in the dissociation experiments, making it impossible to perform the two experiments at the

same instrumental settings (specifically PMT). In order to directly compare amplitudes and rates, the traces were normalized. Association and dissociation experiments were always performed during the same experimental session, so that conditions were as close to identical as possible. Figure 5-2 shows a schematic of the experimental set-up.

Unless otherwise stated, the conditions for experiment were as follows. The asymmetric complex was formed using 40  $\mu\text{M}$  GroEL and 40  $\mu\text{M}$  GroES in 20 mM Tris, pH 7.5, 10 mM MgAc, 100 mM KAc, 2 mM DTT, and 300  $\mu\text{M}$  ATP. This was allowed to incubate for 30 minutes or more at room temperature, so that all the ATP was converted to ADP. The solution was then desalted on a PD-10 column equilibrated with 20 mM Tris, pH 7.5, 10 mM MgAc, 100 mM KAc, and 2 mM DTT in order to remove excess nucleotide and any ADP bound to the *trans* ring, which is freely exchangeable. ADP could then be added back to the solution, if desired, with a final concentration of 15  $\mu\text{M}$  ADP and 3  $\mu\text{M}$  GroEL. This constituted the solution used in syringe A. Syringe B contained 15  $\mu\text{M}$  competitor GroES (5-fold excess over GroEL and GroES in syringe A) and 4 mM ATP in the same buffer as used in syringe A. Both solutions were degassed on 0.2  $\mu\text{m}$  filters prior to use. The solutions from each syringe were mixed 1:1 in the flow cell and acceptor emission (maximum at 519 nm) was followed over time using a 530 nm cut-off filter.

For each condition measured, oversampling was used to reduce the amount of noise in the signal. This is a feature where the instrument takes data every 40  $\mu\text{sec}$ , and then averages several consecutive readings to give a total of 1000 data points. To also reduce noise, several traces were averaged to obtain the final trace shown. The number of traces used in the average depended on the time being monitored. Measurements less

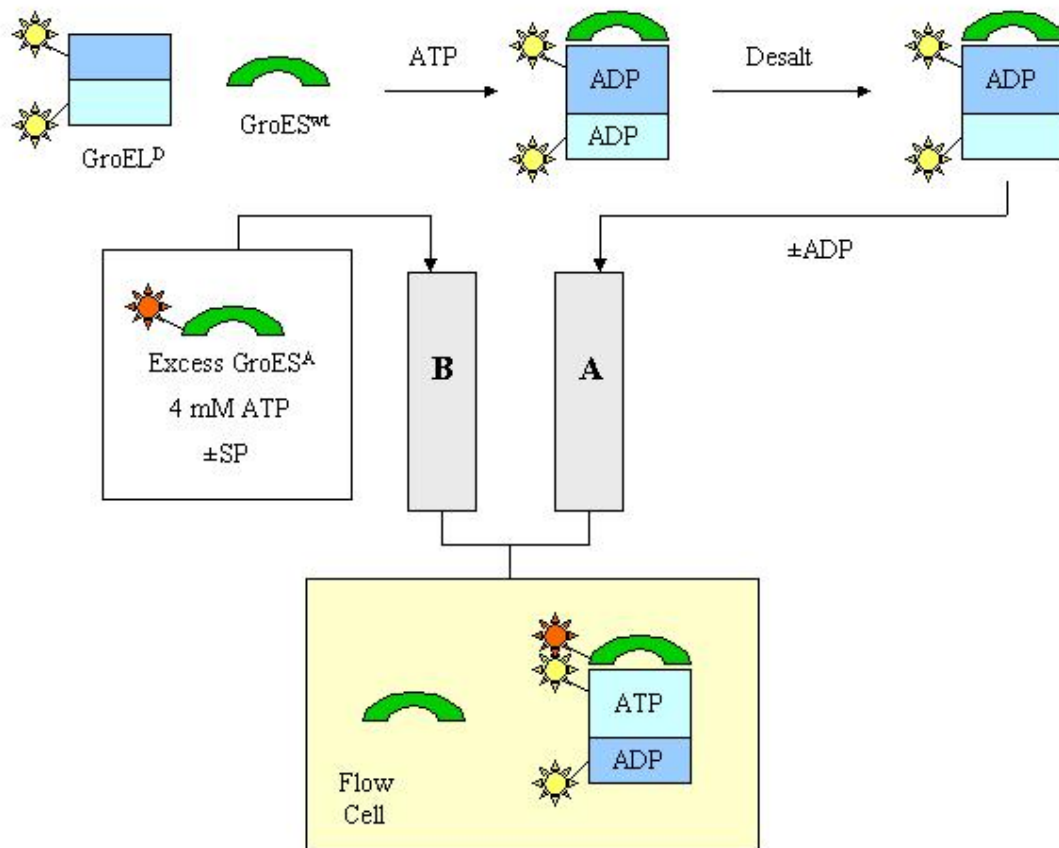


**Figure 5-2: Schematic of Stopped Flow Experiment** This set-up is similar to experimental designs used previously [20, 49]. The asymmetric complex was formed by combining GroEL<sup>D</sup>, GroES<sup>wt</sup>, and ATP in a buffered solution of 20 mM Tris, pH 7.5, 10 mM MgAc, 100 mM KAc, and 2 mM DTT. All of the ATP was consumed over the course of 30 minutes at room temperature. The complex was then desalted on a PD-10 column to remove excess nucleotide from the solution and the *trans* ring of GroEL<sup>D</sup>-GroES<sup>wt</sup> complex. The ADP in the *cis* ring remains trapped. Before adding the desalted complex to syringe A, ADP may be added back at the desired concentration. Syringe B contained 4 mM ATP, GroES<sup>A</sup>, and where noted, denatured substrate protein, in the same buffered solution as syringe A. The solutions were rapidly mixed 1:1 in the flow cell, where emission from the acceptor fluorophore could be monitored over time. The set-up as shown here is for association reactions. Dissociation can be monitored by switching the GroES used to make the asymmetric complex and in syringe B.

than 0.2 sec contain 8-12 traces, whereas measurements at 5 sec contain 5-8 traces. It is possible to hold the pneumatic pressure on the syringes for traces of 5 sec or less. This was done whenever possible, since traces without the pressure held often contained slight interferences. The dead time of the instrument, as stated in the accompanying instrumental documentation, is approximately 1 msec. For this reason, data collected before 3 msec were not used.

**5.2.3 GroEL versus GroES Competitor Experiments** These experiments were designed to test for the existence of symmetric complexes by examining whether the presence of GroES in the challenge solution stimulated dissociation of the *cis* ring. For this set of experiments, the syringe A solution was prepared exactly as described in section 5.2.2. Syringe B contained either 15  $\mu\text{M}$  GroEL<sup>wt</sup> or GroES<sup>wt</sup> along with the other components previously described. Because symmetric complexes are favored when the ADP concentrations are low, we also tried utilizing an ATP regeneration system consisting of 13 units of rabbit muscle Type VII pyruvate kinase (Sigma) and 2 mM PEP in addition to the other components in syringe B. To test whether increasing amounts of substrate protein affected the traces, acid-denatured MDH (0.11  $\mu\text{M}$ ) was added to syringe A and allowed to reach equilibrium.

### 5.3 Results

**5.3.1 GroES Association to the Trans Ring is Diffusion Limited** The FRET pair used in this study, IAEDANS labeled GroEL E315C and F5M labeled GroES 98C, come within approximately 36Å when GroES is bound to GroEL. Previous experiments verified that energy transfer is responsible for the signal change in donor and acceptor channels upon ATP binding to the *trans* ring of a GroEL<sup>D</sup>-GroES<sup>A</sup> complex [20, 49].

Thus, the binding of GroES<sup>A</sup> to the *trans* ring of a GroEL<sup>D</sup>-GroES<sup>wt</sup> asymmetric complex should result in an increase in acceptor fluorescence.

The basic experimental design was similar to that used in the previous experiments [20, 49]. The asymmetric complex was formed and desalted as described. This was then loaded into syringe A of the stopped-flow instrument, with a final GroEL concentration of 3  $\mu$ M. Syringe B contained GroES<sup>A</sup> (usually at a 5-fold excess) and 4 mM ATP in the same buffered solution as used in syringe A. When mixed 1:1, GroES<sup>A</sup> binds to the *trans* ring, causing an increase in the observed signal. Since GroES<sup>A</sup> is in excess over the GroES<sup>wt</sup>, a small adjustment to the final signal is observed over long time traces as the system proceeds past the initial turnover and reaches equilibrium (Figure 5-3).

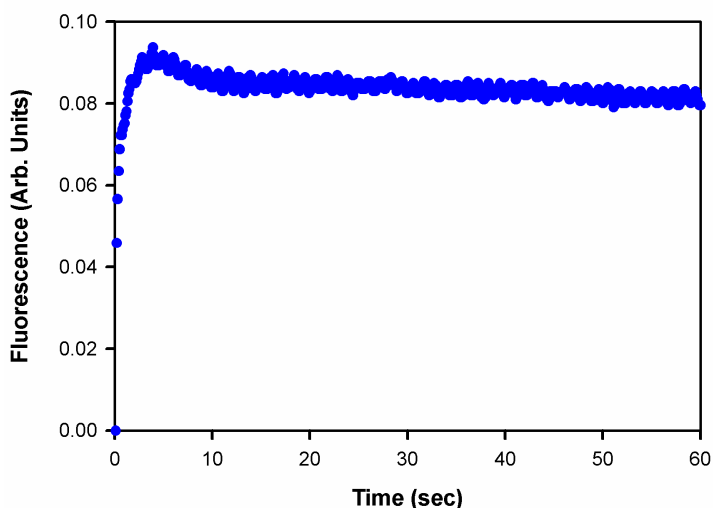


**Figure 5-3: Long Time Course Association Data** Binding of GroES<sup>A</sup> to an asymmetric complex of GroEL<sup>D</sup>-GroES<sup>wt</sup> causes an increase in acceptor fluorescence. The small decrease observed after  $\sim$ 5 seconds is due to the equilibrium between GroES<sup>A</sup> and GroES<sup>wt</sup> after the first turnover. The linear decline is due to a gradual quench of the fluorophor.

Previous experiments found that binding of GroES<sup>A</sup> to GroEL<sup>D</sup> tetradecamers in the presence of ATP was fast and bimolecular, with a rate constant of  $5 \times 10^7 \text{ M}^{-1}\text{s}^{-1}$  [20, 40]. However, they found that the kinetics of GroES<sup>A</sup> binding to the *trans* ring of GroEL<sup>D</sup>-ADP bullets was independent of concentration [20]. Because the rate of association also matched the rate of dissociation, the authors concluded that GroES could not bind to the *trans* ring of GroEL until the *cis* ligands, particularly the *cis* GroES, had departed.

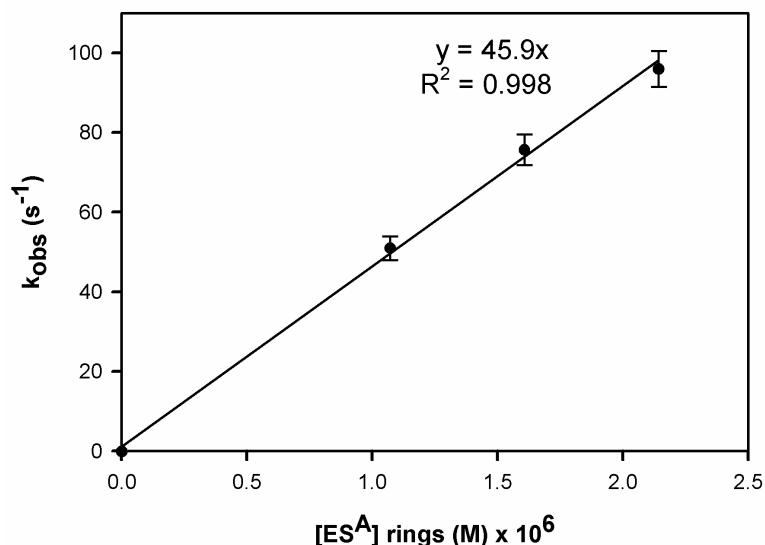
Here, a limited pseudo first-order experiment was performed, where the concentration of GroEL<sup>D</sup> and ATP was held constant and the concentration of GroES<sup>A</sup> rings in syringe B was varied between a 5-fold and 10-fold excess over asymmetric complexes. The asymmetric complex, GroEL<sup>D</sup>-GroES<sup>wt</sup>, was desalted prior to being loaded into syringe A. The association reaction was complete after 0.2 seconds. Eleven traces for each condition were averaged and then fit to a double exponential equation using Sigma Plot 8.0. The rate constants obtained from these fits are shown in Table 5-1.

	<b>5x</b>	<b>7.5x</b>	<b>10x</b>
$k_{\text{obs}} (1)$	$51.00 \pm 2.96$	$75.71 \pm 3.85$	$96.06 \pm 4.52$
$k_{\text{obs}} (2)$	$11.19 \pm 2.68$	$10.64 \pm 2.05$	$12.00 \pm 1.72$

**Table 5-1: Observed Rate Constants at Variable GroES<sup>A</sup> Concentrations**

Only one of the observed rate constants varied with concentration. This was plotted, as shown in Figure 5-4, and a bimolecular rate constant of  $4.6 \times 10^7 \text{ M}^{-1}\text{s}^{-1}$  was derived from a linear regression of the data. This value is nearly identical to results obtained by previous researchers for GroEL<sup>D</sup> tetradecamers alone, but is in contrast with the result

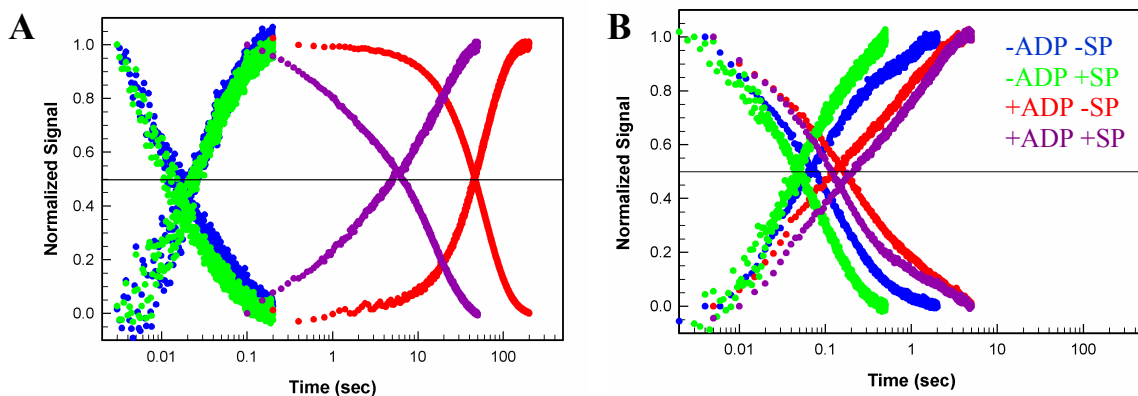
measuring association to the *trans* ring of the GroEL<sup>D</sup>-GroES<sup>wt</sup> asymmetric complex [20]. Our results clearly indicate that association under these conditions is bimolecular and diffusion limited [109].



**Figure 5-4: GroES Association is Diffusion Limited** A limited, pseudo first-order experiment in which the GroEL<sup>D</sup> and ATP concentration were maintained at 1.5  $\mu$ M and 2 mM, respectively, while the concentration of competitor GroES<sup>A</sup> was varied. A plot of the pseudo first-order rate constants ( $k_{\text{obs}}$ ) versus the concentration of competitor GroES<sup>A</sup> in rings is shown. The bimolecular rate constant obtained from the linear regression is  $4.6 \times 10^7 \text{ M}^{-1}\text{s}^{-1}$ .

**5.3.2 Comparing the Kinetics of Association and Dissociation** Previous studies in our lab have shown that the rate limiting step in the dissociation of GroES from the *cis* ring of the asymmetric complex is the release of ADP from the *trans* ring [49]. We wanted to examine whether this was also true for GroES association to the *trans* ring, and whether the addition of SP or the removal of exchangeable ADP from the *trans* ring had the same effects on association as it does for dissociation. The only difference between the experimental set-ups for association and dissociation was the GroES used to form the starting asymmetric complex and as a competitor in syringe B. For association, GroES<sup>wt</sup>

is used to make the complex, and GroES<sup>A</sup> is the competitor. The reverse is true for dissociation (see Figure 5-1). ADP was added to syringe A at a concentration of 15  $\mu\text{M}$ , while substrate protein (acid denatured  $\alpha$ -LA) was added to syringe B at a concentration of 1.1  $\mu\text{M}$ , a 5-fold excess over asymmetric complexes. Substrate protein was added to syringe B to prevent equilibrium binding effects. All experiments were performed with 100 mM KAc. Because association and dissociation could not be measured at the same PMT voltages, the averaged traces were normalized and then plotted (Figure 5-5A).



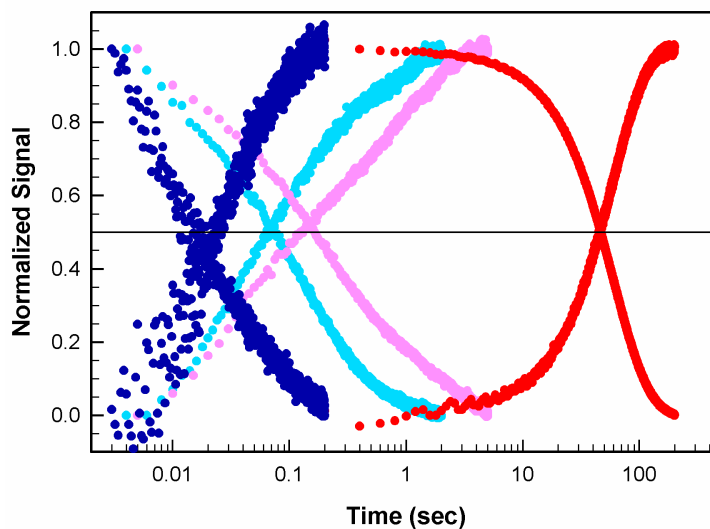
**Figure 5-5: Association and Dissociation Data,  $\pm$ ADP and  $\pm$ SP, at 100 mM and 10 mM  $\text{K}^+$**  The kinetics of GroES binding and release are strongly affected by ADP, SP, and  $\text{K}^+$ . The place where the horizontal line crosses the data marks the mean residence time for GroES binding or release. The fact that association and dissociation have the same mean residence times is coincidental. As revealed in the previous experiment, the rate of association is bimolecular and dependent on the concentration of free GroES. **A)** Data taken at 100 mM  $\text{K}^+$ . **B)** Data taken at 10 mM  $\text{K}^+$ .

Figure 5-5A demonstrates a number of the principles derived from previous experiments: 1) removal of ADP from the *trans* ring results in a nearly 3,000-fold stimulation in the rate of GroES release from the asymmetric complex, 2) even a relatively small amount of the weak binding  $\alpha$ -lactalbumin provides a noticeable rate stimulation [49]. What it also shows is that association and dissociation are nearly mirror images of each other. The line drawn across the mid-point of the y-axis represents the

mean residence time (MRT) for GroES binding or release. Within error, the intersections of all the traces,  $\pm$ ADP and  $\pm$ SP, coincide with the MRT. Previous studies have examined the kinetics of association and dissociation in order to determine if symmetric complexes are formed [20]. The theory was that if association preceded dissociation, then most likely footballs are formed as part of the reaction cycle [20]. However, this reasoning is not viable because, as demonstrated in the previous section, association is a bimolecular process and therefore depends on the concentration of free GroES. Thus, the fact that the association and dissociation traces have identical mean residence times in these experiments is purely coincidental and depends on the experimental set-up. What it does demonstrate is that the association event is affected by the removal of ADP and the presence of SP in the same manner as dissociation.

**5.3.3 The Effects of  $K^+$  on Association and Dissociation** Experiments were performed exactly as described in the previous section except that the asymmetric complex was desalted into buffer containing 10 mM  $K^+$ . Ionic strength was kept constant through addition of TMA. The result (Figure 5-5B) is that the MRT measured in the absence of ADP *increased* approximately 4-fold, and the MRT in the presence of ADP *decreased* approximately 300-fold, compared to traces at 100 mM  $K^+$  (Figure 5-4A). It should be noted that the effect in the presence of ADP is dependent on the concentration of ADP added back to the desalted complex. In this case, the final ADP concentration after mixing 1:1 in the stopped flow was 7.5  $\mu$ M. Previous work shows that at slightly higher concentrations of ADP (15  $\mu$ M), changing the potassium concentration from 100 mM to 10 mM results in only a 10-fold decrease in MRT (J. Grason, unpublished results). Thus, the balance between allosteric ligands is delicate. Substrate protein had very little

effect at 10 mM  $K^+$ , but again, was not present in saturating amounts. Table 5-2 compares the mean residence times at both  $K^+$  concentrations. A direct comparison of traces at the two potassium concentrations in the presence and absence of ADP is shown in Figure 5-6.



**Figure 5-6: The Effects of  $K^+$  on Mean Residence Time,  $\pm$ ADP** As discussed in Chapter 4, the nucleotide binding affinity is directly proportional to the  $[K^+]$ . Association and dissociation data at 100 mM  $K^+$  (+ADP and -ADP) and 10 mM  $K^+$  (+ADP and -ADP) are shown.

Sample (ADP, SP)	100 mM $K^+$ (sec)	10 mM $K^+$ (sec)
-, -	0.015	0.065
-, +	0.015	0.050
+, -	50.00	0.150
+, +	6.00	0.150

**Table 5-2: Comparison of Mean Residence Times at 100 mM and 10 mM  $K^+$**

**5.3.4 Utilizing GroEL Traps to Study Symmetric Complex Formation** One way of examining the issue of football formation is to determine whether GroES binding to the *trans* ring is a requirement for GroES dissociation from the *cis* ring. If this is the case, as might be expected if symmetric complexes are part of the reaction cycle, then dissociation should be slower (if it occurs at all) when the asymmetric FRET complex is challenged only with ATP and no competitor GroES. However, in order to visualize a change in the FRET signal, there must either be competitor GroES<sup>wt</sup>, or some way of sequestering the GroES<sup>A</sup> once it has been released from GroEL<sup>D</sup>. This problem was solved by the Rye group, where they utilized GroEL<sup>wt</sup> as a trap for GroES<sup>A</sup> once it was released into solution [20]. In their experiment, they found that GroEL<sup>wt</sup> and GroES<sup>wt</sup> traps yielded identical kinetics. We repeated their experiment, both in the presence and absence of 20  $\mu$ M ADP. Asymmetric complexes were prepared for dissociation experiments as previously described. ADP was added back to the desalted complex to a final concentration of 20  $\mu$ M. Because GroEL could not easily be added to syringe B, which contains the ATP, it was added to syringe A at a concentration of 15  $\mu$ M for the GroEL<sup>wt</sup> trap traces. For consistency, competitor GroES<sup>wt</sup> was also added to syringe A for GroES<sup>wt</sup> trap traces at the same concentration. Syringe B contained 4 mM ATP in 20 mM Tris, pH 7.5, 10 mM MgAc, 100 mM KAc, and 2 mM DTT.

In the absence of ADP (Figure 5-7A), the kinetics using GroEL and GroES traps were nearly identical. However, in the presence of ADP (Figure 5-7B), the reaction clearly proceeded faster in the presence of excess GroES<sup>wt</sup> as opposed to the GroEL trap. It is difficult to understand why footballs would be forming in one scenario (+ADP) and not the other (-ADP). We were concerned that the difference seen with ADP was not due

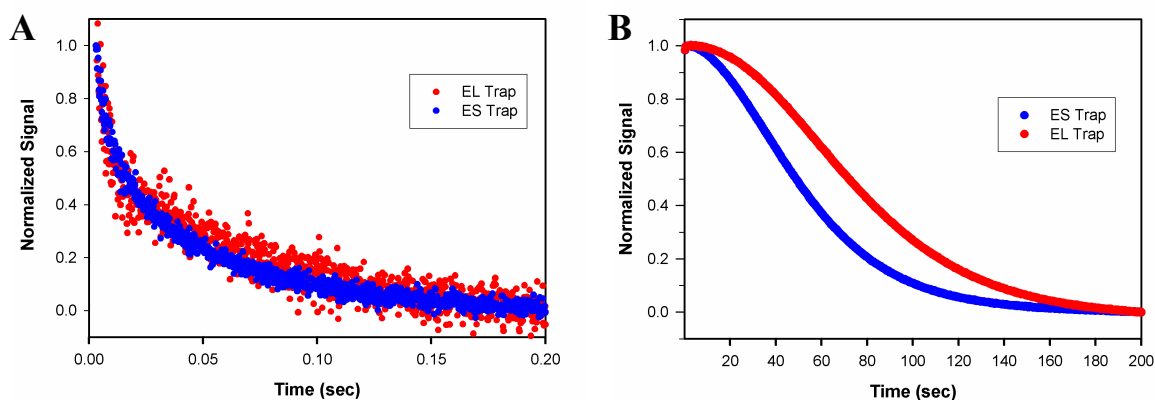


**Figure 5-7: Monitoring Dissociation Using an EL and ES Trap,  $\pm$ ADP** An excess of either GroEL<sup>wt</sup> or GroES<sup>wt</sup> can be used to sequester or out compete the GroES<sup>A</sup>, allowing the dissociation reaction to be monitored over time. If symmetric complexes are forming as an intermediate in the GroEL reaction cycle, it is expected that the rate of dissociation will be dependent on the concentration of GroES. A) ADP was removed from the *trans* ring. The MRT using the GroEL and GroES trap is roughly the same, approximately 15 msec. B) A small amount of ADP was added back to the *trans* ring of the asymmetric complex. Now, the MRT varies using the two different traps: 75 sec for the GroEL<sup>wt</sup> trap, and 50 sec for the GroES<sup>wt</sup> trap.

to the presence of symmetric complexes, but rather the scavenging of contaminating substrate protein from the *trans* ring of the FRET complexes. Since GroEL<sup>wt</sup> was added to syringe A, there was plenty of time for the solution to reach equilibrium prior to mixing in the stopped-flow. As revealed in section 5.3.2, the effect of substrate protein is most apparent when ADP is present, and this might explain why the two conditions yielded different results.

We performed the experiment again, this time adding the GroEL and GroES trap to syringe B. Because the ATP would be consumed by the GroEL over time, we also included an ATP regeneration system, similar to that used in the steady-state ATPase assay described in chapter 2. This time, syringe B contained 15  $\mu$ M GroEL<sup>wt</sup> or GroES<sup>wt</sup> and 4 mM ATP as before, but also 2 mM PEP and 13 units of pyruvate kinase. Once again, in the presence of ADP, the GroEL<sup>wt</sup> trap yielded slower kinetics (data not shown).

To test whether the difference was, in fact, due to substrate protein being transferred to the GroEL trap, the experiment was repeated again, this time with a small amount of denatured MDH added to syringe A (0.5x compared to EL<sub>14</sub>). If the difference in observed rates using the two traps were due to scavenged substrate protein, one would expect the difference to be even greater when SP was added. MDH is a relatively tight binding protein which might simulate the kind of protein that would remain bound to GroEL after purification. As shown in Figure 5-8, while the MRT of the GroEL trap remains about the same in the presence of additional MDH, the MRT using the GroES trap is significantly decreased. This strongly suggests that the disparity in mean residence times observed when using the two traps is due, at least in large part, to the presence of contaminating substrate. Moreover, it demonstrates that ligand release from the *cis* ring does not *require* GroES association to the *trans* ring.

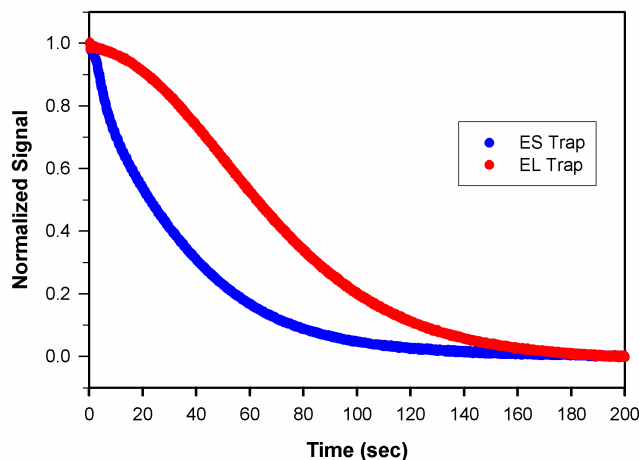


**Figure 5-8: Adding Denatured Substrate Protein to the GroEL and GroES Trap Experiments** It was conjectured that the difference in half-times using the EL and ES traps shown in Figure 5-7 B was due to contaminating substrate protein being scavenged from the *trans* ring of the asymmetric complex by the excess GroEL in the trap. Here, a small amount of denatured malate dehydrogenase (0.5x compared to GroEL<sub>14</sub>) is added to syringe A. While the MRT using the GroEL trap remains about the same (70 sec), the half-time for the GroES trap decreases significantly (25 sec).

### 5.3.5 Testing for Symmetric Complexes Using a Steady State FRET Analysis

We considered the possibility that we had not detected formation of symmetric complexes because they could only be observed under steady state conditions, whereas all the previous experiments were performed under pre-steady state conditions. Some researchers have conjectured that ATP hydrolysis cannot occur in the *cis* ring until ADP has departed from the *trans* ring [110]. However, the evidence for this conclusion is rather tenuous, and we considered the possibility that the *cis* ring in our experiments contained ADP instead of ATP. There is some evidence to support this conclusion. Rates obtained from previous work with the FRET system match very well with those obtained in the steady state ATPase assay [49]. Thus, the resting state complex used in the FRET experiments must include ATP hydrolysis in the *cis* ring, or the rates between the two assays would not match. This relates to the formation of symmetric complexes since it was discovered that the symmetric complex is asymmetric with respect to nucleotide [59]. This means that symmetric complexes would not be able to form in pre-steady experiments because ADP is present in both the *cis* and *trans* rings.

We decided to examine the FRET signal of an asymmetric complex under steady state conditions in the presence of ATP and an excess of GroES<sup>A</sup>, but with no competitor GroES<sup>wt</sup>. The idea behind this experiment was that the FRET signal should increase over time, beyond the starting point, if symmetric complexes were forming in the steady state, since a second GroES<sup>A</sup> would be added to the opposite ring. A control with a buffer challenge (no ATP) would be performed for comparison.

Asymmetric complexes were formed using 40  $\mu$ M GroEL<sup>D</sup>, 60  $\mu$ M GroES<sup>A</sup> (a 3-fold excess of GroES rings over 14-mers), and 300  $\mu$ M ATP. The complex was

incubated for 30 minutes to exhaust the ATP and then split into two samples: one was desalted while the other was not. Each was diluted to a final concentration of 3.1  $\mu$ M GroEL and loaded separately into syringe A. This was then challenged with either 4 mM ATP or buffer alone. Material that was not desalted showed no change in signal, even over 500 second time traces, either with the control or the ATP challenge (data not shown). However, the desalted material (Figure 5-9) displayed a rapid decrease followed by a relatively slow rise, which gradually leveled off above the starting signal. The decrease can be attributed to the initial dissociation event as ATP binds to the *trans* ring and initiates release of the GroES<sup>A</sup> from the *cis* ring. The increase, which begins before the dissociation event is complete, proceeds past the starting point when monitored for 1 second (Figure 5-9A). In order to ensure that the apparent increase beyond the starting point was not due to missing amplitude in the initial fast phase, traces were taken for 0.2 seconds (Figure 5-9B). The shorter time course data indicates there is some missing amplitude in the longer time course data, but that the steady state equilibrium probably exists slightly beyond the starting signal. What is clear from this experiment is that dissociation of the *cis* GroES takes place before association to the *trans* ring begins, due to the fact that the excess of GroES<sup>A</sup> available to bind the *trans* ring is now only a 2-fold excess, instead of the 5-fold excess used in previous experiments. This supports the conclusion that the reciprocal dissociation and association events observed in the previous experiments is accidental. Based on the time scale of this event, it is not surprising there was no change in the +ADP sample. Dissociation of all the ADP occurs on the hundreds of seconds timescale, while the association takes less than a second. In this case, it would be nearly impossible to detect the change.

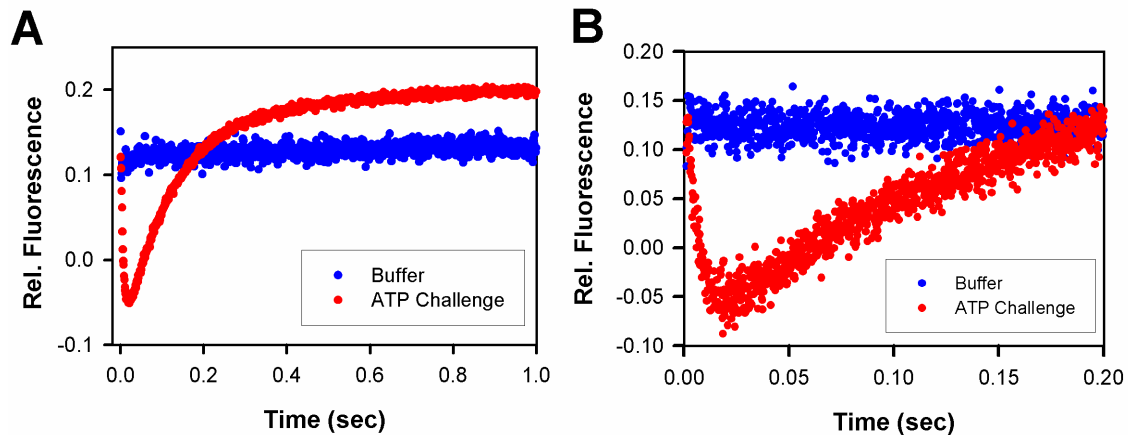


**Figure 5-9: Looking for Symmetric Complex Formation Using Steady State FRET** GroEL<sup>D</sup> was incubated with a 3-fold excess of GroES<sup>A</sup> and ATP. The ATP was allowed to exhaust and the sample was split, one which was desalted and the other which was used directly (i.e. with ADP present on the *trans* ring). This was then challenged in the stopped flow with either ATP (red traces) or buffer (blue traces). The material which was not desalted had no change in signal (data not shown). This shows the result in the absence of ADP at **A**) 1 second and **B**) 0.2 seconds.

## 5.4 Discussion

### 5.4.1 GroES Association and Dissociation Are Tightly Coupled Events

GroEL is a highly efficient nano-machine which functions as a two-stroke motor, where the two rings are 180° out of phase with one another [21]. Thus, events leading to the dissociation of the *cis* ligands should also facilitate association of the incoming GroES to the *trans* ring. The results show that actions which drastically reduce the MRT for dissociation also reduce the time for association, and vice versa. This supports the model of the GroEL reaction cycle shown in Figure 5-1 [49]. Removal of the *trans* ring ADP primes the asymmetric complex for dissociation. This is supported by the fact that gel filtration alone is enough to cause a slow dissociation of the asymmetric complex (J. Grason, unpublished results). SP stimulates *cis* dissociation (and also *trans* association) by

shifting the equilibrium of the *trans* ring subunits toward the T state, which has a lower affinity for nucleotide and hastens removal of the ADP [49].

To this point, the nature of the allosteric signal responsible for *cis* ligand release has not been known. The results here suggest the signal is likely to be an event common to both association and dissociation. The GroEL trap results indicate that GroES association to the *trans* ring is not required for *cis* disassembly. Thus, the signal transmitted between the rings must be an event that occurs between ATP binding and GroES association. Previous experiments in our lab with GroEL<sup>IAX</sup> demonstrated that the *cis* ring GroES could be released even when the *trans* ring was locked in the T state (G. Curien, unpublished results). Moreover, the mutation R197C/E386C, which eliminates a key inter-subunit salt bridge that stabilizes the T state, greatly impairs the release of GroES and ADP from the *cis* ring [49]. This leaves ATP binding to *trans* ring in the T state conformation, or an unidentified event preceding it, as a likely candidate for the allosteric signal.

**5.4.2 The Effects of Potassium** The effects of potassium on GroES association are similar to those reported for dissociation [49]. When ADP has been removed from the *trans* ring, increasing the potassium from 10 mM to 100 mM results in an approximately 4.5-fold decrease in the mean residence time (Figure 5-6). Since the ADP has been removed, subunits in the *trans* ring are expected to be in the T state, as evidenced by the value of the allosteric constant reported in Chapter 4 and elsewhere [50]. The difference between the binding affinities for the T state at 10 mM and 100 mM potassium, determined from fits in Chapter 4, is approximately 5.5-fold, where binding is favored at the higher concentration of potassium. Thus, the reduction in the mean

residence time at 100 mM  $K^+$  is directly related to the higher binding affinity for ATP. In the presence of *trans* ring ADP, the situation is more complicated; increasing the potassium concentration from 10 mM to 100 mM results in a significant *increase* in the mean residence time. Here, the effect is due to a higher affinity for the ADP at the higher potassium concentration, resulting in a longer residence time. The magnitude of this result cannot be directly compared to the values for  $k_R$  at the two potassium concentrations for several reasons: 1) the derived constants are for ATP, not ADP, 2) the constants were derived for GroEL in the absence of GroES, and 3) the mean residence time will be affected by ADP release and ATP binding, both of which are affected by the potassium concentration.

The effects of substrate protein at the two potassium concentrations are shown in Figure 5-5A and B. Substrate protein shifts the equilibrium of subunits in the *trans* ring to the T state, which has a lower affinity for nucleotide than the R state. Thus, at high potassium concentrations, there is a significant stimulation in GroES release as the ADP is discharged more quickly. But at low potassium concentrations, the affinity for nucleotide in both the T and R states is significantly reduced, such that the stimulatory effect of substrate protein essentially disappears.

**5.4.3 The Evidence for Symmetric Complexes** Although the studies here did not show a kinetic requirement for symmetric complex formation, it cannot be ruled out that such particles form. Indeed, in light of the multiple experiments that have chronicled their existence, it would be hard to argue otherwise. The difficulty is that if such complexes form due to association of ATP and GroES preceding dissociation of the *cis* ligands, such a complex would be extremely transitory. In the presence of ADP, the rate

limiting step in the GroES association and dissociation reactions is the release of ADP from the *trans* ring. Thus, the majority of the mean hemicycle time is spent as an asymmetric complex. In this case, it is difficult to imagine they would make up a significant fraction of the total population as reported [18, 111]. Since reciprocity was observed between association and dissociation under a variety of conditions, including conditions of high  $K^+$  and low ADP (which presumably favors the formation of footballs), it is difficult to reconcile such a high percentage of symmetric particles. The slight increase in signal in Figure 5-9A above the starting point suggests they might be forming in the steady state. A final possibility is an off-pathway mechanism, where ATP and GroES bind to the *trans* ring once ADP has departed, but before it has relaxed to back to the T state and sent the signal for *cis* dissociation.

Although the GroEL and GroES traps did not conclusively demonstrate formation of “footballs,” it did highlight the importance of sample preparation and experimental conditions. This experiment becomes an exquisitely sensitive method for determining the degree of substrate contamination. The fact that others observed no difference in the traces using the two traps [20], however, does not indicate that their preparations are especially clean. On the contrary, we believe one reason the results from our lab differ so dramatically from those previously reported is that our preparations are significantly less contaminated with substrate protein due to the acetone precipitation step in the GroEL purification [49]. However, their experiments were performed at 10 mM  $K^+$ , where substrate protein, as shown in Figure 5-5B, has very little effect. It becomes clear that understanding the consequences of the various allosteric effectors is critical to experimental design and interpretation.

## **Chapter 6**

### **Summary and Final Discussion**

Examining the allosteric properties of a large, macromolecular assembly such as GroEL can be overwhelming. Not only are there interactions to account for within and between the rings, but there are also a host of allosteric ligands: ATP, ADP, SP,  $K^+$ ,  $Mg^{2+}$ , and GroES [51]. Yet it is a complex array of allosteric interactions that allows for such exquisite control of many biological systems and makes GroEL a particularly interesting model for study. A nested cooperativity model was proposed to explain the steady-state kinetics of ATP hydrolysis by GroEL [50]. The model made two assumptions: 1) ATP could be bound and hydrolyzed only by the R state, and 2) the activity of subunits in the R state of a RR ring is less than the activity of subunits in the R state of a TR ring. The primary goal of the work presented in this dissertation was to examine the fine details of this model and to test its applicability with allosteric ligands such as potassium, which had not been previously addressed.

Previous studies with GroEL<sup>IAX</sup> (G. Curien and G. Lorimer, unpublished results), along with work presented in Chapter 3, support the broad outlines of the nested cooperativity model. Subunits within a ring transition from the T to R state in a concerted fashion, in accordance with the MWC model. The principle of negative cooperativity was supported by mutants that lacked an opposing ring (SR1) or were deficient in inter-ring signaling (GroEL<sup>LSM</sup>); no decrease in ATPase activity at higher concentrations of ATP was evident for either mutant (Figures 3-8A and 3-15).

However, in the process of confirming the concerted nature of allosteric transitions within a ring, it became apparent that the T state not only bound ATP, it hydrolyzed it at a rate similar to that of the R state (Figure 3-12). This led to the development of a new set of equations for nested cooperativity where the exclusive

binding assumption was not invoked. Moreover, the results with potassium, both from the fitting and from the FRET experiments detailed in Chapter 5 and elsewhere [49], reveal that the other assumption of the original nested cooperativity model is also unnecessary. Negative cooperativity is not due to a difference in the  $k_{\text{cat}}$  of the various allosteric conformations, but is a direct result of the time it takes for ADP to dissociate from the *trans* ring [49]. The corollary to this is that conditions which enhance the R state thereby decrease the rate of ADP dissociation from the *trans* ring and slow the rate of steady state turnover. Fits to the ATPase data collected at various potassium concentrations revealed that potassium affects the binding affinity for ATP without altering the allosteric equilibrium constant, L (Figures 4-6 and 4-9). Increasing the binding affinity for nucleotide has the result of increasing the population of rings in the R state, thereby inhibiting the release of ADP from the *trans* ring. ATP hydrolysis in the *cis* ring is unaffected (J. Grason, unpublished data). Thus, it now becomes clear why potassium alters the  $V_{\text{max}}$  of GroEL and not SR1; the result is a direct reflection of the decreased negativity cooperativity as the concentration of potassium is lowered (Figure 4-7). In the absence of a second ring, potassium exerts no effect (Figure 4-5). Likewise, substrate protein shifts the equilibrium to the T state, which has a lower affinity for nucleotide, thus speeding release of ADP from the *trans* ring and stimulating the overall rate of hydrolysis. Again, this effect is seen only with GroEL and not SR1 (Figure 3-8B).

The results of the FRET experiments in the presence of various potassium concentrations and substrate protein can be explained similarly. Conditions which speed the dissociation reaction also increase the rate of association (Figure 5-5). This is because the key event, ATP binding to the T state of the *trans* ring, is a prerequisite for

both dissociation and association. It makes sense that visiting the T state should be an obligatory part of the reaction cycle. The T state has a higher affinity for unfolded substrate protein and the role of the chaperonin is to capture and refold such proteins. Thus, ATP binding to the T state serves three purposes: 1) it is likely the allosteric signal transmitted between the rings that allows for *cis* ligand release, 2) it induces the formation of the R state in the *trans* ring, a necessary step for GroES association, and 3) it captures substrate protein, and in the process of switching to the R conformation, pulls the substrate binding sites apart (Figure 1-4).

Chapter 5 also explored the possibility of symmetric complex formation. Although the literature has offered ample evidence for their existence (negatively stained and cryo-EM images as well as analytical ultracentrifugation) [105, 107, 108], there is no explanation for how this occurs in the reaction cycle postulated in Figure 5-1. Based on the criteria that symmetric complexes are asymmetric with respect to the nucleotide present in each ring [59], this leaves only three mechanisms for their formation. First, because the rate of association is dependent on the concentration of free GroES (Figure 5-4), it is possible that association could precede dissociation and lead to the formation of a symmetric complex, where the *cis* ring contained ADP and the *trans* ring contained ATP. However, while this event is on-pathway and can be accounted for in the reaction cycle in Figure 5-1, the relative amount of time spent in this configuration would be extremely short. Since researchers have reported populations consisting of more than 50% “footballs” [18], this does not seem the likely mechanism for their formation. Likewise, if complexes are formed in the steady state by GroES adding to the ADP-bound form of the *trans* ring before ATP had been hydrolyzed in the *cis* ring, the fraction of symmetric

complexes would again be small. This means the most likely mechanism is an off-pathway, nonproductive one where ATP and GroES add to the *trans* ring once ADP has departed, but before the ring has relaxed back to the T state. This mechanism also makes sense in light of the dependence on  $K^+$  and ADP concentrations. It has been reported that low  $K^+$  and high ADP disfavor formation of symmetric complexes [16]. If the concentration of ADP were high, it would likely out compete ATP for rebinding to the unoccupied R state. Low potassium would decrease the affinity of both nucleotides, increasing the chance that the ring would relax to the T state before ATP and GroES could bind. This off-pathway mechanism, however, makes it unlikely that substrate protein would be trapped inside both rings simultaneously, as has been reported [105].

The new model of nested cooperativity presented here is consistent with the data collected by this lab and underscores the necessity of scrupulous experimental set-up and design. Much of the GroEL data in the literature is confusing and contradictory because allosteric ligands, especially contaminating substrate protein, have not been accounted for. A new model also presents an opportunity for further experimentation and refinement. It would be interesting to apply the equations presented in Chapter 4 to various GroEL mutants to see if the derived parameters continue to match with experimental results. Applying these equations in the presence of GroES would also be useful to see if the value for  $L_2'$ , which describes the allosteric equilibrium of the *trans* ring of the asymmetric complex, differs significantly from its previously reported value [64]. Further study is also needed to verify our hypothesis that ATP binding to the *trans* ring is the allosteric signal transmitted between the rings, perhaps by making use of a GroEL

D83C/K327C/D398A triple mutant, which could be locked in the T state with chemical cross-linkers but would not be capable of hydrolyzing ATP.

The model of nested cooperativity presented here proposes a novel look at negative cooperativity and offers fresh insights into the role played by allosteric ligands such as substrate protein and the potassium ion. The mean residence times obtained from the FRET experiments here and previously [49] make clear that, in the absence of substrate protein, the chaperonin conserves its fuel (ATP) and spends most of its time in the resting state. However, in the presence of substrate protein, the rate of turnover is accelerated nearly 17 fold and approaches the speed limit, that is the time it take for ATP to be hydrolyzed in the *cis* ring [49]. Thus, the chaperonin is designed in a way that allows for the maximum number of turnovers in the presence of SP, with the timing device for the system located on the *trans* ring. This is consistent with the iterative annealing mechanism, which advocates that the efficiency of the machine increases with multiple turnovers [44, 70].

## Appendix: Derivations of Equations for Nested Cooperativity

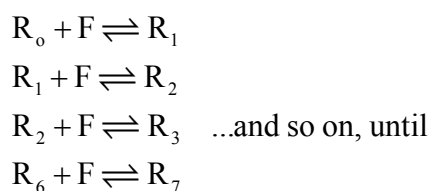
All the equations used to fit the data in Chapter 4 have been previously described [50]. However, due to an error in the published derivation, the equations are derived in full here. An excellent reference for the algebraic treatment of allosteric models is the Biophysical Chemistry text by Cantor and Schimmel [112].

### *A.1 Equations for the Single Ring*

Interactions within a single ring of GroEL are modeled according to MWC theory, meaning that all the subunits move in a concerted motion such that subunits within a ring must be either in the T state or R state [52]. The MWC model makes a number of assumptions:

- 1) Each protomer (in this case, a single subunit) contains a unique ligand binding site.
- 2) The two conformational states, T and R, are defined by a reversible equilibrium. The affinity for ligand in each of these states may be different.
- 3) The binding affinity is determined solely by the conformational state of the subunit, and not on the occupancy of neighboring sites.

With this in mind, the microscopic dissociation constants can be defined for ATP binding to the T and R states as  $k_T$  and  $k_R$ , respectively. The ligand is presumed to bind preferentially to one state over the other, in this case, the R state, such that  $k_T \neq k_R$ . The binding equilibria for the R state can be defined as follows:



R represents the macromolecule, which is defined here as the single ring of GroEL in the R conformation, and contains n sites for the ligand F. In this case, n equals 7, and F is ATP. However, this describes the microscopic species present after each successive round of ligand binding. For example, there are seven different microscopic species that are possible upon the binding of 1 ATP molecule to a ring containing seven binding sites, as shown in Figure A-1.

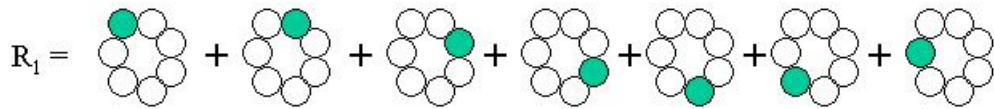


**Figure A-1: The Microscopic Species Possible with One Ligand Bound to the Single Ring.** Each subunit within the ring is represented by a circle. The subunit with ATP bound is colored cyan. If only one ATP is bound, there are seven different conformations which describe the microscopic state.

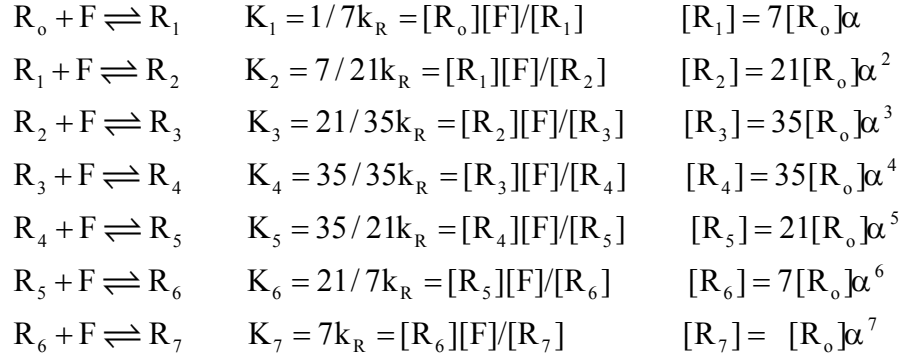
The number of microscopic species is defined by  $\Omega_{n,i}$ , which describes the number of microscopic forms that make up  $R_i$ , or put another way, the number of distinct ways  $i$  ligands can be arranged on  $n$  sites:

$$\Omega_{n,i} = \frac{n!}{(n-i)!i!}$$

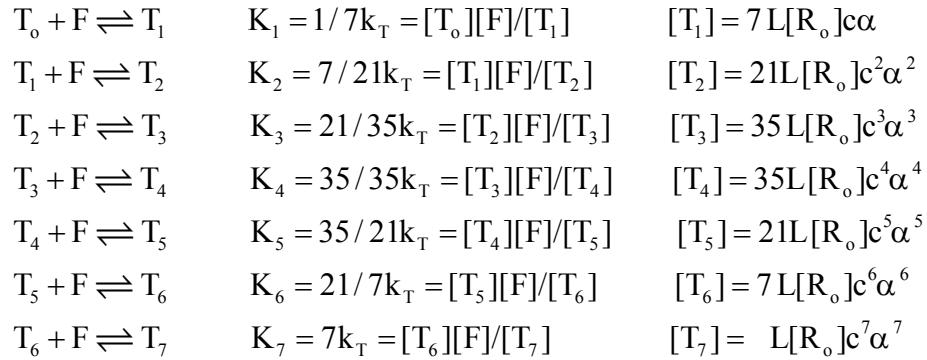
The more familiar macroscopic equilibrium constant,  $K$ , can be distinguished from the microscopic constant,  $k$ , by the statistical factors,  $\Omega_{n,i}$ :

$$K = \frac{\Omega_{n,i-1}}{\Omega_{n,i}} \times k$$

By defining the dimensionless constant  $\alpha$  as  $[F]/k_R$ , then the equilibrium expressions for the R state become:



Similar expressions may be derived for the T state. In order to express the T state equilibria in the same terms used for the R state equilibria, two new constants are defined. The ratio between the two dissociation constants is  $k_T = k_R/c$ , and the conformational equilibrium between the T and R state in the absence of ligand is  $L = [T_0]/[R_0]$ . Thus, the T state equilibria are defined as follows:



The fractional saturation,  $\bar{y}_F$ , with respect to F is defined as:

$$\bar{y}_F = \frac{\sum_i i(R_i) + \sum_i i(T_i)}{7\left[\sum_i (R_i) + \sum_i (T_i)\right]}$$

where the numerator represents the total occupied sites and the denominator is the total number of sites. These terms are defined from the T and R state equilibria equations:

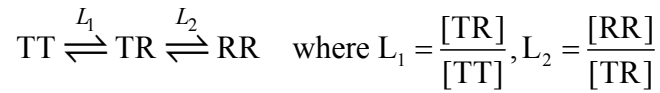
$$\begin{aligned}\sum_{i=0}^7 (R_i) &= [R_o](1 + 7\alpha + 21\alpha^2 + 35\alpha^3 + 35\alpha^4 + 21\alpha^5 + 7\alpha^6 + \alpha^7) = [R_o](1 + \alpha)^7 \\ \sum_{i=0}^7 (T_i) &= L[R_o](1 + \alpha\alpha)^7 \\ \sum_{i=0}^7 i(R_i) &= \alpha \frac{d}{d\alpha} \sum_{i=0}^7 (R_i) = 7[R_o]\alpha(1 + \alpha)^6 \\ \sum i(T_i) &= 7L[R_o]\alpha\alpha(1 + \alpha\alpha)^6\end{aligned}$$

Substituting these expressions into the equation for fractional saturation, and using the relationship:  $\bar{y}_F = V_o / V_{\max}$  where  $V_o$  and  $V_{\max}$  are the initial and maximal velocities, Equation 1, as presented in Chapter 4, is obtained. This describes the binding of ATP to a single ring using MWC formalism, assuming ATP can bind to both the T and R states.

$$V_o = \frac{V_R\alpha(1 + \alpha)^6 + V_T L\alpha\alpha(1 + \alpha\alpha)^6}{(1 + \alpha)^7 + L(1 + \alpha\alpha)^7}$$

## ***A.2 Equations for Nested Cooperativity in the Double Ring***

Interactions between the rings proceeds sequentially, according to KNF theory [53]. The equilibria between the various allosteric states in the double ring can be represented by:



The fractional saturation again is defined as the total occupied sites divided by the total available sites:

$$\bar{y}_F = \frac{\sum_i i(TT_i) + \sum_i i(TR_i) + \sum_i i(RR_i)}{2N \left[ \sum_i (TT_i) + \sum_i (TR_i) + \sum_i (RR_i) \right]}$$

N refers to the number of subunits in a ring, such that  $2N = 14$ . Thus, the terms are defined similarly as in the case of the single ring:

$$\sum_{i=0}^{2N} (TT_i) = [TT_o](1 + c\alpha)^{2N} \quad \sum_{i=0}^{2N} (TR_i) = [TR_o](1 + \alpha)^N (1 + c\alpha)^N \quad \sum_{i=0}^{2N} (RR_o) = [RR_o](1 + \alpha)^{2N}$$

$$\sum_{i=0}^{2N} i(TT_i) = 2Nc\alpha[TT_o](1 + c\alpha)^{2N-1} \quad \sum_{i=0}^{2N} i(RR_i) = 2N\alpha[RR_o](1 + \alpha)^{2N-1}$$

$$\sum_{i=0}^{2N} i(TR_i) = \alpha[TR_o] \left[ N(1 + \alpha)^{N-1} (1 + c\alpha)^N + cN(1 + \alpha)^N (1 + c\alpha)^{N-1} \right]$$

In order to express all concentrations in terms of TT,  $[TR] = L_1[TT]$  and  $[RR] = L_1L_2[TT]$ . As before,  $\alpha = [F]/k_R$  and  $k_T = k_R/c$ . Substituting these expressions into the above equation for fractional saturation, the reduced equation becomes the one presented in Chapter 4:

$$V_o = \frac{V_{TT}c\alpha(1 + c\alpha)^{13} + 0.5V_{TR}\alpha L_1(1 + \alpha)^6(1 + c\alpha)^7 + 0.5V_{TR}c\alpha L_1(1 + \alpha)^7(1 + c\alpha)^6 + V_{RR}\alpha L_1L_2(1 + \alpha)^{13}}{(1 + c\alpha)^{14} + L_1(1 + \alpha)^7(1 + c\alpha)^7 + L_1L_2(1 + \alpha)^{14}}$$

## REFERENCES

1. Onuchic, J. N., Luthey-Schulten, Z. & Wolynes, P. G. (1997) Theory of protein folding: the energy landscape perspective, *Annu. Rev. Phys. Chem.* **48**: 545-600.
2. Fayet, O., Ziegelhoffer, T. & Georgopoulos, C. (1989) The GroES and GroEL heat shock gene products of *Escherichia coli* are essential for bacterial growth at all temperatures, *J. Bacteriol.* **171**: 1379-1385.
3. McLennan, N. & Masters, M. (1998) GroE is vital for cell-wall synthesis, *Nature*. **392**: 139.
4. Born, W., Harbeck, R. & O'Brien, R. L. (1991) Possible links between immune system and stress response: the role of gamma delta T lymphocytes, *Semin. Immunol.* **3**: 43-48.
5. Shinnick, T. M. (1991) Heat shock proteins as antigens of bacterial and parasitic pathogens, *Curr. Top. Microbiol. Immunol.* **167**: 145-160.
6. Hemmingsen, S. M., Woolford, C., van der Vies, S. M., Tilly, K., Dennis, D. T., Georgopoulos, C., Hendrix, R. W. & Ellis, R. J. (1988) Homologous plant and bacterial proteins chaperone oligomeric protein assembly, *Nature*. **333**: 330-334.
7. Braig, K., Otwinowski, Z., Hegde, R., Boisvert, D. C., Joachimiak, A., Horwich, A. L. & Sigler, P. B. (1994) The crystal structure of the bacterial chaperonin GroEL at 2.8 Å, *Nature*. **371**: 578-586.
8. Sigler, P. B., Xu, Z. H., Rye, H. S., Burston, S. G., Fenton, W. A. & Horwich, A. L. (1998) Structure and function in GroEL-mediated protein folding, *Ann. Rev. Biochem.* **67**: 581-608.
9. Braig, K., Adams, P. D. & Brunger, A. T. (1995) Conformational variability in the refined structure of the chaperonin GroEL at 2.8 resolution, *Nat. Struct. Biol.* **2**: 1083-94.
10. Xu, Z. H., Horwich, A. L. & Sigler, P. B. (1997) The crystal structure of the asymmetric GroEL-GroES-(ADP)<sub>7</sub> chaperonin complex, *Nature*. **388**: 741-750.
11. Boisvert, D. C., Wang, J. D., Otwinowski, Z., Horwich, A. L. & Sigler, P. B. (1996) The 2.4 Å crystal structure of the bacterial chaperonin GroEL complexed with ATP<sub>γ</sub>S, *Nat. Struct. Biol.* **3**: 170-177.
12. Brocchieri, L. & Karlin, S. (2000) Conservation among Hsp60 sequences in relation to structure, function, and evolution, *Protein Sci.* **9**: 476-486.
13. Fenton, W. A., Kashi, Y., Furtak, K. & Horwich, A. L. (1994) Residues in chaperonin GroEL required for polypeptide binding and release, *Nature*. **371**: 614-619.

14. Goloubinoff, P., Gatenby, A. A. & Lorimer, G. H. (1989) GroE heat-shock proteins promote assembly of foreign prokaryotic ribulose bis-phosphate carboxylase oligomers in *Escherichia coli*, *Nature*. **337**: 44-47.
15. Hunt, J. F., Weaver, A. J., Samuel, J. L., Gierasch, L. M. & Deisenhofer, J. (1996) The crystal structure of the GroES-cochaperonin at 2.9 Å resolution, *Nature*. **402**: 147-154.
16. Llorca, O., Carrascosa, J. L. & Valpuesta, J. M. (1996) Biochemical characterization of symmetric GroEL-GroES complexes, *J. Biol. Chem.* **271**: 68-76.
17. Grallert, H., Rutkat, K. & Buchner, J. (2000) Limits of protein folding inside GroE complexes, *J. Biol. Chem.* **275**: 20424-30.
18. Beißinger, M., Rutkat, K. & Buchner, J. (1999) Catalysis, commitment and encapsulation during GroE-mediated folding, *J. Mol. Biol.* **289**: 1075-1092.
19. Grallert, H. & Buchner, J. (2001) Review: A structural view of the GroE chaperone cycle, *J. Struct. Biol.* **135**: 95-103.
20. Rye, H. S., Roseman, A. M., Chen, S., Furtak, K., Fenton, W. A., Saibil, H. & Horwich, A. L. (1999) GroEL-GroES cycling: ATP and non-native polypeptide direct alternation of folding-active rings, *Cell*. **97**: 325-338.
21. Lorimer, G. H. (1997) Protein folding: Folding with a two-stroke motor, *Nature*. **388**: 720-721.
22. Thirumalai, D. & Lorimer, G. H. (2001) Chaperonin-mediated protein folding, *Ann. Rev. Biophys. Biomol. Struct.* **30**: 245-269.
23. Viitanen, P. V., Gatenby, A. A. & Lorimer, G. H. (1992) Purified chaperonin 60 (groEL) interacts with the nonnative states of a multitude of *Escherichia coli* proteins, *Protein Sci.* **1**: 363-369.
24. Lorimer, G. H. (1996) A quantitative assessment of the role of the chaperonin proteins in protein folding *in vivo*, *FASEB Journal*. **10**: 5-9.
25. Ellis, R. J. & Hartl, F. U. (1996) Protein folding in the cell: Competing models of chaperonin function, *FASEB J.* **10**: 20-26.
26. Ben-Zvi, A. P. & Goloubinoff, P. (2001) Review: mechanisms of disaggregation and refolding of stable protein aggregates by molecular chaperones, *J. Struct. Biol.* **135**: 84-93.

27. Jaenicke, R. (1995) Folding and association versus misfolding and aggregation of proteins, *Philos. Trans. R. Soc. London B Biol. Sci.* **348**: 97-105.
28. Ewalt, K. L., Hendrick, J. P., Houry, W. A. & Hartl, F. U. (1997) *In vivo* observation of polypeptide flux through the bacterial chaperonin system, *Cell.* **90**: 491-500.
29. Lin, Z., Schwartz, F. P. & Eisenstein, E. (1995) The hydrophobic nature of GroEL-substrate binding, *J. Biol. Chem.* **270**: 1011-1014.
30. Buckle, A. M., Zahn, R. & Fersht, A. R. (1997) A structural model for GroEL-polypeptide recognition, *Proc. Natl. Acad. Sci. U.S.A.* **94**: 3571-3575.
31. Houry, W. A., Frishman, D., Eckerskorn, C., Lottspeich, F. & Hartl, F. U. (1999) Identification of *in vivo* substrates of the chaperonin GroEL, *Nature.* **402**: 147-154.
32. Landry, S. J. & Gierasch, L. M. (1994) Polypeptide interactions with molecular chaperones and their relationship to *in vivo* protein folding, *Annu. Rev. Biophys. Biomol. Struct.* **23**: 645-669.
33. Fedorov, A. N. & Baldwin, T. O. (1997) GroE modulates kinetic partitioning of folding intermediates between alternative states to maximize the yield of biologically active protein, *J. Mol. Biol.* **268**: 712-23.
34. Stan, G., Brooks, B. R., Lorimer, G. H. & Thirumalai, D. (2004) Identifying natural substrates for chaperonins using a sequence-based approach, *Proc. Natl. Acad. Sci. U.S.A.* **In Press**.
35. Aoki, K., Motojima, F., Taguchi, H., Yomo, T. & Yoshida, M. (2000) GroEL binds artificial proteins with random sequences, *J. Biol. Chem.* **275**: 13755-8.
36. Xu, Z. H. & Sigler, P. B. (1998) GroEL/GroES: Structure and function of a two-stroke folding machine, *J. Struct. Biol.* **124**: 129-141.
37. Chen, S., Roseman, A. M., Hunter, A. S., Wood, S. P., Burston, S. G., Ranson, N. A., Clarke, A. R. & Saibil, H. (1994) Location of a folding protein and shape changes in GroEL-GroES complexes imaged by cryo-electron microscopy, *Nature.* **371**: 261-264.
38. Thiyagarajan, P., Henderson, S. J. & Joachimiak, A. (1996) Solution structures of GroEL and its complex with rhodanese from small-angle neutron scattering, *Structure.* **4**: 79-88.
39. Farr, G. W., Furtak, K., Rowland, M. B., Ranson, N. A., Saibil, H. R., Kirchhausen, T. & Horwich, A. L. (2000) Multivalent binding of nonnative substrate proteins by the chaperonin GroEL, *Cell.* **100**: 561-573.

40. Burston, S. G., Ranson, N. A. & Clarke, A. R. (1995) The origins and consequences of asymmetry in the chaperonin reaction cycle, *J. Mol. Biol.* **249**: 138-152.
41. Ranson, N. A., Farr, G. W., Roseman, A. M., Gowen, B., Fenton, W. A., Horwich, A. L. & Saibil, H. R. (2001) ATP-bound states of GroEL captured by cryo-electron microscopy, *Cell.* **107**: 869-879.
42. White, H., Chen, S., Roseman, A. M., Yifrach, O., Horovitz, A. & Saibil, H. (1997) Structural basis of allosteric changes in the GroEL mutant Arg197Ala, *Nat. Struct. Biol.* **4**: 690-694.
43. Anfinsen, C. B. (1973) Principles that govern the folding of protein chains, *Science.* **181**: 223-230.
44. Betancourt, M. R. & Thirumalai, D. (1999) Exploring the kinetic requirements for enhancement of protein folding rates in the GroEL cavity, *J. Mol. Biol.* **287**: 627-644.
45. Chaudhry, C., Farr, G. W., Todd, M. J., Rye, H. S., Brunger, A. T., Adams, P. D., Horwich, A. L. & Sigler, P. B. (2003) Role of the  $\gamma$ -phosphate of ATP in triggering protein folding by GroEL-GroES: function, structure, and energetics, *EMBO J.* **22**: 4877-4887.
46. Weissman, J. S., Hohl, C. M., Kovalenko, O., Kashi, Y., Chen, S. X., Braig, K., Saibil, H. R., Fenton, W. A. & Horwich, A. L. (1995) Mechanism of GroEL action - productive release of polypeptide from a sequestered position under GroES, *Cell.* **83**: 577-587.
47. Rye, H. S., Burston, S. G., Fenton, W. A., Beechem, J. M., Xu, Z. H., Sigler, P. B. & Horwich, A. L. (1997) Distinct actions of cis and trans ATP within the double ring of the chaperonin GroEL, *Nature.* **388**: 792-798.
48. Todd, M. J., Viitanen, P. V. & Lorimer, G. H. (1994) Dynamics of the Chaperonin ATPase Cycle: Implications for Facilitated Protein Folding, *Science.* **265**: 659-666.
49. Grason, J. P. (2003) *Allostery in GroEL: Its role in the refolding of protein substrates*, University of MD, College Park.
50. Yifrach, O. & Horovitz, A. (1995) Nested cooperativity in the ATPase activity of the oligomeric chaperonin GroEL, *Biochemistry.* **34**: 5303-5308.
51. Horovitz, A., Fridmann, Y., Kafri, G. & Yifrach, O. (2001) Review: allostery in chaperonins, *J. Struct. Biol.* **135**: 104-14.
52. Monod, J., Wyman, J. & Changeux, J.-P. (1965) On the nature of allosteric interactions: a plausible model, *J. Mol. Biol.* **12**: 88-118.

53. Koshland, D. E., Jr., Nemethy, G. & Filmer, D. (1966) Comparison of experimental binding data and theoretical models in proteins containing subunits, *Biochemistry*. **5**: 365-385.
54. Hellmann, N. & Decker, H. (2002) Nested MWC model describes hydrolysis of GroEL without assuming negative cooperativity in binding, *Biochim Biophys Acta*. **1599**: 45-55.
55. Gray, T. E. & Fersht, A. R. (1991) Cooperativity in ATP hydrolysis by GroEL is increased by GroES, *FEBS Letters*. **292**: 254-258.
56. Roseman, A. M., Chen, S., White, H., Braig, K. & Saibil, H. (1996) The chaperonin ATPase cycle: Mechanism of allosteric switching and movements of substrate-binding domains in GroEL, *Nature*. **87**: 241-251.
57. Ma, J., Sigler, P. B., Xu, Z. & Karplus, M. (2000) A dynamic model for the allosteric mechanism of GroEL, *J. Mol. Biol.* **302**: 303-13.
58. Danziger, O., Rivenzon-Segal, D., Wolf, S. G. & Horovitz, A. (2003) Conversion of the allosteric transition of GroEL from concerted to sequential by the single mutation Asp155 to Ala, *Proc. Natl. Acad. Sci. USA*. **100**: 13797-802.
59. Gorovits, B. M., Ybarra, J., Seale, J. W. & Horowitz, P. M. (1997) Conditions for nucleotide-dependent GroES-GroEL interactions, *J. Biol. Chem.* **272**: 20424-20430.
60. Viitanen, P. V., Lubben, T. H., Reed, J., Goloubinoff, P., O'Keefe, D. P. & Lorimer, G. H. (1990) Chaperonin-facilitated refolding of ribulose-bisphosphate carboxylase and ATP hydrolysis by chaperonin 60 (groEL) are K<sup>+</sup> dependent, *Biochemistry*. **29**: 5665-5671.
61. Clark, A. C., Karon, B. S. & Frieden, C. (1999) Cooperative effects of potassium, magnesium and magnesium-ADP on the release of *Escherichia coli* dihydrofolate reductase from the chaperonin GroEL, *Protein Sci.* **8**: 2166-2176.
62. Todd, M. J., Viitanen, P. V. & Lorimer, G. H. (1993) Hydrolysis of adenosine 5'-triphosphate by *Escherichia coli* GroEL: effects of GroES and potassium ion, *Biochemistry*. **32**: 8560-7.
63. Widjaja, L. (2002) *Allosteric control by ATP on GroEL: Effects of monovalent and divalent cations*, University of MD, College Park.
64. Inbar, E. & Horovitz, A. (1997) GroES promotes the T to R transition of the GroEL ring distal to GroES in the GroEL-GroES complex, *Biochemistry*. **36**: 12276-81.
65. Yifrach, O. & Horovitz, A. (1996) Allosteric control by ATP of non-folded protein binding to GroEL, *J. Mol. Biol.* **255**: 356-361.

66. Saibil, H. (2000) Molecular chaperones: containers and surfaces for folding, stabilising or unfolding proteins, *Curr. Opin. Struct. Biol.* **10**: 251-8.
67. Brinker, A., Pfeifer, G., Kerner, M. J., Naylor, D. J., Hartl, F. U. & Hayer-Hartl, M. (2001) Dual function of protein confinement in chaperonin-assisted protein folding, *Cell.* **107**: 223-233.
68. Smith, C. M., Kohler, R. J., Barho, E., El-Thaher, T. S. H., Preuss, M. & Miller, A. D. (1999) Characterisation of Cpn60 (GroEL) bound cytochrome c: the passive role of molecular chaperones in assisted folding/refolding of proteins, *Journal of the Chemical Society-Perkin Transactions 2*: 1537-1546.
69. Shtilerman, M., Lorimer, G. H. & Englander, S. W. (1999) Chaperonin function: Folding by forced unfolding, *Science.* **284**: 822-825.
70. Todd, M. J., Lorimer, G. H. & Thirumalai, D. (1996) Chaperonin-facilitated protein folding: Optimization of rate and yield by an iterative annealing mechanism, *Proc. Natl. Acad. Sci. USA.* **93**: 4030-4035.
71. Ranson, N. A., Burston, S. G. & Clarke, A. R. (1997) Binding, encapsulation and ejection: Substrate dynamics during a chaperonin-assisted folding reaction, *J. Mol. Biol.* **266**: 656-664.
72. Baumketner, A., Jewett, A. & Shea, J. E. (2003) Effects of confinement in chaperonin assisted protein folding: rate enhancement by decreasing the roughness of the folding energy landscape, *J. Mol. Biol.* **332**: 701-13.
73. Farr, G. W., Fenton, W. A., Chaudhuri, T. K., Clare, D. K., Saibil, H. & Horwich, A. L. (2003) Folding with and without encapsulation by cis- and trans-only GroEL-GroES complexes, *EMBO J.* **22**: 3220-3230.
74. Chaudhuri, T. K., Farr, G. W., Fenton, W. A., Rospert, S. & Horwich, A. L. (2001) GroEL/GroES-mediated folding of a protein too large to be encapsulated, *Cell.* **107**: 235-246.
75. Inobe, T., Makio, E. T.-I., Terada, T. P. & Kuwajima, K. (2001) Nucleotide binding to chaperonin GroEL: non-cooperative binding of ATP analogs and ADP, and cooperative effect of ATP, *Biochim Biophys Acta.* **1545**: 160-173.
76. Bradford, M. (1976) A rapid and sensitive method for the quantitation of microgram quantities of protein utilizing the principle of protein-dye binding, *Anal. Biochem.* **72**: 248-254.
77. Laemmli, U. K. (1970) Cleavage of proteins during the assembly of the head of bacteriophage T4, *Nature.* **227**: 680-685.

78. Sambrook, J., Fritsch, E. F. & Maniatis, T. (1989) *Molecular Cloning, A Laboratory Manual, Second Edition*, Cold Spring Harbor Press.
79. Clark, A. C., Ramanathan, R. & Frieden, C. (1998) Purification of GroEL with Low Fluorescence Background, *Meth. Enzymol.* **290**: 100-118.
80. Voziyan, P. A. & Fisher, M. T. (2000) Chaperonin-assisted folding of glutamine synthetase under nonpermissive conditions: off-pathway aggregation propensity does not determine the co-chaperonin requirement, *Protein Sci.* **9**: 2405-2412.
81. Horwich, A. L., Burston, S. G., Rye, H. S., Weissman, J. S. & Fenton, W. A. (1998) Construction of single-ring and two-ring hybrid versions of bacterial chaperonin GroEL, *Methods Enzymol.* **290**: 141-6.
82. Eisenstein, E., Reddy, P. & Fisher, M. T. (1998) Overexpression, purification, and properties of GroES from *Escherichia coli*, *Meth. Enzymol.* **290**: 119-135.
83. Kreuzer, K. N. & Jongeneel, C. V. (1983) *Escherichia coli* phage T4 topoisomerase, *Meth. Enzymol.* **100**: 144-160.
84. Okazaki, A., Ikura, T., Nikaido, K. & Kuwajima, K. (1994) The chaperonin GroEL does not recognize apo- $\alpha$ -lactalbumin in the molten globule state, *Nat. Struct. Biol.* **1**: 439-446.
85. Peralta, D., Hartman, D. J., Hoogenraad, N. J. & Hoj, P. B. (1994) Generation of a stable folding intermediate which can be rescued by the chaperonins GroEL and GroES, *FEBS Letters.* **339**: 45-49.
86. Ranson, N. A., Dunster, N. J., Burston, S. G. & Clarke, A. R. (1995) Chaperonins can catalyse the reversal of early aggregation steps when a protein misfolds, *J. Mol. Biol.* **250**: 581-586.
87. Martz, E. (2002) Protein Explorer: Easy yet powerful macromolecular visualization, *Trends in Biochemical Sciences.* **27**: 107-109.
88. Sot, B., Galán, A., Valpuesta, J. M., Bertrand, S. & Muga, A. (2002) Salt Bridges at the Inter-ring Interface Regulate the Thermostat of GroEL, *J. Biol. Chem.* **277**: 34024-34029.
89. Weber, F., Keppel, F., Georgopoulos, C., Hayer-Hartl, M. K. & Hartl, F. U. (1998) The oligomeric structure of GroEL/GroES is required for biologically significant chaperonin function in protein folding, *Nature Struct. Biol.* **5**: 977-985.
90. Nielsen, K. & Cowan, N. (1998) A single-ring is sufficient for productive chaperonin-mediated folding in vivo, *Mol. Cell.* **2**: 1-7.

91. Nielsen, K., McLennan, N., Masters, M. & Cowan, N. (1999) A single ring mitochondrial chaperonin (Hsp 60/Hsp 10) can substitute for GroEL/GroES *in vivo*, *J. Bact.* **181**: 5871-5875.
92. Sun, Z., Scott, D. J. & Lund, P. A. (2003) Isolation and characterisation of mutants of GroEL that are fully functional as single rings, *J. Mol. Biol.* **332**: 715-728.
93. Levy-Rimler, G., Viitanen, P. V., Weiss, C., Sharkia, R., Greenberg, A., Niv, A., Lustig, A., Delarea, Y. & Azem, A. (2001) The effect of nucleotides and mitochondrial chaperonin 10 on the structure and chaperone activity of mitochondrial chaperonin 60, *Eur. J. Biochem.* **268**: 3465-3472.
94. Chen, J. W., Walter, S., Horwich, A. L. & Smith, D. L. (2001) Folding of malate dehydrogenase inside the GroEL-GroES cavity, *Nat. Struct. Biol.* **8**: 721-728.
95. Murai, N., Makino, Y. & Yoshida, M. (1996) GroEL locked in a closed conformation by an interdomain cross-link can bind ATP and polypeptide but cannot process further reaction steps, *J. Biol. Chem.* **271**: 28229-34.
96. Uebel, M. H. (2001) *Recovering intact GroEL complexes formed in vivo*, University of Maryland, College Park.
97. Kosower, N. & Kosower, E. (1995) Diamide: An Oxidant Probe for Thiols, *Meth. Enzymol.* **251**: 123-129.
98. Poso, D., Clarke, A. R. & Burston, S. G. (2004) A kinetic analysis of the nucleotide-induced allosteric transitions in a single-ring mutant of GroEL, *J. Mol. Biol.* **338**: 969-977.
99. Eaton, W. A., Henry, E. R., Hofrichter, J. & Mozzarelli, A. (1999) Is cooperative oxygen binding by hemoglobin really understood?, *Nat. Struct. Biol.* **6**: 351-358.
100. Gutsche, I., Essen, L. O. & Baumeister, W. (1999) Group II chaperonins: new TRiC(k)s and turns of a protein folding machine, *J. Mol. Biol.* **293**: 295-312.
101. Laughlin, L. T. & Reed, G. H. (1997) The monovalent cation requirement of rabbit muscle pyruvate kinase is eliminated by substitution of lysine for glutamate 117, *Arch. Biochem. Biophys.* **348**: 262-267.
102. Roseman, A. M., Ranson, N. A., Gowen, B., Fuller, S. D. & Saibil, H. (2001) Structures of unliganded and ATP-bound states of the Escherichia coli chaperonin GroEL by cryoelectron microscopy, *J. Struct. Biol.* **135**: 115-125.

103. Wang, J. D. & Boisvert, D. C. (2003) Structural basis for GroEL-assisted protein folding from the crystal structure of (GroEL-KMgATP)<sub>14</sub> at 2.0Å resolution, *J. Mol. Biol.* **327**: 843-855.
104. Taniguchi, M., Tatsunari, Y., Hongo, K., Mizobata, T. & Kawata, Y. (2004) Stopped-flow fluorescence analysis of the conformational changes in the GroEL apical domain: relationships between movements in the apical domain and the quaternary structure of GroEL, *J. Biol. Chem.* **279**: 16368-16376.
105. Sparrer, H., Rutkat, K. & Buchner, J. (1997) Catalysis of protein folding by symmetric chaperone complexes, *Proc. Natl. Acad. Sci. USA.* **94**: 1096-1100.
106. Behlke, J., Ristau, O. & Schonfeld, H. (1997) Nucleotide-dependent complex formation between the *Escherichia coli* chaperonins GroEL and GroES studied under equilibrium conditions, *Biochemistry.* **36**: 5149-5156.
107. Azem, A., Diamant, S., Kessel, M., Weiss, C. & Goloubinoff, P. (1995) The protein-folding activity of chaperonins correlates with the symmetric GroEL<sub>14</sub>(GroES)<sub>2</sub> heterooligomer, *Proc. Natl. Acad. Sci. USA.* **92**: 12021-12025.
108. Llorca, O., Marco, S., Carrascosa, J. L. & Valpuesta, J. M. (1994) The formation of symmetrical GroEL-GroES complexes in the presence of ATP, *FEBS Letters.* **345**: 181-186.
109. Fersht, A. R. (1977) *Enzyme Structure and Mechanism*, W. H. Freeman and Co., San Francisco.
110. Kad, N. M., Ranson, N. A., Cliff, M. J. & Clarke, A. R. (1998) Asymmetry, commitment and inhibition in the GroE ATPase cycle impose alternating functions on the two GroEL rings, *J. Mol. Biol.* **278**: 267-278.
111. Sparrer, H. & Buchner, J. (1997) How GroES regulates binding of nonnative protein to GroEL, *J. Biol. Chem.* **272**: 14080-14086.
112. Cantor, C. R. & Schimmel, P. R. (1980) *Biophysical Chemistry Part III: The Behavior of Biological Molecules*, W. H. Freeman and Co., San Francisco.